Atmos. Chem. Phys., 16, 4283–4305, 2016
www.atmos-chem-phys.net/16/4283/2016/
doi:10.5194/acp-16-4283-2016

Atmospheric Chemistry and Physics Open Access EGU

Non-OH chemistry in oxidation flow reactors for the study of atmospheric chemistry systematically examined by modeling

Zhe Peng[1,2], Douglas A. Day[1,2], Amber M. Ortega[1,3,a], Brett B. Palm[1,2], Weiwei Hu[1,2], Harald Stark[1,2,5], Rui Li[1,3,4,b], Kostas Tsigaridis[6], William H. Brune[7], and Jose L. Jimenez[1,2]

[1]Cooperative Institute for Research in Environmental Sciences, University of Colorado, Boulder, CO 80309, USA
[2]Department of Chemistry and Biochemistry, University of Colorado, Boulder, CO 80309, USA
[3]Department of Atmospheric and Oceanic Sciences, University of Colorado, Boulder, CO 80309, USA
[4]Chemical Sciences Division, Earth System Research Laboratory, National Oceanic and Atmospheric Administration, Boulder, CO 80305, USA
[5]Aerodyne Research, Inc., Billerica, MA 01821, USA
[6]Center for Climate Systems Research, Columbia University, and NASA Goddard Institute for Space Studies, New York, NY 10025, USA
[7]Department of Meteorology, Pennsylvania State University, University Park, PA 16802, USA
[a]now at: Chemical and Environmental Engineering, University of Arizona, Tucson, AZ 85721, USA
[b]now at: Markes International, Inc., Cincinnati, OH 45242, USA

Correspondence to: Jose L. Jimenez (jose.jimenez@colorado.edu)

Received: 30 July 2015 – Published in Atmos. Chem. Phys. Discuss.: 1 September 2015
Revised: 14 March 2016 – Accepted: 15 March 2016 – Published: 6 April 2016

Abstract. Oxidation flow reactors (OFRs) using low-pressure Hg lamp emission at 185 and 254 nm produce OH radicals efficiently and are widely used in atmospheric chemistry and other fields. However, knowledge of detailed OFR chemistry is limited, allowing speculation in the literature about whether some non-OH reactants, including several not relevant for tropospheric chemistry, may play an important role in these OFRs. These non-OH reactants are UV radiation, $O(^1D)$, $O(^3P)$, and O_3. In this study, we investigate the relative importance of other reactants to OH for the fate of reactant species in OFR under a wide range of conditions via box modeling. The relative importance of non-OH species is less sensitive to UV light intensity than to water vapor mixing ratio (H_2O) and external OH reactivity (OHR_{ext}), as both non-OH reactants and OH scale roughly proportionally to UV intensity. We show that for field studies in forested regions and also the urban area of Los Angeles, reactants of atmospheric interest are predominantly consumed by OH. We find that $O(^1D)$, $O(^3P)$, and O_3 have relative contributions to volatile organic compound (VOC) consumption that are similar or lower than in the troposphere. The impact of O atoms can be neglected under most conditions in both OFR and troposphere. We define "riskier OFR conditions" as those with either low H_2O ($< 0.1\,\%$) or high OHR_{ext} ($\geq 100\,s^{-1}$ in OFR185 and $> 200\,s^{-1}$ in OFR254). We strongly suggest avoiding such conditions as the importance of non-OH reactants can be substantial for the most sensitive species, although OH may still dominate under some riskier conditions, depending on the species present. Photolysis at non-tropospheric wavelengths (185 and 254 nm) may play a significant ($> 20\,\%$) role in the degradation of some aromatics, as well as some oxidation intermediates, under riskier reactor conditions, if the quantum yields are high. Under riskier conditions, some biogenics can have substantial destructions by O_3, similarly to the troposphere. Working under low O_2 (volume mixing ratio of 0.002) with the OFR185 mode allows OH to completely dominate over O_3 reactions even for the biogenic species most reactive with O_3. Non-tropospheric VOC photolysis may have been a problem in some laboratory and source studies, but can be avoided or lessened in future studies by diluting source emissions and working at lower precursor concentrations in laboratory studies and by humidification. Photolysis of secondary organic aerosol (SOA) samples is estimated to be significant ($> 20\,\%$) under

the upper limit assumption of unity quantum yield at medium (1×10^{13} and 1.5×10^{15} photons cm^{-2} s^{-1} at 185 and 254 nm, respectively) or higher UV flux settings. The need for quantum yield measurements of both VOC and SOA photolysis is highlighted in this study. The results of this study allow improved OFR operation and experimental design and also inform the design of future reactors.

1 Introduction

For decades, environmental chambers have been employed to study atmospheric chemical processes, particularly volatile organic compound (VOC) oxidation processes in the atmosphere (Cocker et al., 2001; Carter et al., 2005; Presto et al., 2005; Wang et al., 2011; Platt et al., 2013), without the interference of some transport processes (e.g., advection and wet deposition). These oxidation processes are the key to secondary organic aerosol (SOA) formation (Odum et al., 1996; Hoffmann et al., 1997; Hallquist et al., 2009) and air pollutant removal (Levy, 1971). Atmospheric simulation chambers usually have volumes on the order of several m^3 and use light sources longer than 300 nm (e.g., sunlight or UV black lights) to generate oxidants (mainly OH). These settings leads to OH concentrations (10^6–10^8 molecules cm^{-3}) that are not much higher than the typical ambient values (10^6–10^7 molecules cm^{-3}; Mao et al., 2009). Relatively low OH concentrations require long residence/simulation times (generally hours) and limit the ability of those setups to reach very high photochemical ages that are atmospherically relevant (George et al., 2007; Kang et al., 2007; Carlton et al., 2009; Seakins, 2010; Wang et al., 2011). Residence times are ultimately limited due to losses of gases and particles to Teflon walls with timescales of tens of minutes to several hours (Cocker et al., 2001; Matsunaga and Ziemann, 2010; Zhang et al., 2014) as well as by the limited volume of the bag relative to the sampling instrumentation (Nguyen et al., 2014). Besides, large sizes and support systems (e.g., clean air generators) make it difficult to use large chambers in field or source studies.

Oxidation flow reactors (OFRs) are an alternative that offers some advantages over environmental chambers, especially for rapid changes of experimental conditions and/or for field experiments. They generally have a smaller size (on the order of 10 L) and typically use low-pressure Hg lamps as light sources for producing OH in large amounts via O_3 and/or H_2O photolysis. These design choices lead to good portability, short experimental timescales, ability to reach long photochemical ages, and potentially reduced wall losses.

Due to these advantages, OFRs have been employed in many recent field and laboratory studies in atmospheric chemistry, particularly in SOA-related research (George et al., 2007; Kang et al., 2007, 2011; Smith et al., 2009; Massoli et al., 2010; Cubison et al., 2011; Lambe et al., 2011a, b, 2012, 2013; Bahreini et al., 2012; Saukko et al., 2012; Wang et al., 2012; Ortega et al., 2013; Li et al., 2013). OFRs are also used in related applied fields, such as scrubbing of pollution from air (Johnson et al., 2014). In contrast to their popularity, the chemistry occurring in OFRs is still incompletely characterized, although the formation and interconversion reactions of most oxidants in OFRs have been well characterized (Sander et al., 2011; Ammann et al., 2015). To our knowledge, there are only three studies of OFR radical oxidation chemistry to date. Ono et al. (2014) focused on the dependence of O_3 destruction on H_2O concentration. We have recently made progress on the characterization of HO_x radical chemistry in OFRs (Li et al., 2015; Peng et al., 2015). We have developed a kinetic model for OFRs, which provides predictions in good agreement with laboratory experiments. This model has also shown that OH exposure (OH_{exp}, i.e., OH concentration integrated over the reactor residence time) increases with H_2O concentration and UV intensity, and decreases with external OH reactivity ($OHR_{ext} = \sum k_i c_i$, i.e., the sum of the products of concentrations of externally introduced OH-consuming species (c_i) and rate constants of their reactions with OH (k_i)). The OH_{exp} decrease due to OHR_{ext} was defined as "OH suppression" and can reach 2 orders of magnitude in some cases (Li et al., 2015; Peng et al., 2015). We also showed that relative uncertainties of the outputs of our box model (e.g., OH_{exp}) due to uncertain kinetic parameters are typically only 20 % (Peng et al., 2015). However, none of these studies directly address the fate of VOCs (including oxygenated VOCs), simply regarded as external OH reactants in the prior studies.

The primary reason for the use of the OFRs studied here is for the study of reactions of species or mixtures of atmospheric relevance with the OH radical. However, other highly reactive species are also present at very elevated concentrations, including the radicals $O(^1D)$ and $O(^3P)$, 185 and 254 nm photons, and O_3. If a substantial fraction of the species of interest reacted with those non-OH reactants, then the chemistry in the OFR would deviate from the OH radical chemistry intended to investigate. The absence of systematic research on VOC fate in OFRs leaves room for some speculation that non-OH or non-tropospheric chemistry can play a major role in OFRs; for example, Johnson et al. (2014) suggested that $O(^1D)$ and $O(^3P)$ significantly consumed VOCs. Klems et al. (2015) concluded that photons at 254 nm from Hg-lamp emission played an important role in their OFR experiment, especially for downstream chemistry. Lack of clarity about these types of questions and of clear guidelines about how to apply OFRs to avoid such problems have limited the application of OFRs for years. In this paper, we apply the model in Peng et al. (2015) to systematically investigate whether significant non-tropospheric or non-OH chemistry occurs in OFRs and what experimental conditions make it more important. Considering the enormous complexity of organic radical (particularly organic peroxy) chemistry, we

only examine the non-OH fate of stable species in the present work. The fate of organic radicals should be the subject of future studies. The results allow improved OFR operation and experimental design, as well as guidance for the design of future reactors.

2 Methods

The OFR and the model used here have been described in detail elsewhere (Kang et al., 2007; Li et al., 2015; Peng et al., 2015). Here, we only present a brief introduction for each.

2.1 Potential Aerosol Mass (PAM) flow reactor

Kang et al. (2007) first introduced the PAM flow reactor. Although there were earlier versions of the PAM reactor, the version of cylindrical geometry with a volume of ~ 13 L has been widely used and is currently in use in many SOA research groups (Massoli et al., 2010; Cubison et al., 2011; Kang et al., 2011; Lambe et al., 2011a, b, 2012, 2013; Bahreini et al., 2012; Saukko et al., 2012; Wang et al., 2012; Li et al., 2013; Ortega et al., 2013). The reactor is made of aluminum or of glass and aluminum and equipped with 1–4 low-pressure Hg lamps (model no. 82-9304-03, BHK Inc.) located inside the flow tube. The Hg lamps produce UV emissions at 185 and 254 nm, the intensity of which can be rapidly computer-controlled. The operation mode using both 185 and 254 nm emissions is called "OFR185". In this mode, photons at 185 nm dissociate H_2O and O_2 molecules to produce OH + H and $O(^3P)$, respectively. Recombination of $O(^3P)$ with O_2 forms O_3. UV light at 254 nm then photolyzes O_3 to produce $O(^1D)$, which reacts with H_2O and produces additional OH. OFR can also be operated in another mode where photons at 185 nm are filtered by quartz sleeves around the lamps. In this case, only 254 nm UV light is active to generate OH ("OFR254" mode), and injection of externally generated O_3 into the reactor is required for OH production. The amount of injected O_3 plays a critical role in the OFR chemistry (Peng et al., 2015). For this reason this amount (X ppm) is also included in OFR operation mode notation in the form of OFR254-X. For example, OFR254-70 and OFR254-7 denote experiments with 70 and 7 ppm O_3 injected, respectively. We use the PAM as the basic OFR design. Other designs will be specified below if needed. Rapid computer-controlled UV lamp setting allows rapidly scanning UV lamp settings during an experiment and has unique applications to OFR experiments in field studies (Hu et al., 2015; Ortega et al., 2015; Palm et al., 2016). In these experiments, OFRs enable the exploration of a very large range of photochemical age during a short period (~ 2 h) when ambient conditions often do not significantly change.

2.2 Model description

We use the same model as in Peng et al. (2015), a standard chemical-kinetic model under plug-flow conditions. The effect of non-plug-flow residence time distributions (RTDs) was also investigated in that study. Non-plug-flow models result in similar OH_{exp} than plug flow in most cases, except under specific conditions with very high UV, H_2O, and OHR_{ext} (Peng et al., 2015). Therefore, plug-flow OH_{exp} is used in this study, as a proxy of OH_{exp} estimated from OHR_{ext} decay and to avoid the much increased computational expense for complex RTDs. All O_x and HO_x reactions available in the JPL Chemical Kinetic Data Evaluation (Sander et al., 2011) are taken into account. Reactions of some external OH reactants (externally introduced reactants destructing OH), such as SO_2, CO, and NO_x, are also included. SO_2 is used as a proxy of other external OH reactants (e.g., VOCs). We believe that this is a realistic approximation in terms of OHR_{ext} decay vs. OH_{exp} for many precursors, as discussed in Peng et al. (2015).

When studying the OFR, we assume a residence time of 180 s and use typical temperature (295 K) and atmospheric pressure (835 mbar) in Boulder, CO, USA. H_2O mixing ratio (abbr. H_2O hereafter) ranges from 0.07 to 2.3 % (equivalent to relative humidity, RH, of 2–71 %). According to Li et al. (2015), UV photon fluxes (abbr. UV hereafter) at 185 and 254 nm are estimated to be in the ranges 1.0×10^{11}–1.0×10^{14} and 4.2×10^{13}–8.5×10^{15} photons $cm^{-2}\,s^{-1}$, respectively. OHR_{ext} at 0 and between 1 and 1000 s^{-1}, covering the range of most field and laboratory studies, are investigated. In the explored parameter space, the same three-character labels as in Peng et al. (2015) are used to denote typical cases (Table 1). For OFR254, we study OFR254-7 to -70, representing OFR254 experiments with low (Kang et al., 2011; Liu et al., 2015) and high O_3 (Palm et al., 2016), respectively. To model literature OFR studies, we adopt corresponding parameters (reactor volume, H_2O, residence time, etc.), and estimate parameters that are specified or measured (e.g., UV) as needed. In particular, for some field studies, where long time-series of experimental data (42 days in BEACHON-RoMBAS (Palm et al., 2016), 42 days in SOAS (Hu et al., 2015), and 15 days in CalNex-LA (Ortega et al., 2015)) were recorded, we model all valid data points and present outputs in the form of histograms. Note that the outputs for field studies, i.e., histograms, have a complex dependence on ambient temperature, H_2O, and OHR_{ext}, as well as UV steps used. The specific histogram shapes for different field campaigns are influenced by both ambient and experimental parameters.

3 Results and discussions

In the following sections we explore the relative importance of five non-OH pathways (photons at 185 and 254 nm,

Table 1. Code of the labels of typical cases. A case label is composed of three characters denoting the water mixing ratio, the photon flux, and the external OH reactivity, respectively.

	Water mixing ratio	Photon flux	External OH reactivity
Options	L is low (0.07 %)	L is low (10^{11} photons cm^{-2} s^{-1} at 185 nm; 4.17×10^{13} photons cm^{-2} s^{-1} at 254 nm)	0
	M is medium (1 %)	M is medium (10^{13} photons cm^{-2} s^{-1} at 185 nm; 1.45×10^{15} photons cm^{-2} s^{-1} at 254 nm)	L is low ($10\,s^{-1}$) typically for remote or clean urban air
	H is high (2.3 %)	H is high (10^{14} photons cm^{-2} s^{-1} at 185 nm; 8.51×10^{15} photons cm^{-2} s^{-1} at 254 nm)	H is high ($100\,s^{-1}$) typically for polluted urban air
		"L" is lowest in PAM by Li et al. (2015) (7.9×10^{11} photons cm^{-2} s^{-1} at 185 nm; 2.04×10^{14} photons cm^{-2} s^{-1} at 254 nm)	V is very high ($1000\,s^{-1}$) only for laboratory experiments
Example	LH0:	low water mixing ratio, high photon flux, no external OH reactivity	

$O(^1D)$, $O(^3P)$, and O_3) vs. the OH reaction for species of atmospheric interest, including a variety of typical biogenic and anthropogenic VOCs and a few important inorganic species (e.g., SO_2 and NO_2). Because of the huge complexity of VOC oxidation mechanisms, only consumption/oxidation of specific VOCs is investigated. In such an investigation, a large amount of kinetic data is required. We collected the required data (Tables S1–S3 in the Supplement) according to the principles in Sect. S1. Photolysis of SOA is also investigated.

3.1 Fractional loss of VOCs to non-OH reactants

As shown in Peng et al. (2015), OH_{exp} in OFRs depends on various physical conditions, e.g., H_2O and OHR_{ext}. However, the non-OH reactants are much less dependent on these parameters. H_2O and external OH reactants only contribute less than 1 % to absorption at 185 and 254 nm. Therefore, they have almost no impact on effective UV. O_3 can absorb a fraction of the 254 nm radiation, but the optical depth due to 70 ppm O_3 in the reactor is ~ 0.11, and thus the attenuation of 254 nm photons by O_3 absorption is a minor effect. The dominant fates of $O(^1D)$ and $O(^3P)$ are the quenching by air and the recombination with O_2, respectively, with which no reactions involving H_2O or external OH reactants can compete. Thus the concentrations of $O(^1D)$ and $O(^3P)$ in the reactor depend on UV intensity and H_2O, but not on OHR_{ext}. Since OH can be strongly modulated by OHR_{ext}, changing input conditions may result in very different relative importance of OH to other reactive species. To fully evaluate this issue, it is necessary to explore a very wide range of conditions as in Peng et al. (2015).

3.1.1 Common features of all the non-OH reactants

Figures 1–5 show the relative consumption of several species vs. ratio of exposures to individual non-OH species (X) to OH exposure (X_{exp}/OH_{exp}) for 185 and 254 nm photons, $O(^1D)$, $O(^3P)$, and O_3, respectively. Figures S1–S5 present the same information in an alternative format that may be useful to evaluate the fate of species not included in our study. They show ratios of rate constants of species with OH to those with non-OH species (X), mathematically equivalent to the X_{exp}/OH_{exp} where corresponding $X/(OH+X)$ is 50 %. $X/(OH+X)$ denotes the fractional importance of X in the sum of the contribution of OH and X to VOC. If a VOC has a higher ratio of rate constant with OH to that with a non-OH reactant (X) than with another reactant (Y), the relative contribution of X, $X/(OH+X)$, should be smaller than that of Y. In these figures, we also show the X_{exp}/OH_{exp} fractional occurrence distribution for OFR254 and OFR185, under different conditions, including key laboratory and field studies, and identify the X_{exp}/OH_{exp} ranges where non-OH contribution to species fate is significant. Unless specifically stated, a dissociation quantum yield of unity is assumed for the photolysis reactions, which results in upper limits for the relative importance of those pathways.

In these figures, the relationships of all non-OH reactive species to OH are similar for certain common conditions. We define three types of conditions to help guide experimental design and evaluation in terms of the relative importance of non-OH reactants. Under "riskier conditions" of high/very high OHR_{ext} ($\geq 100\,s^{-1}$ in OFR185 and $> 200\,s^{-1}$ in OFR254-7 to -70) and/or low H_2O (<0.1 %), non-OH reactions can be significant depending on the species. Conversely, under "safer conditions" with relatively low OHR_{ext} ($< 30\,s^{-1}$ in OFR185 and $< 50\,s^{-1}$ in OFR254) *and* high H_2O (> 0.8 % in OFR185 and > 0.5 % in OFR254), and moderate or higher UV ($> 1 \times 10^{12}$ photons cm^{-2} s^{-1} at 185 nm) in OFR185, reaction with OH is dominant (Figs. 1–5 and S1–5). We denote all other conditions as "transition conditions". High H_2O and zero/low OHR_{ext} lead to strong OH production and no/weak OH suppression, respectively. Thus, OH

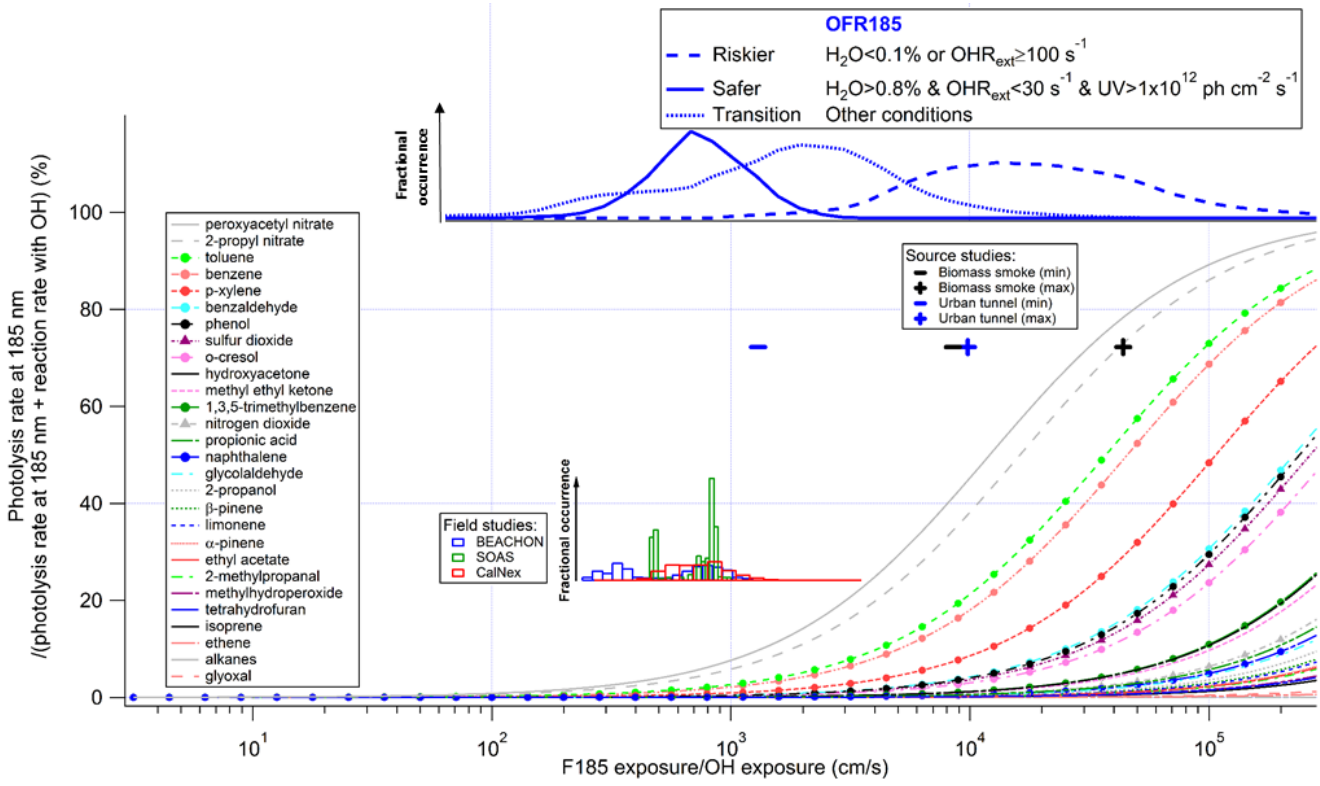

Figure 1. Fractional importance of the photolysis rate at 185 nm of several species of interest vs. the reaction rate with OH, as a function of the ratio of exposure to 185 nm photons (F185) and OH. F185 exposure (in photons cm^{-2}) is the product of 185 nm photon flux (in photons $cm^{-2}\ s^{-1}$) and time (in s). F185 exposure / OH exposure is thus in $cm\ s^{-1}$. The modeled frequency distributions of ratios of 185 nm photon exposure to OH exposure under riskier, safer, and transition conditions for OFR185 are also shown. The curves of aromatics and inorganic gases are highlighted by solid dots and upward triangles, respectively. The lower inset shows histograms of model-estimated F185 / OH exposures for three field studies where OFR185 was used to process ambient air. Their ordinate is the fractional occurrence of a given condition (X_{exp}/ OH_{exp}). All histograms are normalized to be of identical total area (i.e., total probability of 1). The upper inset (black and blue markers) shows similar information for source studies of biomass smoke (FLAME-3; Ortega et al., 2013) and an urban tunnel (Tkacik et al., 2014). All curves, markers, and histograms in this figure share the same abscissa.

is more abundant and dominates species consumption under those conditions. In the case of low H_2O and high OHR_{ext}, OH is generally lower because of less production and more suppression. These conditions increase the relative contribution of non-OH species. UV light intensity is generally less influential on non-OH VOC fate than H_2O and OHR_{ext}, although OH production is nearly proportional to UV (Peng et al., 2015), because the non-OH reactive species also scale (nearly) proportional to UV. As a result, UV generally has smaller effects on exposure ratios between OH and the non-OH reactants. However, under a UV near the lower bound of the explored range in this study ($< 1 \times 10^{12}$ photons $cm^{-2}\ s^{-1}$ at 185 nm) in OFR185, OH production is so small that the effect of OHR_{ext} on OH suppression can be amplified and hence some exposure ratios may be affected. In OFR254 OH is more resilient to suppression even at low UV because of the OH recycling by initially injected O_3 (Peng et al., 2015). Note that we call these conditions "riskier" and "safer" mainly in terms of non-tropospheric VOC fate but not of VOC fate by all non-OH reactants, as some of the non-OH reactant studied in this work may also play a role under some tropospheric conditions (see Sect. 3.1.4 and 3.1.5). In addition to the common features above, individual non-OH reactants have their own features as well as a few exceptions to the above mentioned general observations, which we will detail below.

3.1.2 Reactions with OH vs. photolysis at 185 nm

Under riskier reactor conditions, photolysis at 185 nm of several aromatic compounds, such as toluene, benzene, and p-xylene, are estimated to be significant and even dominant vs. the OH reactions (Fig. 1). This results from their aromatic ring, which is not only highly efficient as a chromophore but also relatively resistant to OH attack.

It is not common to perform field studies for SOA at H_2O as low as 0.1 % or $OHR_{ext} \geq 100\ s^{-1}$ (Table 1). According to $F185_{exp}$/ OH_{exp} calculated from the field studies where

OFR185 was deployed, i.e., BEACHON-RoMBAS (Palm et al., 2016), SOAS (Hu et al., 2015) and CalNex-LA (Ortega et al., 2015), all these studies are generally under safer conditions (infrequent low H_2O mixing ratio and ambient OH reactivity estimated to be $\sim$ 15–25 s^{-1}). For instance, none of these field studies fell into the conditions where the fractional importance of photolysis at 185 nm was significant for aromatic species. However, in some source studies using OFRs, e.g., when sampling biomass burning smoke (FLAME-3; Ortega et al., 2013) or air in a traffic tunnel (Tkacik et al., 2014), OHR_{ext} can be very high, reaching values of several 100 s^{-1} (Table S4). Especially on the smoke study, photolysis of aromatics may have played a role. However, it has long been known that excited aromatic molecules may undergo various deactivation pathways (e.g., vibronic coupling, intersystem crossing, and collisional quenching) without molecular fragmentation (Beddard et al., 1974; Nakashima, 1982; Nakashima and Yoshihara, 1983; Fang and Phillips, 2002), preventing unity quantum yields. Therefore, the photolysis of aromatics at 185 nm in the above mentioned source studies may not be as significant as estimated in Fig. 1.

Under riskier conditions, some organic peroxy nitrates and nitrates (e.g., peroxyacetyl nitrate and 2-propyl nitrate in Fig. 1) have an estimated contribution from photolysis at 185 nm to their fate that is comparable to or even larger than that of reaction with OH. Nevertheless, this does not mean that we need to make extra efforts to avoid the photolysis of organic nitrates and peroxy nitrates at 185 nm. Although they have cross sections at 185 nm $\sim$ 10–100 times smaller than those of aromatics, these organic compounds react remarkably slowly with OH ($\sim$ 2 orders of magnitude slower than reactions of aromatics with OH), so photolysis appears substantial with respect to reaction with OH, but really two slow rates are being compared. Thus, absolute photolyzed amounts of these species are not substantial. For example, only $\sim$ 10 % of peroxyacyl nitrate is photolyzed by 185 nm photons at the highest OFR185 lamp setting. Even if photolysis of nitrates and peroxy nitrates by low-pressure Hg lamp emission proceeds to a significant extent, it may still not be a problem, as it generally leads to the same products as their ambient photolysis (Renlund and Trott, 1984; Roberts and Fajer, 1989). Nitrate and peroxy nitrate photolysis is actually much more important in the atmosphere than in OFRs for the same photochemical age (see below and Fig. 6).

SO_2 has been used in some studies to calibrate OH_{exp} (Lambe et al., 2015; Li et al., 2015). It does undergo significant photolysis at 185 nm under riskier conditions. However, this photolysis does not lead to an overestimation of OH_{exp}, since the S-bearing product of SO_2 photolysis at 185 nm, SO, converts back to SO_2 very rapidly through its reaction with O_2.

Oxidation intermediates may also photolyze at 185 nm. However, their photolysis is unlikely to be significant when OFR is operated under safer conditions. To clarify this issue, a detailed discussion about the photolysis of oxidation intermediates at 254 nm is required as a premise. We thus discuss oxidation intermediate photolysis at both 185 and 254 nm in Sect. 3.1.3.

3.1.3 Reactions with OH vs. photolysis at 254 nm

The photon flux in the reactor at 254 nm is 80–250 times larger than at 185 nm (Li et al., 2015). Although absorption cross sections of all molecules investigated in this study are significantly lower at 254 than 185 nm, the higher photon flux compensates, at least partially, for this effect, so that in OFR185 photolysis of many species at 254 nm is of similar relative importance as photolysis at 185 nm, with potentially important effects at low H_2O and/or high OHR_{ext} (Figs. 2 and S2). As for 185 nm, 254 nm photolysis is a concern mainly for aromatic compounds, because of the high light absorptivity and low OH reactivity of aromatic rings as previously discussed. Again, note that this concern may be less serious than shown in Fig. 2 because of possible lower quantum yields. Photolysis of organic nitrates and peroxy nitrates at 254 nm also appears to be important relative to reactions with OH and is still not a concern for the same reasons as photolysis at 185 nm. SO_2 can absorb efficiently at 254 nm, but it is still not a problem for SO_2-based OH_{exp} calibration, since photons at 254 nm are not sufficiently energetic to dissociate SO_2 molecules.

High UV generally appears to be more problematic than low UV in OFR254 (Fig. S2). This is in contrast to the trend of OFR185. In OFR254, O_3 is the only primary OH source, and a substantial fraction of O_3 can be photolyzed at the highest lamp settings, leading to a substantial reduction of OH production (compared with proportional scaling with UV). OFR254-70 appears to be less prone to riskier conditions than OFR254-7, since higher O_3 favors HO_2-to-OH recycling, making OH more resilient to suppression (Peng et al., 2015).

Under highly risky conditions ($H_2O < 0.1$ % and $OHR_{ext} \geq 100\ s^{-1}$ for OFR185, and $H_2O < 0.1$ % and $OHR_{ext} > 200\ s^{-1}$ for OFR254), some saturated carbonyl compounds (e.g., pyruvic acid, methyl ethyl ketone, and hydroxyacetone) have significant photolysis at 254 nm relative to reactions with OH. This significant relative contribution of photolysis also results from remarkably slow reactions of saturated carbonyl compounds with OH. Although secondary species without C=C double bond, e.g., saturated carbonyls, hydroperoxides, and nitrates, can be photolyzed in OFRs at low H_2O and/or high OHR_{ext}, their photolysis only proceeds to a $\sim$ 10–1000 times smaller extent than ambient photolysis at the same photochemical age (Fig. 6).

Unsaturated carbonyls may have much higher absorption cross sections if their C=C bonds are conjugated with carbonyls. However, according to our following analysis, conjugated unsaturated carbonyl compounds do not often cause problems of non-tropospheric photolysis at 254 nm. Car-

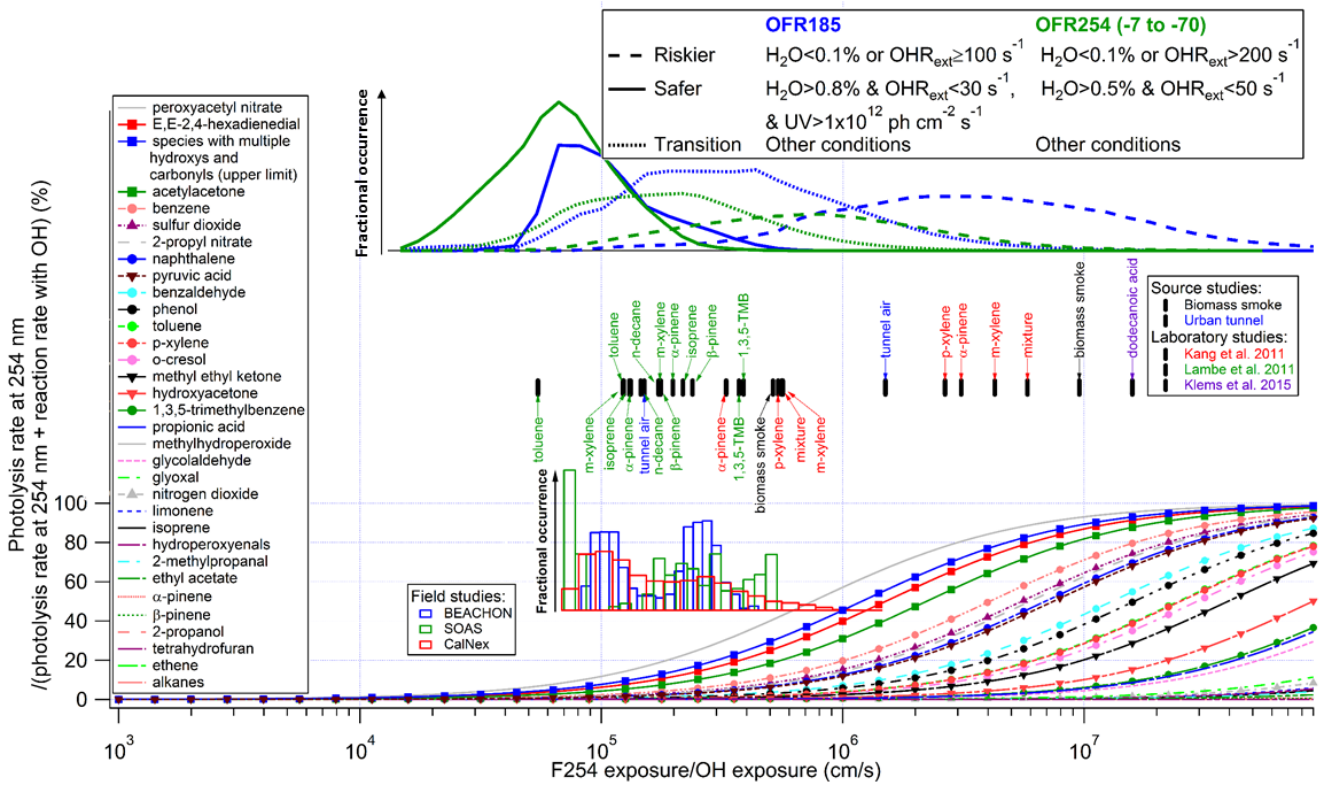

Figure 2. Same format as Fig. 1, but for the fractional importance of the photolysis rate at 254 nm vs. the reaction rate with OH as a function of the ratio of exposure to 254 nm (F254) and OH. The modeled frequency distributions of ratios of 254 nm photon exposure to OH exposure under riskier, safer, and transition conditions for OFR185 and OFR254 (-7 to -70) are also shown. The curves of saturated carbonyl compounds and possible highly absorbing oxidation intermediates are highlighted by downward triangles and squares, respectively. The insets show histograms of model-estimated F254/OH exposures for three field studies where OFR185 was used to process ambient air. In addition to source studies of biomass smoke (FLAME-3) and urban tunnel (Tkacik et al., 2014), F254 exposure / OH exposure ratios in two laboratory studies (Kang et al., 2011; Lambe et al., 2011b) are shown in the upper inset. Colored tags indicate species used in the laboratory experiments. The lower and upper limits of F254 exposure / OH exposure ratios in the experiments with a certain source in a certain study are denoted by tags below and above the markers, respectively.

bonyls have π–π^* and n–π^* transitions. The former corresponds to high cross section (typically $> 10^{-18}$ cm^2) and typically occurs around or below 200 nm. The latter is forbidden and thus has weak absorption (cross section on the order of 10^{-19} cm^2 or lower) and typically occurs around or above 300 nm (Turro et al., 2009). Conjugation usually does not substantially enhance the absorption of n–π^* transition, but it does for π–π^* transitions (Turro et al., 2009). As a result, through conjugation, the only reason why cross sections of carbonyls at 254 nm may be elevated above 10^{-18} cm^2 is the redshift of the maximum absorption wavelength of their π–π^* transitions due to conjugation. According to Woodward's rules (Pretsch et al., 2009) and available cross-section data of α,β-unsaturated carbonyls in Keller-Rudek et al. (2015), a conjugation of at least 3–4 double bonds is required for the excitation at 254 nm to dominantly correspond to π–π^* transition. Conjugated oxidation intermediates containing at least 3–4 double bonds including C=C bond(s) are virtually impossible to form from aliphatic hydrocarbon oxidation in OFRs. Nevertheless, such intermediates may form via ring-opening pathways of aromatic oxidation (Calvert et al., 2002; Atkinson and Arey, 2003; Strollo and Ziemann, 2013). *E*,*E*-2,4-hexadienedial may be regarded as an example of this type of intermediates. Even under assumption of a unity quantum yield, its fraction of photolysis at 254 nm is not much higher than that of aromatic precursors (Fig. 2). Therefore, 254 nm photolysis of conjugated intermediates should not be problematic as long as safer experimental conditions are adopted.

To our knowledge, the only exception that has strong absorption at 254 nm due to conjugation with <2 double bonds are β-diketones, which may be formed in aliphatic hydrocarbon oxidation, particularly that of long-chain alkanes (Ziemann and Atkinson, 2012). The peculiarity of β-diketones is that their enol form may have a highly conjugated ring structure due to very strong resonance (Scheme S1) and hence cross sections on the order of 10^{-17} cm^2 at 254 nm (Messaadia et al., 2015). However, even under the assumption of unity quantum yield, the fractional contribution of 254 nm

photolysis of acetylacetone (representative of β-diketones) is only slightly larger than for aromatic VOCs (Fig. 2), since its enol form also contains a C=C bond leading to very high reactivity toward OH. Furthermore, we argue that the actual probability that a concrete structural change (in number and type of functional groups, O / C ratio, average C oxidation state, etc.) of β-diketones resulting from photoexcitation at 254 nm may be low. As their excitation at 254 nm corresponds to π–π^* transition, their rigid ring structure likely hinders cyclic structural change at the first singlet excited state ($S_1(\pi,\pi^*)$) while the biradical structure of the first triplet state ($T_1(\pi,\pi^*)$) may favor H shift between two O atoms, which ends up with the same/similar structure than prior to the H shift (Scheme S1). Also, the excitation of β-diketones at 254 nm may also lead to charge transfer complex formation via direct excitation and/or radiationless transition from a local excited state (Phillips and Smith, 2015), which is likely to result in low quantum yields, as discussed in detail below.

In addition to conjugated species, Phillips and Smith (2014, 2015) reported a new type of highly absorbing species that may be formed from VOC oxidation. Although their studies were conducted in the condensed phase, it is likely that the main conclusions of these studies are generally transferable to the gas-phase conditions, since no long-range interactions, which do not exist in normal gases, were involved in these studies. Phillips and Smith (2014, 2015) investigated the photoabsorption enhancement of multifunctional oxygenated species in SOA and found that the high absorptivity of these species can largely be explained by transitions toward the electronic states of charge transfer complex formed between hydroxyl groups (donor) and spatially neighboring carbonyl groups (acceptor). They also pointed out that charge transfer complexes of this kind have a continuum of states whose energy levels range from that of local excited states (radiative transition wavelength < 300 nm) to very low levels (radiative transition wavelength > 600 nm). The latter are insufficient to cause common photochemical reactions. Relaxation through a continuum of states is usually ultrafast according to Fermi's golden rule (Turro et al., 2009), likely leading to low quantum yields of chemical reactions. The low quantum yields may be seen even from species with only one hydroxyl and one carbonyl: the photolysis of 3-hydroxy-3-methyl-2-butanone and 4-hydroxy-2-butanone at wavelengths down to 270 nm has quantum yields around only 0.1 (Bouzidi et al., 2014, 2015). Although measurements of photolysis quantum yield for multifunctional species are challenging and rare, it is reasonable to expect even lower quantum yields for larger and/or highly substituted (by hydroxyl and carbonyl) species, since larger species have more degrees of freedom for relaxation of excited molecules, and more and/or larger complex sites generally lead to more efficient relaxation through a continuum of states, in accordance with common photophysical sense (Sharpless and Blough, 2014). Therefore, even though species with a number of hydroxyls and carbonyls are formed in VOC oxidation and can absorb > 1 order of magnitude more efficiently at 254 nm than mono- and difunctional species, they may still have low effective photolysis rates because of low quantum yields.

For this type of species, we estimate an upper limit of the fractional importance of their photolysis at 254 nm. Molar absorption coefficients of charge transfer transitions of organic molecules are usually $\sim 10^3$–1×10^4 L mol^{-1} cm^{-1}, i.e., cross sections of $\sim 3.9 \times 10^{-18}$–3.9×10^{-17} cm^2 (Foster, 1969). Based on that, it is reasonable to estimate an upper limit of absorption cross sections of charge transfer transitions of 5×10^{-17} cm^2. However, photolysis quantum yields of multifunctional species are unlikely to be larger than that of species with only one carbonyl and one hydroxyl, i.e., ~ 0.1 (see discussion above). We thus take 0.1 as an upper limit of photolysis quantum yields. Besides, 6×10^{-12} cm^3 molecule^{-1} s^{-1} can be a conservative estimate of rate constants of multifunctional oxygenated species with OH, as it is roughly an average value for ketones (Atkinson and Arey, 2003), and the enhancement of H-abstraction by hydroxyl groups (Kwok and Atkinson, 1995; Ziemann and Atkinson, 2012) and the fast abstraction of aldehydic H atoms (Atkinson and Arey, 2003) are completely neglected. With the three estimates combined, the estimated maximum fractional contribution from photolysis at 254 nm to the fate of multifunctional species (Fig. 2) is close to that of *E*,*E*-2,4-hexadienedial and acetylacetone.

The problem of photolysis of oxidation intermediates at 185 nm is unlikely to be worse than at 254 nm. According to available UV spectra of carbonyl compounds in Keller-Rudek et al. (2015), 185 nm is almost always located within the π–π^* transition band, whose maximum cross section is on the order of 10^{-17} cm^2. Even if all types of radiative transitions at normal radiation intensity are considered, an approximate upper limit of absorption cross sections is $\sim 10^{-16}$ cm^2 (Evans et al., 2013). However, UV intensity at 185 nm in the OFR185 mode is ~ 100 times lower than that at 254 nm (Li et al., 2015). The photolysis rate of oxidation intermediates at 185 nm should thus be generally smaller than at 254 nm.

Therefore, in summary, photolysis of oxidation intermediates are, to our knowledge, conservatively estimated to be of limited importance relative to their reactions with OH, as long as the experimental conditions are in the safer range. Although studies on photolysis quantum yields of oxidation intermediates are very sparse, we reason, based on the existing studies on this topic and common photophysical and photochemical rules, that the photolysis quantum yields of these species may be lower than the values assumed in this study (e.g., 1 for *E*,*E*-2,4-hexadienedial and acetylacetone and 0.1 for multifunctional species). As a result, actual rates and relative importance of photolysis might be significantly smaller than the upper limits estimated in our study.

As discussed for photolysis at 185 nm, in all ambient OFR field studies (BEACHON-RoMBAS, SOAS, and CalNex-LA), reactions with OH dominate over photolysis at 254 nm (Fig. 2). The fractional consumption of several anthropogenic aromatic VOCs, such as benzene and naphthalene, in the urban CalNex-LA campaign by 254 nm photolysis is estimated as a few percent under most conditions and at most ∼ 15 %. At the BEACHON-RoMBAS and SOAS forested sites, photolysis at 254 nm should be a negligible contributor to the fate of biogenic VOCs such as isoprene and monoterpenes.

Some laboratory and source studies may have had an appreciable contribution to aromatic species fate from 254 nm at low H_2O and/or high OHR_{ext}. $F254_{exp}/OH_{exp}$ in the biomass smoke and urban tunnel source studies (source OHR_{ext} up to $\sim 300\,s^{-1}$; Ortega et al., 2013; Tkacik et al., 2014) and the Kang et al. (2011) laboratory study (H_2O down to ∼ 0.1 %) can be as high as 10^6–$10^7\,cm\,s^{-1}$. In this range, photolysis of a few aromatic VOCs (e.g., benzene and naphthalene) at 254 nm could account for ∼ 20–80 % of their destruction.

Note that photolysis of oxidation intermediates also needs to be taken into account. If multifunctional species, β-diketones, and extensively conjugated species are photolyzed as shown in Fig. 2, these photolyses would be significant in some previous source and laboratory studies examined here, as they were conducted at relatively low H_2O and/or high OHR_{ext}. To our knowledge, none of these studies reported a significant photolysis of oxidation intermediates. Klems et al. (2015) attributed large amounts of fragmentation products detected in their OFR experiments with dodecanoic acid to photolysis of peroxy radicals. However, these products may also be at least partially accounted for by photolysis of carbonyls leading to carbon-chain cleavage via Norrish reactions (Laue and Plagens, 2005). The OFR used by Klems et al. (2015) has a different design from the PAM, which is regarded as the base design in this study. Their reactor employs a light source stronger than the PAM's highest lamp setting, with UV at 254 nm estimated to be $\sim 3\times10^{16}$ photons $cm^{-2}\,s^{-1}$ (∼ 4 times the value at the highest lamp setting of the PAM OFR) based on the lamp power and the reactor geometry. Such high UV may even result in significant photolysis of saturated carbonyl intermediates, which are very likely formed in the oxidation of long-chain alkane-like dodecanoic acid.

3.1.4 Reactions with OH vs. reactions with $O(^1D)$ and $O(^3P)$

The results for these two radicals are shown in Figs. 3–4. The potential impact of $O(^1D)$ is smaller than for 185 and 254 nm photons, due to the low concentration of $O(^1D)$ in the reactor. Only for methane may reaction with $O(^1D)$ be significant, because the reaction of methane with $O(^1D)$ is close to the collision rate, while CH_4 is the most resistant VOC to H-abstraction by OH. This could be important if CH_4 was used for OH_{exp} calibration under riskier reactor conditions, or if the fate of CH_4 is important to the experiment for other reasons. Other VOCs react much faster with OH. As a result, reactions of VOCs (other than CH_4) with $O(^1D)$ in all laboratory, field, and source studies previously discussed are almost always negligible. We also note that the ratio of $O(^1D)_{exp}/OH_{exp}$ in the OFR is actually much lower than in the troposphere (Monks, 2005), except under some riskier conditions. It is believed that the contribution of $O(^1D)$ to VOC destruction in the atmosphere should be negligible (Calvert et al., 2002), and their relative importance is even lower under most OFR conditions.

Reactions with $O(^3P)$ are small or negligible contributors to VOC consumption except under extreme riskier conditions. Unless at low H_2O (< 0.1 %) and very high external OH reactivity ($\sim 1000\,s^{-1}$), VOC consumption by $O(^3P)$ cannot be larger than 10 % of that by OH (Figs. 4 and S4). This results from both very low concentrations of $O(^3P)$ and relatively low reactivity compared to that of OH. Among the species that we examine, biogenic VOC consumption may have some contribution from $O(^3P)$ under the abovementioned riskier conditions, due to the higher reactivity of double bonds in these species with $O(^3P)$. For example, α-pinene in the mixture experiments in Kang et al. (2011) may have had a ∼ 5 % contribution from $O(^3P)$. Similarly to $O(^1D)$, $O(^3P)_{exp}/OH_{exp}$ in the troposphere (Calvert et al., 2002) is higher than in the OFR except for riskier conditions. Thus the relative importance of both $O(^1D)$ and $O(^3P)$ to OFR chemistry is typically lower than in the troposphere.

3.1.5 Reactions with OH vs. reactions with O_3

Reaction with O_3 is a major, even dominant pathway of the consumption of many biogenic VOCs in the troposphere. However, it is of interest to quantify the relative importance of OH vs. O_3 across OFR experiments (Figs. 5 and S5). This allows comparison with the relative importance in the troposphere, as well as potentially designing experiments where the relative influence of O_3 is minimized or adjusted as desired.

A large amount of O_3 is injected into OFR254, and O_3 concentration in that type of reactor does not change much with UV flux (negligibly under most conditions and up to a factor of ∼ 2 at high H_2O and UV; Peng et al., 2015). Since OH_{exp} is proportional to UV flux, as UV decreases, OH_{exp} is lowered and the fractional species destruction by O_3 increases. In OFR185, O_3 production is almost linearly dependent on UV, while a significant portion of OH production has a quadratic relationship with UV. Thus OH increases faster with increasing UV than O_3. Therefore, lower UV in OFR185 also leads to a higher relative importance of O_3 for VOC consumption.

The distribution of O_{3exp}/OH_{exp} expected for the troposphere was obtained from the GISS ModelE2 climate

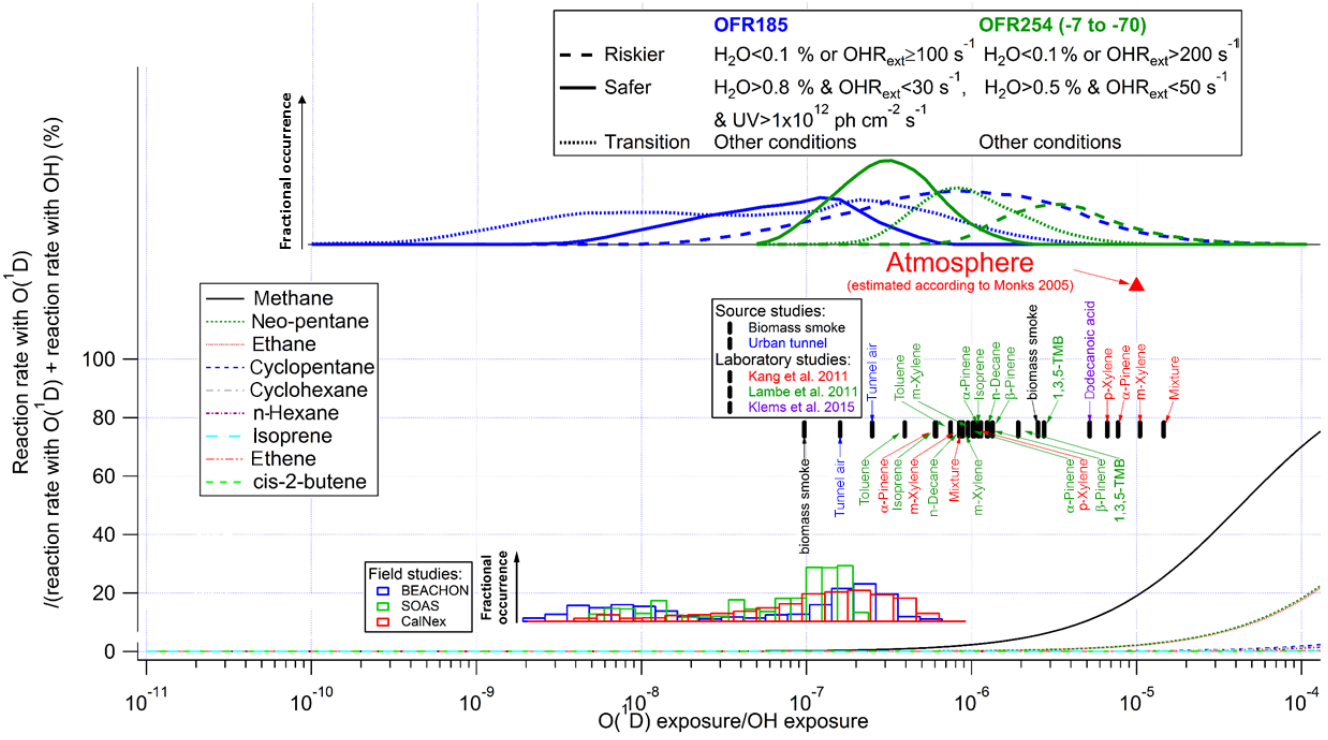

Figure 3. Same format as Fig. 2 but for the ratio of the reaction rate with $O(^1D)$ vs. OH as a function of the relative exposure to $O(^1D)$ and OH. A typical value of the relative exposure of $O(^1D)$ and OH in the troposphere estimated according to Monks (2005) is also shown.

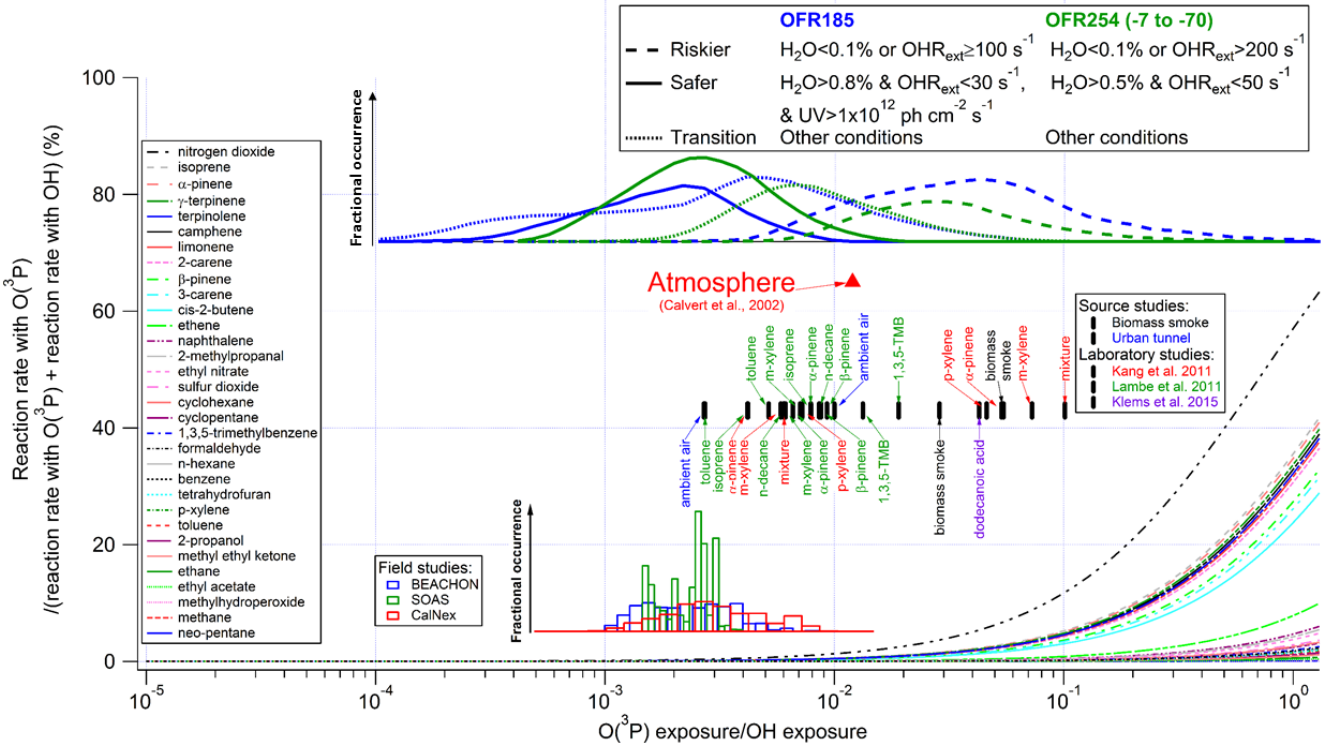

Figure 4. Same format as Fig. 3 but for the ratio of the reaction rate with $O(^3P)$ vs. OH as a function of the relative exposure of $O(^3P)$ and OH. A typical value of the relative exposure of $O(^3P)$ and OH in the troposphere from Calvert et al. (2002) is also shown.

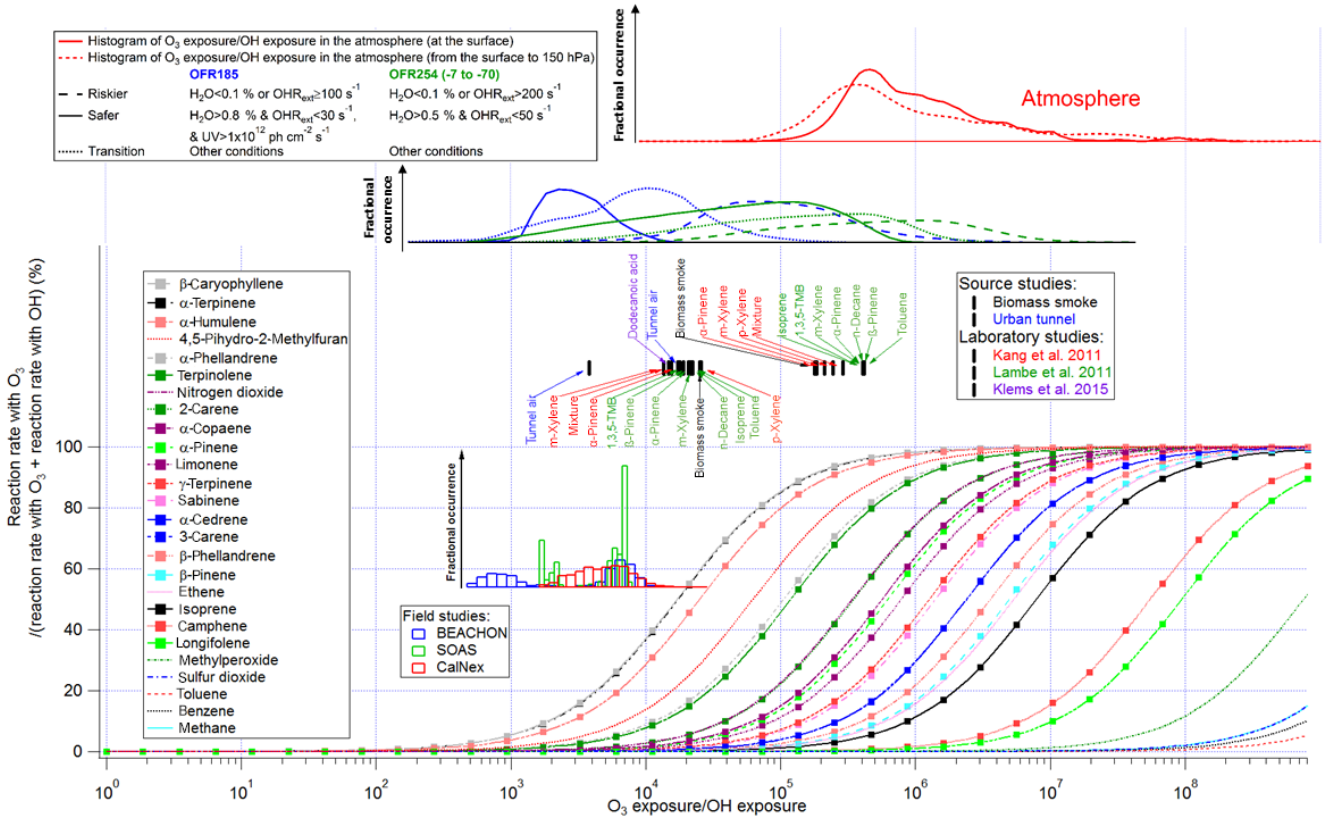

Figure 5. Same format as Fig. 2 but for the fractional importance of the reaction rate with O_3 vs. OH as a function of the relative exposure of O_3 and OH. The curves of biogenics are highlighted by squares. Also shown are modeled distributions of the relative exposure of O_3 and OH at the Earth's surface (solid line) and throughout the column from the surface to a height with a pressure of 150 hPa (dashed line). The distributions were calculated from the mean daily concentrations of O_3 and OH as simulated by the GISS ModelE2.

model (Schmidt et al., 2014) and is estimated as the ratio of the simulated daily mean concentration of O_3 and OH on a horizontal grid of 2° in latitude and 2.5° in longitude for the year 2000. Interestingly, the simulated relative importance of O_3 to OH in the troposphere is higher than when OFRs are operated under safer conditions, and similar to OFRs when they are operated under riskier conditions (Figs. 5 and S5). In those cases, a number of biogenic VOCs can be significantly consumed by O_3. In particular, some monoterpenes (e.g., α-terpinene) and sesquiterpenes (e.g., β-caryophyllene) have a fractional reaction with O_3 close to 100 % in the troposphere. In contrast to biogenics, reactions with O_3 do not play any role in the consumption of most anthropogenic VOCs, e.g., benzene, toluene, and alkanes. Besides, ozonolysis of saturated oxidation intermediates (e.g., carbonyls and alcohols) is minor or negligible in both OFRs and the atmosphere, since they react with OH at $\sim 10^{-13}$–10^{-11} cm^3 molecule^{-1} s^{-1} while their ozonolysis rate constants are $< 10^{-20}$ cm^3 molecule^{-1} s^{-1} (Atkinson and Arey, 2003). However, unsaturated oxidation intermediates may have larger contributions from O_3 because of C=C bonds. In particular, dihydrofurans, possible intermediates of saturated hydrocarbon oxidation (Ziemann and Atkinson, 2012; Aimanant and Ziemann, 2013), may be predominantly oxidized by O_3 in the troposphere. In OFR254, they can still have significant contributions from O_3 even outside riskier conditions.

An experimentalist may be interested in obtaining an O_{3exp}/OH_{exp} in an OFR close to ambient values, which requires lower H_2O and higher OHR_{ext} conditions, although care should be taken to avoid other non-tropospheric reactions under those conditions. However, one may want to study OH-dominated chemistry and thus want to avoid significant ozonolysis of VOCs to reduce the complexity of VOC fate. This is analogous to the addition of excess NO to suppress O_3 in some chamber experiments. In this case the OFRs should be operated under opposite conditions, i.e., high H_2O, high UV, and low OHR_{ext}. This strategy enhancing OH_{exp} is effective for most VOCs, except those with the highest k_{O_3}/k_{OH} ratios, e.g., α-terpinene and β-caryophyllene. To further decrease the importance of reactions of VOC with O_3, it is necessary to lower the O_3 concentration. For OFR254, one can inject less O_3 into the reactor and increase the UV lamp setting. The comparison between

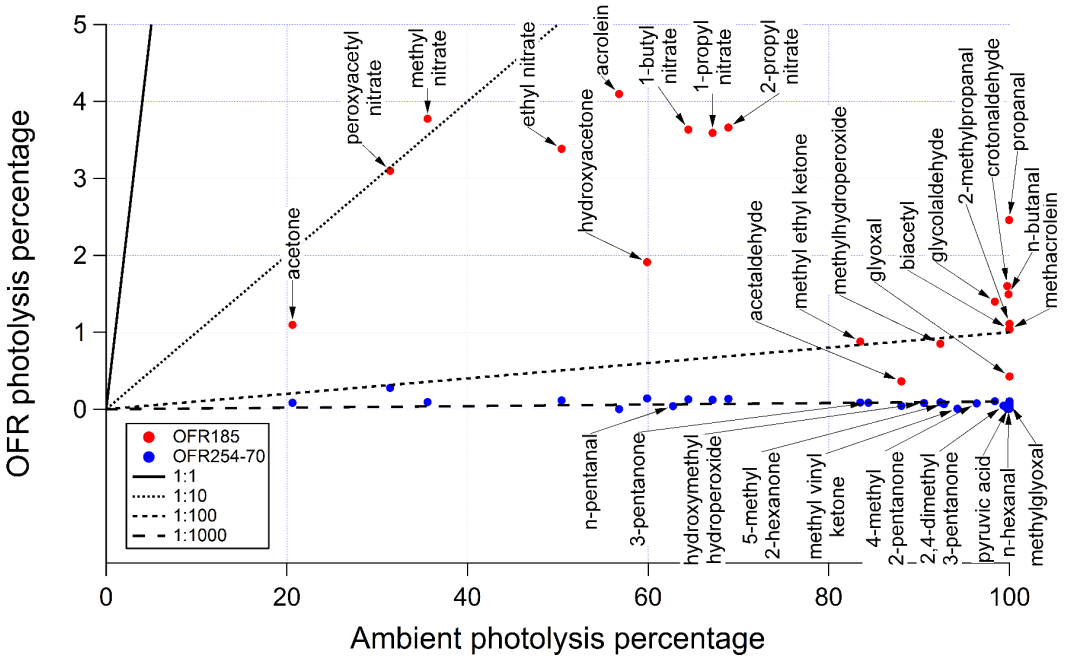

Figure 6. Ambient photolysis fractions of secondary species in a week (calculated from photolysis rates reported in Hodzic et al., 2015) vs. photolysis fractions of those species in OFR185 and OFR254-70 when reaching the same photochemical age (ambient OH concentration of 1.5×10^6 molecules cm^{-3} assumed) under conditions of 44 % relative humidity (water vapor mixing ratio of 1.4 %) and 25 s^{-1} initial OHR_{ext}. If the points of a certain species for both OFR185 and OFR254-70 are available, the species name is tagged on the OFR185 point (downward arrow); otherwise it is tagged on the OFR254-70 point (upward arrow). The 1 : 1, 1 : 10, 1 : 100, and 1 : 1000 lines are also shown for comparison.

OFR254-70 and OFR254-7 in Fig. S5 demonstrates this approach. For OFR185, we propose another strategy, i.e., lowering O_2 concentration in the reactor. This decreases O_3 production but affects OH production to a much lesser extent, thanks to the major OH production by H_2O photolysis. We simulate the OFR185 cases with 2 ‰ O_2 and observe that VOC ozonolysis can be excluded at high H_2O and high UV (Fig. S5).

Among the literature OFR studies, the field studies employing OFRs in urban and forested areas all operated under O_{3exp}/OH_{exp} values 100 times lower than in the atmosphere. In these field studies reaction of almost all VOCs with O_3 can be neglected, except for the most reactive biogenics with O_3, e.g., α-terpinene and β-caryophyllene. The source study in an urban tunnel of Tkacik et al. (2014) operated under similar conditions. Some laboratory studies using OFR254 (Kang et al., 2011; Lambe et al., 2011b) as well as the biomass smoke source study (Ortega et al., 2013) operated at O_{3exp}/OH_{exp} close to tropospheric values, because the injected O_3 plays a key role for OFR254 studies and the biomass smoke experiments were conducted at high OHR_{ext}. Nevertheless, only α-pinene and β-pinene, both biogenics, are significantly consumed by O_3 in these studies. Another OFR254 study, Klems et al. (2015), had O_{3exp}/OH_{exp} significant lower than tropospheric values, since the initial O_3 in their experiment was only 2 ppm, and the UV light in their experiment was stronger than our lamps' highest setting and further reduced effective O_3.

3.1.6 Reactions with $^1O_2$ and HO_2

Singlet oxygen, $^1O_2$, can be produced in various ways in OFRs (Calvert et al., 2002; Ono et al., 2014) and react with alkenes at appreciable rate constants ($\sim 10^{-17}$–10^{-14} cm^3 molecule^{-1} s^{-1}; Huie and Herron, 1973; Eisenberg et al., 1986). We estimate $^1O_2$ concentration by the expression proposed by Ono et al. (2014). Only at the lowest H_2O, the highest lamp setting, and the highest OHR_{ext} in this study (Table 1), may the most reactive alkene (endocyclic conjugated dienes, e.g., cyclopentadiene, α-terpinene, and α-phellandrene) have > 10 % contribution from $^1O_2$ to their fate. For all other species and under all other conditions, reactions of VOCs with $^1O_2$ are negligible. Thus, this reactant is not discussed further in the present work.

HO_2 is a major radical in the OFR chemistry. However, it is much less reactive than OH toward VOCs. Typically, the rate constants of reactions of HO_2 with alkenes are smaller than 10^{-20} cm^3 molecule^{-1} s^{-1} at room temperature, and those with almost all saturated VOCs (except aldehydes and ketones) are even smaller (Tsang, 1991; Baulch et al., 1992, 2005). Therefore, we briefly discuss reactions of HO_2 with aldehydes and ketones and neglect those with all other VOCs

in this study. Ketones react with HO_2 at rate constants on the order of 10^{-16} cm^3 molecule^{-1} s^{-1} or lower (Gierczak and Ravishankara, 2000; Cours et al., 2007). Therefore, only at low H_2O, low UV, and high OHR_{ext}, the reaction of acetone with HO_2 may compete with that with OH. The same is likely true for the reactions of acetaldehyde and larger aldehydes with HO_2, as their rate constants are likely to be around or less than 1×10^{-14} cm^3 molecule^{-1} s^{-1} (da Silva and Bozzelli, 2009). Formaldehyde is the only stable carbonyl compound that may react with HO_2 (rate constant: 7.9×10^{-14} cm^3 molecule^{-1} s^{-1}; Ammann et al., 2015) at a rate competing with that with OH under conditions that are not low H_2O, low UV, and high OHR_{ext}. Note that the reaction of formaldehyde with HO_2 is also significant in the atmosphere (Pitts and Finlayson, 1975; Gäb et al., 1985). However, its product, hydroxymethylperoxy radical, dominantly undergoes decomposition via thermal reaction and photolysis (Kumar and Francisco, 2015), compared to the hydroxymethyl hydroperoxide formation pathway via a further reaction with HO_2 (Ziemann and Atkinson, 2012). Even if hydroxymethyl hydroperoxide is produced in appreciable amounts, in the high-OH environment of OFRs, this species can be easily predicted to convert into formic acid (Francisco and Eisfeld, 2009) and eventually CO_2. All these products have very few interactions with other VOCs and hence should not significantly perturb the reaction system of OFRs.

3.1.7 Overall contribution of non-OH reactants to gas-phase chemistry

In this section we summarize the combined effect of all non-OH reactants to VOC consumption. However, we can no longer use X_{exp}/OH_{exp} to express total non-OH VOC consumption as for individual reactants. Total non-OH VOC consumption is thus discussed case by case.

In the explored range of conditions (i.e., H_2O, UV, OHR_{ext}, and initial O_3 for OFR254), there are obviously conditions where all non-OH fates of VOCs are negligible. Most simply, the highest H_2O and UV in this study and a very small non-zero OHR_{ext} result in a VOC consumption nearly 100 % by OH, regardless of the VOC type (Table S6). Lowering UV can make non-OH contribution even smaller for OFR185, but not for OFR254. This difference occurs because OH production is reduced while O_3 roughly remains at the same level in OFR254, leading to enhanced relative contribution from O_3 to the fate of biogenics. At the lowest non-zero UV in the PAM reactor (7.9×10^{11} photons cm^{-2} s^{-1} at 185 nm; 2.0×10^{14} photons cm^{-2} s^{-1} at 254 nm) of Li et al. (2015), the fractional destructions of α-pinene (representative of biogenic VOCs) by O_3 are 21 and 4.2 % in OFR254-70 and OFR254-7, respectively. Other OFR designs may reach lower UV, e.g., the "low UV" case defined in this study (1.0×10^{11} photons cm^{-2} s^{-1} at 185 nm; 4.2×10^{13} photons cm^{-2} s^{-1} at 254 nm). At these UV levels, the fate of α-pinene by O_3 further increases to 44 and 13 % in OFR254-70 and OFR254-7, respectively.

However, non-OH reactants can dominate VOC fate under opposite conditions that lead to low OH production and strong OH suppression. At the lowest H_2O and UV and the highest OHR_{ext} in this study, > 95 % of α-pinene and ∼ 80 % of toluene are consumed by non-OH reactants in OFR185. In OFR254, almost all α-pinene has non-OH fate while non-OH fate of toluene is still minor or negligible. If OFRs are operated at the low UV setting from the PAM by Li et al. (2015), ∼ 8 times higher the lowest UV in this study, the situation hardly changes, as a very large OH suppression persists. Nevertheless, if UV is increased to the highest level, non-OH fate of α-pinene is lowered to ∼ 60–70 % and that of toluene in OFR185 decreases to 24 %. When H_2O is at the highest level, non-OH fate is systematically lower than at low H_2O in all types of OFRs. In particular, the HHV case has non-OH fates of α-pinene only up to ∼ 10 % and negligible non-OH fates of toluene, despite very high OHR_{ext}.

We also summarize VOC fate for key laboratory, source, and field studies examined in the present work in Fig. 7. For each case, the fate of one or a few typical VOCs is investigated. In laboratory studies, Kang et al. (2011) performed experiments with a mixture of α-pinene, m-xylene, and p-xylene, and one of experiments by Lambe et al. (2011b) used biogenics (α-pinene and isoprene, respectively) as precursors. In both cases, O_3 plays a role in the fate of biogenics when H_2O is low (Kang et al., 2011), or OHR_{ext} is high and UV is low (Lambe et al., 2011b), as shown in Fig. 7. The fate of isoprene by O_3 is less significant despite the very high OHR_{ext}, because isoprene, compared to α-pinene, is more reactive with OH and less reactive with O_3. Besides, $O(^3P)$ contributes up to a few percent to the fate of biogenics. In the literature experiments performed at a higher H_2O (Kang et al., 2011) or a higher UV (Lambe et al., 2011b), non-OH fate of both VOCs significantly decreases because of increases in OH_{exp}. About 20 % of p-xylene in the Kang et al. (2011) mixture experiment at very low H_2O may be destroyed by 254 nm photons, under the assumption of unity quantum yield. Other laboratory study cases with aromatics have lower non-OH fates because of higher H_2O. N-decane in one of Lambe et al.'s experiments and dodecanoic acid in the Klems et al. (2015) study are consumed ∼ 100 % by OH, as these alkane(-like) species neither react rapidly with O_3, nor absorb UV efficiently. However, as previously discussed, some carbonyl compounds may be formed and significantly photolyzed at 254 nm in the Klems et al. (2015) experiments, although the huge complexity of intermediates and limited knowledge of reaction mechanisms prevents a quantitative assessment of the fate of carbonyl intermediates by photons at 254 nm.

Source and field studies usually have highly complex precursors. For the urban tunnel study (Tkacik et al., 2014) and the CalNex-LA study in the Los Angeles basin (Ortega et al., 2015), we choose toluene as a representative of

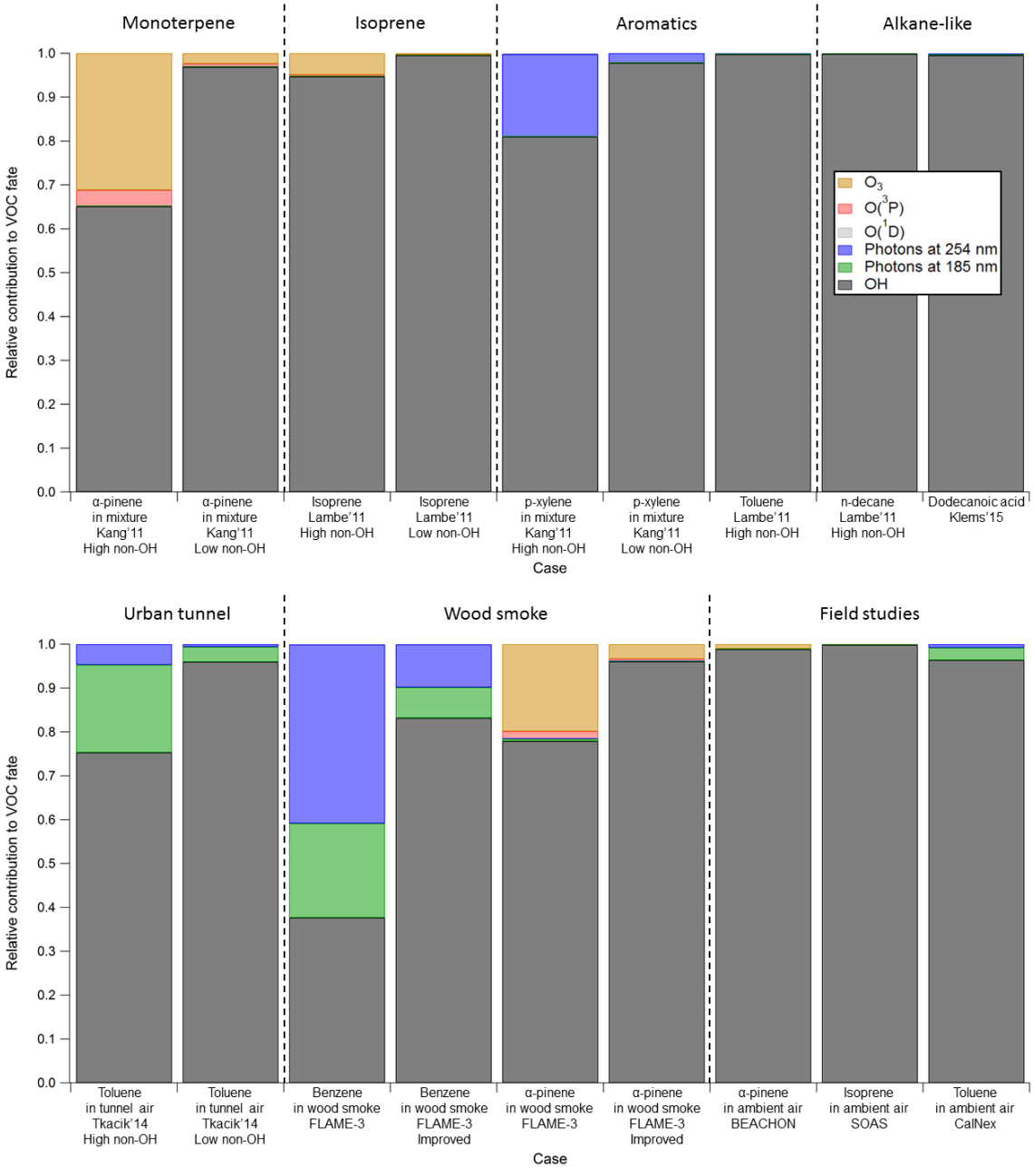

Figure 7. VOC fate in several representative cases of the laboratory, source, and field studies examined in this work. More details on VOC fate in these studies can be found in Table S4.

aromatic species, as these are major anthropogenic VOCs and SOA precursors in urban environment (Dzepina et al., 2009; Borbon et al., 2013; Hayes et al., 2015; Jathar et al., 2015). Although alkanes are also major anthropogenic VOCs, their non-OH fate is not quantitatively assessed for the same reason as discussed for dodecanoic acid in the Klems et al. (2015) experiment. For the smoke aging study, FLAME-3 (Ortega et al., 2013), we select benzene and α-pinene, which are important VOCs in biomass burning emissions (Warneke et al., 2011). For the BEACHON-RoMBAS and SOAS studies at forested sites, α-pinene and isoprene are chosen, respectively, as they are major emitted biogenic VOCs at those corresponding sites. Both the urban tunnel and FLAME-3 studies have aromatic precursors significantly photolyzed at 185 and 254 nm (assuming quantum yield = 1) under the conditions of high source concentrations (Fig. 7). The toluene fate by UV in the tunnel study is less substantial than that of benzene in FLAME-3, since NO_x, the largest fraction of external OH reactant in the tunnel study, is converted into HNO_3 very rapidly (Li et al., 2015) and does not

further suppress OH. In the cases of lower OHR_{ext} (e.g., the tunnel experiments with low source concentration and CalNex), toluene is dominantly consumed by OH. It also holds for biogenic VOCs that non-OH fate decreases with decreasing OHR_{ext} due to less OH suppression. The non-OH fate of α-pinene in FLAME-3, dominated by reaction with O_3, is larger than 20 %, while the non-OH fates of α-pinene in BEACHON-RoMBAS and of isoprene in SOAS are both negligible, since OHR_{ext} in the former study is > 10 times higher than in the latter two studies.

3.2 SOA photolysis

Recently, photolysis in the UV range has been found to be a potentially significant sink of some types SOA in the troposphere (Updyke et al., 2012; Lambe et al., 2013; Liu et al., 2013, 2015; Hodzic et al., 2015; Wong et al., 2015; Romonosky et al., 2016). It is necessary to also investigate SOA photolysis in OFRs, as photons used in OFRs are highly energetic and non-tropospheric. UV extinction due to aerosol optical scattering and in-particle absorption under OFR conditions is generally negligible (Hodzic et al., 2015). For simplicity, we estimate photodegradation ratios of various SOA component surrogates as well as several SOA samples whose absorptivity was measured in previous studies (Updyke et al., 2012; Lambe et al., 2013; Liu et al., 2013; Romonosky et al., 2016) (Fig. 8) under the assumption of unity quantum yield to obtain upper limits of photodegradation ratios, as well as under the assumption of lower (0.1 and 0.01) quantum yields.

Most SOA functional groups are oxygenated (e.g., peroxides, carbonyls, carboxylic acids, alcohols). The absorption cross sections of most of these functional groups are too low at 185 and 254 nm given the OFR residence time and UV light intensity, leading to a small contribution of photolysis to SOA degradation (Fig. 8). For example, glycolaldehyde has a negligible fractional contribution of photolysis except at the highest lamp setting, when only $\sim$ 5 % of this species photolyzes at each wavelength. Species (e.g., isoprene) with conjugated double bonds as efficient chromophores will not be present in SOA because of their high reactivity with OH and O_3. Nitrate groups may have a $\sim$ 30 % contribution from photolysis at the highest UV settings and a negligible contribution at intermediate or low UV settings.

Aromatic rings are more resistant to OH attack and usually strongly absorb UV light. Under our assumptions, the photolysis of some aromatic SOA components (e.g., o-cresol at 185 nm and naphthalene at 254 nm) is already important at medium UV flux. At the highest lamp setting, most aromatics in SOA would be destroyed if the quantum yields are indeed near unity. However, as previously discussed, photolysis quantum yields of aromatics may be significantly lower than 1. This is more probable in the condensed phase (Damschen et al., 1978; Baker et al., 2015) than in the gas phase, as quenching processes in the condensed-phase matrix are usually much more efficient than through gas-phase molecular collisions. It has recently been reported that photolysis quantum yields of aromatics in SOA were low under UVB irradiation (Romonosky et al., 2015). Although the range and relevance of the species investigated in that study are limited, it is reasonable to assume low quantum yield for aromatic photolysis in SOA at 185 and 254 nm.

Wong et al. (2015) conducted α-pinene-derived SOA photolysis experiments in a chamber under UVB irradiation (down to 284 nm). They observed at 85 % RH $\sim$ 30 % SOA photolyzed after > 30 min irradiation and a photolysis quantum yield of $\sim$ 1 during the first 10 min. However, in OFRs such a high SOA photodegradation percentage would not occur, since the Wong et al. (2015) experiments had a high photon flux ($\sim 4 \times 10^{15}$ photons cm^{-2} s^{-1}) and a long irradiation time, and hence a photon flux exposure that is $\sim$ 5 times that at the highest lamp setting in the OFRs modeled in our work. According to the measurements of Wong et al. (2015), a photolysis fraction of $\sim$ 6 % would be expected for this type of SOA in our OFRs under the highest UV flux, with lower percentages at lower UV settings. In addition, the approximate unity quantum yield observed in Wong et al. (2015) may be due to (hydro)peroxides in α-pinene-derived SOA, since peroxides have high photolysis quantum yields (Goldstein et al., 2007; Epstein et al., 2012), while other functional groups (i.e., mainly hydroxyl and carbonyl) in oxygenated species in SOA are unlikely to have for reasons discussed below.

Note that a simple addition of absorptivities of different functional groups may not explain SOA absorptivity (Phillips and Smith, 2015). According to the absorption data of SOA samples from Lambe et al. (2013) and Romonosky et al. (2016), real SOA absorbs $\sim$ 1–3 orders of magnitude more than non-aromatic component surrogate species shown in Fig. 8 at 254 nm. As discussed for multifunctional oxidation intermediates (with carbonyls and hydroxyls), SOA absorption enhancement may be largely due to transitions of charge transfer complexes formed between carbonyls and hydroxyls in multifunctional oxygenated SOA components (Phillips and Smith, 2014, 2015). These complexes between carbonyls and hydroxyls also have continua of states likely leading to ultrafast relaxation and hence low photolysis quantum yields. Charge transfer transitions have been extensively shown in measurements (Alif et al., 1991; Gao and Zepp, 1998; Johannessen and Miller, 2001; O'Sullivan et al., 2005; Zhang et al., 2006; Osburn et al., 2009; Sharpless and Blough, 2014) to have very low quantum yields in the condensed phase. Sharpless and Blough (2014) compiled quantum yields of various products of humic-like matter photolysis down to 280 nm. No quantum yields except those of the product $^1O_2$, which is generally unimportant for OFRs (see Sect. 3.1.6), are higher than 0.01. If the photolysis quantum yields of the SOA samples in Fig. 8 at 254 nm are no more than 0.01, no SOA samples will be photolyzed by 20 % even at the highest OFR lamp setting, and photolysis of most SOA samples at 254 nm will be minor or negligible in OFRs. Thus, to our current knowledge, lack of solid information on quantum yields

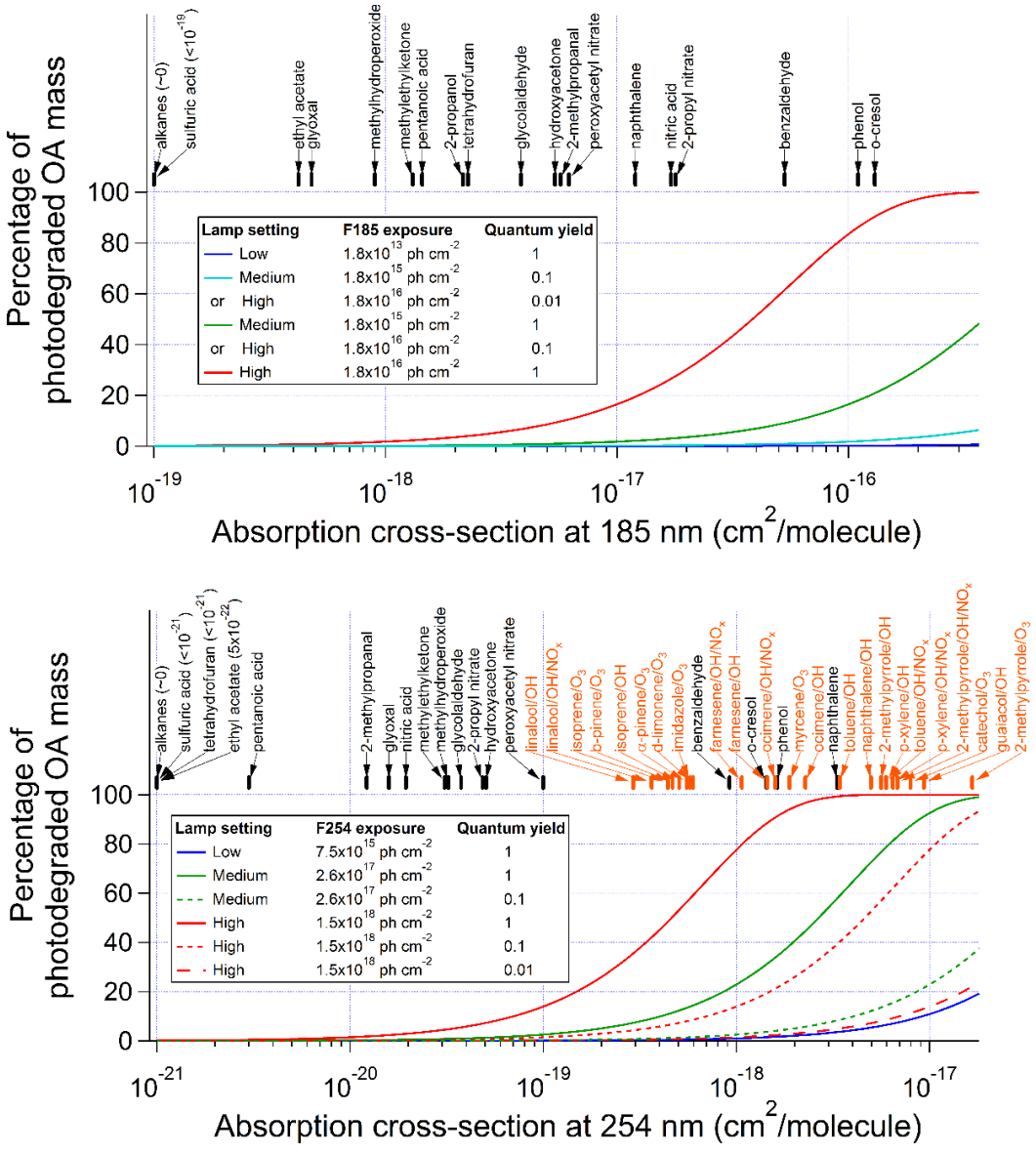

Figure 8. Percentage of SOA photodegradation at (upper panel) 185 and (lower panel) 254 nm at different UV levels as a function of absorption cross section under the assumptions of quantum yields of 1, 0.1, and 0.01. Absorption cross sections of some SOA component surrogates (black tag) and SOA samples (orange tag; calculated from data in Lambe et al., 2013, and Romonosky et al., 2016) are also shown.

of SOA components with multiple carbonyls and hydroxyls at 254 nm prevents a clear assessment of SOA photolysis in OFRs at the medium and high UV. Nonetheless, direct measurements are desirable for this issue and caution should still be exercised for OFR experiments at relatively high UV.

SOA photolysis at 185 nm may be lower compared to that at 254 nm. SOA absorptivity data at 185 nm are not available. According to SOA mass-specific absorption cross-section (MAC) data between 250 and 300 nm in Romonosky et al. (2016), there is a linear relationship between the logarithm of MAC and wavelength for most SOA samples: MAC increases by a factor of ~ 3 per 50 nm decrease in wavelength. We thus extrapolate this relationship to 185 nm, where MAC is estimated to be ~ 3.5 times higher than that at 254 nm. However, the UV flux at 185 nm in our OFR is ~ 100 times lower than at 254 nm.

Based on the discussion above, the SOA photodegradation ratio of ~ 30 % in the non-OFR setup of Wong et al. (2015) may be explained. α-Pinene-derived SOA has ~ 20–50 % weight fraction of peroxides (Docherty et al., 2005; Epstein et al., 2014), which may undergo photolysis in SOA to convert into carbonyls (and hydroxyls) (Epstein et al., 2014). We speculate that after the formation of carbonyls from peroxides, SOA materials cannot proceed significantly further

with photolysis as discussed for charge transfer between carbonyl and hydroxyl above. In the experiments of Wong et al. (2015), as well as Epstein et al. (2014), effective photolysis rate constants/quantum yields decreased as SOA photolysis proceeded. Photolysis rates were substantially reduced after a ∼ 30 % mass loss due to photolysis in the Wong et al. (2015) experiments. This mass loss ratio is consistent with the mass percentage of peroxides in α-pinene-derived SOA. Again, we note that, according to the extrapolation from the results from Wong et al. (2015), the mass loss percentage expected in our OFR under the highest UV flux is ∼ 6 % for α-pinene-derived SOA. This value is much lower than that shown in Fig. 8 under the assumption of unity quantum yield (∼ 40 %) because of a substantially decreasing quantum yield in the real photolysis experiments. Therefore, in OFRs, even if (hydro)peroxides in SOA may be photolyzed in appreciable amounts, SOA mass is unlikely to be largely destroyed by photons in OFRs, as (hydro)peroxides may convert into carbonyls and hydroxyls, which may substantially lower subsequent photolysis quantum yields.

According to the discussion above, measurements of quantum yields and/or products of SOA photolysis are highly desirable, especially for the photolysis of SOA containing dominantly carbonyl and hydroxyl groups, as (hydro)peroxides, which are likely to form in OFRs, may convert into hydroxyls and carbonyls. With more data on quantum yields of SOA photolysis, a clearer strategy for including or excluding SOA photolysis in OFRs can be made.

Even though SOA photolysis can be significant in OFRs, it only proceeds to a much lesser extent compared to ambient SOA photolysis. We calculate the numbers of e-fold decay of SOA photolysis in OFR254-70 and the troposphere according to the effective ambient photolysis lifetime of SOA from Romonosky et al. (2016). Under the condition of 44 % RH ($H_2O = 1.4$ %) and $OHR_{ext} = 25\,s^{-1}$ (typical of ambient conditions), SOA samples are estimated to undergo ∼ 0.01–0.5 e-fold photolysis timescales (i.e., ∼ 1–35 % OA photolyzed) in OFR254-70 at an equivalent photochemical age of 1 week under the upper limit assumption of unity quantum yields (Table S8). However, in the atmosphere, those samples may proceed with 10^2–10^4 e-fold decays of photolysis (i.e., virtually complete destruction) at the same photochemical age, if ambient SOA photolysis quantum yields are assumed to be those of H_2O_2 (unity below 400 nm). Even if the quantum yield of acetone (non-zero below 320 nm; see Romonosky et al., 2016) is taken as a surrogate for SOA, most types of SOA would still be completely or nearly completely photolyzed under ambient conditions. These results demonstrate that ambient SOA photolysis is likely to be much more important than in OFRs. However, they also highlight the need for studies of ambient SOA photolysis quantum yields and photolytic aging, as ambient SOA is unlikely to be completely destroyed by photons within only 1 week. Either their quantum yields are much lower than used in this study or the photolabile groups are destroyed and leave behind others that are not (or less) photolabile during photolytic aging.

3.3 Guidelines for OFR experimental design and operation

It is necessary to avoid significant non-tropospheric chemistry in OFRs in order to more accurately simulate tropospheric aging. Only photolysis at 185 and 254 nm are important non-tropospheric pathways in OFRs and reactions with O atoms are generally unimportant. Ozonolysis is also a major VOC sink in the troposphere, and the desirability of including or excluding its effects depends on the goals of each experiment.

In the cases where the exclusion of VOC ozonolysis is desired, there is no dilemma for the experimental design, as the exclusion of both VOC ozonolysis and non-tropospheric VOC consumption requires similar conditions, i.e., safer conditions. As shown above, all examined field studies do not have significant non-tropospheric contribution to VOC fate, while some past laboratory and source studies do because of low H_2O and/or very high OHR_{ext} in those experiments. It is possible to improve the latter experiments by increasing H_2O and/or lowering OHR_{ext}. In detail, source humidification and dilution can be feasible measures to increase H_2O and decrease OHR_{ext}, respectively. For example, increasing RH from 3 to 60 % (H_2O from ∼ 0.08 to ∼ 1.6 %) lowers the percentage of non-tropospheric consumption of p-xylene in the Kang et al. (2011) mixture experiment from ∼ 20 to 1.5 %. Humidifying the average condition of the BEACHON-RoMBAS (Palm et al., 2016) campaign from $H_2O = 1.6$ % (RH = 63 %) to $H_2O = 2.3$ % (RH = 92 %) leads to a ∼ 50 % decrease in non-tropospheric photolysis of α-pinene (Table S4). Also, a 5-fold source dilution in FLAME-3 reduces the non-tropospheric fate of benzene from > 60 to ∼ 15 % (Table S4 and "Improved" cases in Fig. 7). Injecting less precursor is a simple way to keep a reasonably low OHR_{ext} in laboratory studies. The comparison between the cases with high and low concentrations in the urban tunnel study (Tkacik et al., 2014) is a good example (Table S4 and Fig. 7). Note that when taking the measures above to limit non-tropospheric VOC fate, one generally reduces the contribution from all non-OH reactants. Increasing H_2O and source dilution also significantly lower the relative importance of ozonolysis in the fate of α-pinene in the Kang et al. (2011) mixture experiments and the FLAME-3 study (Table S4 and Fig. 7). Although increasing UV may increase OH production, OH reactant destruction, and hence the relative contribution of OH to VOC fate in some cases, one has to be cautious when taking this measure to reduce effective OHR_{ext}, as high UV may cause non-tropospheric photolysis of SOA.

In laboratory experiments, running OFRs under safer conditions ensures a minor contribution of non-tropospheric photolysis, based on the current knowledge of oxidation in-

termediate photolysis (Fig. 2). This also reduces the relative contribution of ozonolysis to VOC fate. However, when more information becomes available about photolysis quantum yields of oxidation intermediates (vs. the upper limits assumed here), there may be additional flexibility to include ozonolysis while excluding non-tropospheric VOC consumption. As the precursor composition is usually relatively simple in laboratory experiments, it is sufficient to ensure the insignificance of non-tropospheric consumption of only the precursor(s) and possible intermediates (usually oxygenated species), rather than for a large variety of VOC precursors and intermediates. For example, in the case of quantum yields significantly lower than used in the present work, we may perform OFR254-70 experiments with a large amount of biogenics at medium H_2O and UV. In this case, a tropospheric O_{3exp}/OH_{exp} ratio can be obtained without major side effects, because the fractional contribution of photolysis of possible intermediates is still minor due to low quantum yields. However, OFR experiments with some anthropogenic VOCs, such as alkanes, can just be conducted at high H_2O and low OHR_{ext} to avoid the contribution of all non-OH reactants, since ozonolysis of alkanes is negligible even at a tropospheric O_{3exp}/OH_{exp}.

OFR experiments can be simply conducted under safer conditions to avoid non-tropospheric VOC fate, while riskier conditions can lead to significant non-tropospheric VOC fate, depending on the species under study. The conditions in between, i.e., "transition" conditions, are explicitly discussed above. However, one may want to be able to more quantitatively estimate the relative importance of non-OH reactants under different conditions so that a more detailed experimental planning becomes possible that simultaneously ensures insignificant non-tropospheric VOC fate and specific experimental goals. For this purpose, we provide a series of estimation equations for non-OH reactant exposures (Sect. S3, Table S9, and Fig. S6, as well as Excel file). With these equations, the relative contribution of non-OH reactants under all conditions explored in this study can be easily estimated. In OFR studies where a different OFR design is adopted and/or chemistry beyond the approximations in our model is involved, a new model may need to be established, which can be done in similar manner as Peng et al. (2015), to obtain the relative importance of non-OH VOC fate and then perform experimental design.

4 Conclusions

We used a kinetic model to investigate non-OH contribution (from 185 and 254 nm photons, $O(^1D)$, $O(^3P)$, and O_3) to VOC destruction, as well as to SOA photolysis at 185 and 254 nm in OFRs. We assessed the relative significance of the VOC consumption by non-OH reactants to that by OH in OFRs and the troposphere. The only non-tropospheric reaction that can play a major role under OFR conditions is photolysis, especially at 254 nm. The relative importance of photolysis is largest under riskier OFR conditions where OH is low due to low H_2O and/or high OHR_{ext}. Due to lack of quantum yield data, we estimated upper limits of the relative importance of photolysis for the few most susceptible oxidation intermediates, which are comparable to those from aromatic precursors. Reactions of O atoms are not competitive and are actually of lower relative importance (vs. OH) in OFRs than in the troposphere. VOC ozonolysis is much less important than in the troposphere under typical OFR conditions and of similar importance under riskier OFR conditions. Photolysis of SOA in OFRs could be significant at medium and high UV, but only if corresponding quantum yields are high. If SOA photolysis quantum yields are of the order of 0.01 or lower, as measured for many humic-like substances (Sharpless and Blough, 2014), SOA photolysis in OFRs may be minor or negligible under most conditions. Although the reaction fates may be different, numbers of e-fold decays of photolysis for a given OH_{exp} are at least an order of magnitude lower in the OFRs compared to the troposphere.

We examined some past field, laboratory, and source studies using OFRs. In the field studies of aged urban and forest ambient air, non-OH VOC fate was not important because of relatively high H_2O and moderate OHR_{ext}. However, some laboratory and source studies were conducted at low H_2O and/or high OHR_{ext} and have significant non-tropospheric VOC consumption. Humidification and/or dilution are recommended in these cases to reduce the importance of non-tropospheric reactants. We proposed different approaches to avoid non-OH VOC consumption, as well as strategies to employ insignificant non-tropospheric photolysis and significant tropospheric ozonolysis simultaneously in laboratory experiments. Our work has implications for the interpretation of past OFR studies and should be useful for designing and conducting future OFR experiments for atmospheric research, as well as in related applied fields.

The need for systematic measurements of photolysis quantum yields, for both VOC and SOA, and both at actinic wavelengths and at 185 and 254 nm, was highlighted in this study. When quantum yield data become available, photolysis of oxidation precursors, oxidation intermediates, and SOA in OFRs can be much better quantified, its relative importance compared to OH oxidation, ambient photolysis, etc. can be better evaluated, and experimental planning might then be able to be less conservative and have more freedom to avoid non-tropospheric photolysis and realize specific experimental objective(s).

The Supplement related to this article is available online at doi:10.5194/acp-16-4283-2016-supplement.

Acknowledgements. We thank Veronica Vaida, Paul Ziemann, Andrew Lambe, and the PAM user community for useful discussions, Andrew Lambe and Daniel Tkacik for providing some OFR experimental data and the reviewers for their useful comments for improving the manuscript. This research was partially supported by CARB 11-305, DOE (BER/ASR) DE-SC0011105, NSF AGS-1243354 & AGS-1360834, and NASA NNX15AT96G. Amber M. Ortega acknowledges fellowships from DOE and CU Graduate School. Rui Li and Brett B. Palm acknowledge CIRES Fellowships. Brett B. Palm is grateful for a Fellowship from US EPA STAR (FP-91761701-0). Resources supporting this work were provided by the NASA High-End Computing (HEC) Program through the NASA Center for Climate Simulation (NCCS) at Goddard Space Flight Center.

Edited by: J. H. Seinfeld

References

Aimanant, S. and Ziemann, P. J.: Chemical Mechanisms of Aging of Aerosol Formed from the Reaction of n-Pentadecane with OH Radicals in the Presence of NO_x, Aerosol Sci. Technol., 47, 979–990, doi:10.1080/02786826.2013.804621, 2013.

Alif, A., Pilichowski, J., and Boule, P.: photochemistry and environment XIII phototransformation of 2-nitrophenol in aqueous solution, J. Photoch. Photobio. A, 59, 209–219, doi:10.1016/1010-6030(91)87009-K, 1991.

Ammann, M., Cox, R. A., Crowley, J. N., Jenkin, M. E., Mellouki, A., Rossi, M. J., Troe, J., Wallington, T. J., Cox, B., Atkinson, R., Baulch, D. L., and Kerr, J. A.: IUPAC Task Group on Atmospheric Chemical Kinetic Data Evaluation, available at: http://iupac.pole-ether.fr/#, last access: November 2015.

Atkinson, R. and Arey, J.: Atmospheric degradation of volatile organic compounds, Chem. Rev., 103, 4605–4638, doi:10.1021/cr0206420, 2003.

Bahreini, R., Middlebrook, A. M., Brock, C. A., de Gouw, J. A., McKeen, S. A., Williams, L. R., Daumit, K. E., Lambe, A. T., Massoli, P., Canagaratna, M. R., Ahmadov, R., Carrasquillo, A. J., Cross, E. S., Ervens, B., Holloway, J. S., Hunter, J. F., Onasch, T. B., Pollack, I. B., Roberts, J. M., Ryerson, T. B., Warneke, C., Davidovits, P., Worsnop, D. R., and Kroll, J. H.: Mass spectral analysis of organic aerosol formed downwind of the Deepwater Horizon oil spill: field studies and laboratory confirmations, Environ. Sci. Technol., 46, 8025–8034, doi:10.1021/es301691k, 2012.

Baker, L. A., Horbury, M. D., Greenough, S. E., Coulter, P. M., Karsili, T. N. V., Roberts, G. M., Orr-Ewing, A. J., Ashfold, M. N. R., and Stavros, V. G.: Probing the Ultrafast Energy Dissipation Mechanism of the Sunscreen Oxybenzone after UVA Irradiation, J. Phys. Chem. Lett., 6, 1363–1368, doi:10.1021/acs.jpclett.5b00417, 2015.

Baulch, D. L., Cobos, C. J., Cox, R. A., Esser, C., Frank, P., Just, T., Kerr, J. A., Pilling, M. J., Troe, J., Walker, R. W., and Warnatz, J.: Evaluated Kinetic Data for Combustion Modelling, J. Phys. Chem. Ref. Data, 21, 411, doi:10.1063/1.555908, 1992.

Baulch, D. L., Bowman, C. T., Cobos, C. J., Cox, R. A., Just, T., Kerr, J. A., Pilling, M. J., Stocker, D., Troe, J., Tsang, W., Walker, R. W., and Warnatz, J.: Evaluated kinetic data for combustion modeling, Supplement II, J. Phys. Chem. Ref. Data, 34, 757–1397, doi:10.1063/1.1748524, 2005.

Beddard, G. S., Fleming, G. R., Gijzeman, O. L. J., and Porter, G.: Vibrational Energy Dependence of Radiationless Conversion in Aromatic Vapours, P. Roy. Soc. A-Math. Phy., 340, 519–533, doi:10.1098/rspa.1974.0168, 1974.

Borbon, A., Gilman, J. B., Kuster, W. C., Grand, N., Chevaillier, S., Colomb, A., Dolgorouky, C., Gros, V., Lopez, M., Sarda-Esteve, R., Holloway, J., Stutz, J., Petetin, H., McKeen, S., Beekmann, M., Warneke, C., Parrish, D. D., and De Gouw, J. A.: Emission ratios of anthropogenic volatile organic compounds in northern mid-latitude megacities: Observations versus emission inventories in Los Angeles and Paris, J. Geophys. Res.-Atmos., 118, 2041–2057, doi:10.1002/jgrd.50059, 2013.

Bouzidi, H., Laversin, H., Tomas, A., Coddeville, P., Fittschen, C., El Dib, G., Roth, E., and Chakir, A.: Reactivity of 3-hydroxy-3-methyl-2-butanone: Photolysis and OH reaction kinetics, Atmos. Environ., 98, 540–548, doi:10.1016/j.atmosenv.2014.09.033, 2014.

Bouzidi, H., Aslan, L., El Dib, G., Coddeville, P., Fittschen, C., and Tomas, A.: Investigation of the Gas-Phase Photolysis and Temperature-Dependent OH Reaction Kinetics of 4-Hydroxy-2-butanone, Environ. Sci. Technol., 49, 12178–12186, doi:10.1021/acs.est.5b02721, 2015.

Calvert, J. G., Atkinson, R., Becker, K. H., Kamens, R. M., Seinfeld, J. H., Wallington, T. H., and Yarwood, G.: The Mechanisms of Atmospheric Oxidation of the Aromatic Hydrocarbons, Oxford University Press, USA, available at: https://books.google.com/books?id=P0basaLrxDMC (last access: November 2015), 2002.

Carlton, A. G., Wiedinmyer, C., and Kroll, J. H.: A review of Secondary Organic Aerosol (SOA) formation from isoprene, Atmos. Chem. Phys., 9, 4987–5005, doi:10.5194/acp-9-4987-2009, 2009.

Carter, W. P. L., Cocker, D. R., Fitz, D. R., Malkina, I. L., Bumiller, K., Sauer, C. G., Pisano, J. T., Bufalino, C., and Song, C.: A new environmental chamber for evaluation of gas-phase chemical mechanisms and secondary aerosol formation, Atmos. Environ., 39, 7768–7788, doi:10.1016/j.atmosenv.2005.08.040, 2005.

Cocker, D. R., Flagan, R. C., and Seinfeld, J. H.: State-of-the-Art Chamber Facility for Studying Atmospheric Aerosol Chemistry, Environ. Sci. Technol., 35, 2594–2601, doi:10.1021/es0019169, 2001.

Cours, T., Canneaux, S., and Bohr, F.: Features of the potential energy surface for the reaction of HO_2 radical with acetone, Int. J. Quantum Chem., 107, 1344–1354, doi:10.1002/qua.21269, 2007.

Cubison, M. J., Ortega, A. M., Hayes, P. L., Farmer, D. K., Day, D., Lechner, M. J., Brune, W. H., Apel, E., Diskin, G. S., Fisher, J. A., Fuelberg, H. E., Hecobian, A., Knapp, D. J., Mikoviny, T., Riemer, D., Sachse, G. W., Sessions, W., Weber, R. J., Weinheimer, A. J., Wisthaler, A., and Jimenez, J. L.: Effects of aging on organic aerosol from open biomass burning smoke in aircraft and laboratory studies, Atmos. Chem. Phys., 11, 12049–12064, doi:10.5194/acp-11-12049-2011, 2011.

Damschen, D. E., Merritt, C. D., Perry, D. L., Scott, G. W., and Talley, L. D.: Intersystem Crossing Kinetics, J. Phys. Chem., 82, 2268–2272, doi:10.1021/j100510a002, 1978.

da Silva, G. and Bozzelli, J. W.: Role of the α-hydroxyethylperoxy radical in the reactions of acetaldehyde and vinyl al-

cohol with HO_2, Chem. Phys. Lett., 483, 25–29, doi:10.1016/j.cplett.2009.10.045, 2009.

Docherty, K. S., Wu, W., Lim, Y. B., and Ziemann, P. J.: Contributions of Organic Peroxides to Secondary Aerosol Formed from Reactions of Monoterpenes with O_3, Environ. Sci. Technol., 39, 4049–4059, doi:10.1021/es050228s, 2005.

Dzepina, K., Volkamer, R. M., Madronich, S., Tulet, P., Ulbrich, I. M., Zhang, Q., Cappa, C. D., Ziemann, P. J., and Jimenez, J. L.: Evaluation of recently-proposed secondary organic aerosol models for a case study in Mexico City, Atmos. Chem. Phys., 9, 5681–5709, doi:10.5194/acp-9-5681-2009, 2009.

Eisenberg, W. C., Taylor, K., and Murray, R. W.: Gas-Phase Kinetics of the Reaction of Singlet Oxygen with Olefins at Atmospheric Pressure, J. Phys. Chem., 90, 1945–1948, doi:10.1021/j100400a041, 1986.

Epstein, S. A., Shemesh, D., Tran, V. T., Nizkorodov, S. A., and Gerber, R. B.: Absorption Spectra and Photolysis of Methyl Peroxide in Liquid and Frozen Water, J. Phys. Chem. A, 116, 6068–6077, doi:10.1021/jp211304v, 2012.

Epstein, S. A., Blair, S. L., and Nizkorodov, S. A.: Direct Photolysis of α-Pinene Ozonolysis Secondary Organic Aerosol: Effect on Particle Mass and Peroxide Content, Environ. Sci. Technol., 48, 11251–11258, doi:10.1021/es502350u, 2014.

Evans, R. C., Douglas, P., and Burrow, H. D. (Eds.): Applied Photochemistry, Springer Netherlands, Dordrecht, the Netherlands, 2013.

Fang, W. H. and Phillips, D. L.: The crucial role of the S1/T2/T1 intersection in the relaxation dynamics of aromatic carbonyl compounds upon $n > \pi^*$ excitation, Chem. Phys. Chem., 3, 889–892, doi:10.1002/1439-7641(20021018)3:10<889::AID-CPHC889>3.0.CO;2-U, 2002.

Foster, R.: Organic Charge-Transfer Complexes, Academic Press, New York, USA, 1969.

Francisco, J. S. and Eisfeld, W.: Atmospheric Oxidation Mechanism of Hydroxymethyl Hydroperoxide, J. Phys. Chem. A, 113, 7593–7600, doi:10.1021/jp901735z, 2009.

Gäb, S., Hellpointner, E., Turner, W. V., and Korte, F.: Hydroxymethyl hydroperoxide and bis(hydroxymethyl) peroxide from gas-phase ozonolysis of naturally occurring alkenes, Nature, 316, 535–536, doi:10.1038/316535a0, 1985.

Gao, H. and Zepp, R. G.: Factors Influencing Photoreactions of Dissolved Organic Matter in a Coastal River of the Southeastern United States, Environ. Sci. Technol., 32, 2940–2946, doi:10.1021/es9803660, 1998.

George, I. J., Vlasenko, A., Slowik, J. G., Broekhuizen, K., and Abbatt, J. P. D.: Heterogeneous oxidation of saturated organic aerosols by hydroxyl radicals: uptake kinetics, condensed-phase products, and particle size change, Atmos. Chem. Phys., 7, 4187–4201, doi:10.5194/acp-7-4187-2007, 2007.

Gierczak, T. and Ravishankara, A. R.: Does the HO_2 radical react with ketones?, Int. J. Chem. Kinet., 32, 573–580, doi:10.1002/1097-4601(2000)32:9<573::AID-KIN7>3.0.CO;2-V, 2000.

Goldstein, S., Aschengrau, D., Diamant, Y., and Rabani, J.: Photolysis of Aqueous H_2O_2?: Quantum Yield and Applications for Polychromatic UV Actinometry in Photoreactors, Environ. Sci. Technol., 41, 7486–7490, doi:10.1021/es071379t, 2007.

Hallquist, M., Wenger, J. C., Baltensperger, U., Rudich, Y., Simpson, D., Claeys, M., Dommen, J., Donahue, N. M., George, C., Goldstein, A. H., Hamilton, J. F., Herrmann, H., Hoffmann, T., Iinuma, Y., Jang, M., Jenkin, M. E., Jimenez, J. L., Kiendler-Scharr, A., Maenhaut, W., McFiggans, G., Mentel, Th. F., Monod, A., Prévôt, A. S. H., Seinfeld, J. H., Surratt, J. D., Szmigielski, R., and Wildt, J.: The formation, properties and impact of secondary organic aerosol: current and emerging issues, Atmos. Chem. Phys., 9, 5155–5236, doi:10.5194/acp-9-5155-2009, 2009.

Hayes, P. L., Carlton, A. G., Baker, K. R., Ahmadov, R., Washenfelder, R. A., Alvarez, S., Rappenglück, B., Gilman, J. B., Kuster, W. C., de Gouw, J. A., Zotter, P., Prévôt, A. S. H., Szidat, S., Kleindienst, T. E., Offenberg, J. H., Ma, P. K., and Jimenez, J. L.: Modeling the formation and aging of secondary organic aerosols in Los Angeles during CalNex 2010, Atmos. Chem. Phys., 15, 5773–5801, doi:10.5194/acp-15-5773-2015, 2015.

Hodzic, A., Madronich, S., Kasibhatla, P. S., Tyndall, G., Aumont, B., Jimenez, J. L., Lee-Taylor, J., and Orlando, J.: Organic photolysis reactions in tropospheric aerosols: effect on secondary organic aerosol formation and lifetime, Atmos. Chem. Phys., 15, 9253–9269, doi:10.5194/acp-15-9253-2015, 2015.

Hoffmann, T., Odum, J. R., Bowman, F., Collins, D., Klockow, D., Flagan, R. C., and Seinfeld., J. H.: Formation of Organic Aerosols from the Oxidation of Biogenic Hydrocarbons, J. Atmos. Chem., 26, 189–222, doi:10.1023/A:1005734301837, 1997.

Hu, W. W., Campuzano-Jost, P., Palm, B. B., Day, D. A., Ortega, A. M., Hayes, P. L., Krechmer, J. E., Chen, Q., Kuwata, M., Liu, Y. J., de Sá, S. S., McKinney, K., Martin, S. T., Hu, M., Budisulistiorini, S. H., Riva, M., Surratt, J. D., St. Clair, J. M., Isaacman-Van Wertz, G., Yee, L. D., Goldstein, A. H., Carbone, S., Brito, J., Artaxo, P., de Gouw, J. A., Koss, A., Wisthaler, A., Mikoviny, T., Karl, T., Kaser, L., Jud, W., Hansel, A., Docherty, K. S., Alexander, M. L., Robinson, N. H., Coe, H., Allan, J. D., Canagaratna, M. R., Paulot, F., and Jimenez, J. L.: Characterization of a real-time tracer for isoprene epoxydiols-derived secondary organic aerosol (IEPOX-SOA) from aerosol mass spectrometer measurements, Atmos. Chem. Phys., 15, 11807–11833, doi:10.5194/acp-15-11807-2015, 2015.

Huie, R. E. and Herron, J. T.: Kinetics of the reactions of singlet molecular oxygen ($O_2{}^1\Delta_g$) with organic compounds in the gas phase, Int. J. Chem. Kinet., 5, 197–211, doi:10.1002/kin.550050204, 1973.

Jathar, S. H., Cappa, C. D., Wexler, A. S., Seinfeld, J. H., and Kleeman, M. J.: Multi-generational oxidation model to simulate secondary organic aerosol in a 3-D air quality model, Geosci. Model Dev., 8, 2553–2567, doi:10.5194/gmd-8-2553-2015, 2015.

Johannessen, S. C. and Miller, W. L.: Quantum yield for the photochemical production of dissolved inorganic carbon in seawater, Mar. Chem., 76, 271–283, doi:10.1016/S0304-4203(01)00067-6, 2001.

Johnson, M. S., Nilsson, E. J. K., Svensson, E. A., and Langer, S.: Gas-Phase Advanced Oxidation for Effective, Efficient in Situ Control of Pollution, Environ. Sci. Technol., 48, 8768–8776, doi:10.1021/es5012687, 2014.

Kang, E., Root, M. J., Toohey, D. W., and Brune, W. H.: Introducing the concept of Potential Aerosol Mass (PAM), Atmos. Chem. Phys., 7, 5727–5744, doi:10.5194/acp-7-5727-2007, 2007.

Kang, E., Toohey, D. W., and Brune, W. H.: Dependence of SOA oxidation on organic aerosol mass concentration and OH expo-

sure: experimental PAM chamber studies, Atmos. Chem. Phys., 11, 1837–1852, doi:10.5194/acp-11-1837-2011, 2011.

Keller-Rudek, H., Moortgat, G. K., Sander, R., and Sörensen, R.: The MPI-Mainz UV/VIS Spectral Atlas of Gaseous Molecules of Atmospheric Interest, available at: www.uv-vis-spectral-atlas-mainz.org, last access: November 2015.

Klems, J. P., Lippa, K. A., and McGivern, W. S.: Quantitative Evidence for Organic Peroxy Radical Photochemistry at 254 nm, J. Phys. Chem. A, 119, 344–351, doi:10.1021/jp509165x, 2015.

Kumar, M. and Francisco, J. S.: Red-Light-Induced Decomposition of an Organic Peroxy Radical: A New Source of the HO_2 Radical, Angew. Chemie Int. Ed., 54, 15711–15714, doi:10.1002/anie.201509311, 2015.

Kwok, E. and Atkinson, R.: Estimation of hydroxyl radical reaction rate constants for gas-phase organic compounds using a structure-reactivity relationship: An update, Atmos. Environ., 29, 1685–1695, doi:10.1016/1352-2310(95)00069-B, 1995.

Lambe, A. T., Ahern, A. T., Williams, L. R., Slowik, J. G., Wong, J. P. S., Abbatt, J. P. D., Brune, W. H., Ng, N. L., Wright, J. P., Croasdale, D. R., Worsnop, D. R., Davidovits, P., and Onasch, T. B.: Characterization of aerosol photooxidation flow reactors: heterogeneous oxidation, secondary organic aerosol formation and cloud condensation nuclei activity measurements, Atmos. Meas. Tech., 4, 445–461, doi:10.5194/amt-4-445-2011, 2011a.

Lambe, A. T., Onasch, T. B., Massoli, P., Croasdale, D. R., Wright, J. P., Ahern, A. T., Williams, L. R., Worsnop, D. R., Brune, W. H., and Davidovits, P.: Laboratory studies of the chemical composition and cloud condensation nuclei (CCN) activity of secondary organic aerosol (SOA) and oxidized primary organic aerosol (OPOA), Atmos. Chem. Phys., 11, 8913–8928, doi:10.5194/acp-11-8913-2011, 2011b.

Lambe, A. T., Onasch, T. B., Croasdale, D. R., Wright, J. P., Martin, A. T., Franklin, J. P., Massoli, P., Kroll, J. H., Canagaratna, M. R., Brune, W. H., Worsnop, D. R., and Davidovits, P.: Transitions from Functionalization to Fragmentation Reactions of Laboratory Secondary Organic Aerosol (SOA) Generated from the OH Oxidation of Alkane Precursors, Environ. Sci. Technol., 46, 5430–5437, doi:10.1021/es300274t, 2012.

Lambe, A. T., Cappa, C. D., Massoli, P., Onasch, T. B., Forestieri, S. D., Martin, A. T., Cummings, M. J., Croasdale, D. R., Brune, W. H., Worsnop, D. R., and Davidovits, P.: Relationship between Oxidation Level and Optical Properties of Secondary Organic Aerosol, Environ. Sci. Technol., 47, 6349–6357, doi:10.1021/es401043j, 2013.

Lambe, A. T., Chhabra, P. S., Onasch, T. B., Brune, W. H., Hunter, J. F., Kroll, J. H., Cummings, M. J., Brogan, J. F., Parmar, Y., Worsnop, D. R., Kolb, C. E., and Davidovits, P.: Effect of oxidant concentration, exposure time, and seed particles on secondary organic aerosol chemical composition and yield, Atmos. Chem. Phys., 15, 3063–3075, doi:10.5194/acp-15-3063-2015, 2015.

Laue, T. and Plagens, A.: Named Organic Reactions, 2nd ed., John Wiley & Sons, Chichester, England, New York, USA, available at: http://www.wiley.com/WileyCDA/WileyTitle/productCd-047001041X.html (last access: November 2015), 2005.

Levy II, H.: Normal atmosphere: large radical and formaldehyde concentrations predicted., Science, 173, 141–143, doi:10.1126/science.173.3992.141, 1971.

Li, R., Palm, B. B., Borbon, A., Graus, M., Warneke, C., Ortega, A. M., Day, D. A., Brune, W. H., Jimenez, J. L., and de Gouw, J. A.: Laboratory Studies on Secondary Organic Aerosol Formation from Crude Oil Vapors, Environ. Sci. Technol., 47, 12566–12574, doi:10.1021/es402265y, 2013.

Li, R., Palm, B. B., Ortega, A. M., Hu, W., Peng, Z., Day, D. A., Knote, C., Brune, W. H., de Gouw, J., and Jimenez, J. L.: Modeling the radical chemistry in an Oxidation Flow Reactor (OFR): radical formation and recycling, sensitivities, and OH exposure estimation equation, J. Phys. Chem. A, 119, 4418–4432, doi:10.1021/jp509534k, 2015.

Liu, P., Zhang, Y., and Martin, S. T.: Complex refractive indices of thin films of secondary organic materials by spectroscopic ellipsometry from 220 to 1200 nm, Environ. Sci. Technol., 47, 13594–13601, doi:10.1021/es403411e, 2013.

Liu, P. F., Abdelmalki, N., Hung, H.-M., Wang, Y., Brune, W. H., and Martin, S. T.: Ultraviolet and visible complex refractive indices of secondary organic material produced by photooxidation of the aromatic compounds toluene and *m*-xylene, Atmos. Chem. Phys., 15, 1435–1446, doi:10.5194/acp-15-1435-2015, 2015.

Mao, J., Ren, X., Brune, W. H., Olson, J. R., Crawford, J. H., Fried, A., Huey, L. G., Cohen, R. C., Heikes, B., Singh, H. B., Blake, D. R., Sachse, G. W., Diskin, G. S., Hall, S. R., and Shetter, R. E.: Airborne measurement of OH reactivity during INTEX-B, Atmos. Chem. Phys., 9, 163–173, doi:10.5194/acp-9-163-2009, 2009.

Massoli, P., Lambe, A. T., Ahern, A. T., Williams, L. R., Ehn, M., Mikkilä, J., Canagaratna, M. R., Brune, W. H., Onasch, T. B., Jayne, J. T., Petäjä, T., Kulmala, M., Laaksonen, A., Kolb, C. E., Davidovits, P., and Worsnop, D. R.: Relationship between aerosol oxidation level and hygroscopic properties of laboratory generated secondary organic aerosol (SOA) particles, Geophys. Res. Lett., 37, L24801, doi:10.1029/2010GL045258, 2010.

Matsunaga, A. and Ziemann, P. J.: Gas-Wall Partitioning of Organic Compounds in a Teflon Film Chamber and Potential Effects on Reaction Product and Aerosol Yield Measurements, Aerosol Sci. Technol., 44, 881–892, doi:10.1080/02786826.2010.501044, 2010.

Messaadia, L., El Dib, G., Ferhati, A., and Chakir, A.: UV–visible spectra and gas-phase rate coefficients for the reaction of 2,3-pentanedione and 2,4-pentanedione with OH radicals, Chem. Phys. Lett., 626, 73–79, doi:10.1016/j.cplett.2015.02.032, 2015.

Monks, P. S.: Gas-phase radical chemistry in the troposphere, Chem. Soc. Rev., 34, 376–395, doi:10.1039/b307982c, 2005.

Nakashima, N.: Laser photolysis of benzene. V. Formation of hot benzene, J. Chem. Phys., 77, 6040, doi:10.1063/1.443847, 1982.

Nakashima, N. and Yoshihara, K.: Laser flash photolysis of benzene. VIII. Formation of hot benzene from the S_2 state and its collisional deactivation, J. Chem. Phys., 79, 2727–2735, doi:10.1063/1.446176, 1983.

Nguyen, T. B., Crounse, J. D., Schwantes, R. H., Teng, A. P., Bates, K. H., Zhang, X., St. Clair, J. M., Brune, W. H., Tyndall, G. S., Keutsch, F. N., Seinfeld, J. H., and Wennberg, P. O.: Overview of the Focused Isoprene eXperiment at the California Institute of Technology (FIXCIT): mechanistic chamber studies on the oxidation of biogenic compounds, Atmos. Chem. Phys., 14, 13531–13549, doi:10.5194/acp-14-13531-2014, 2014.

Odum, J. R., Hoffmann, T., Bowman, F., Collins, D., Flagan, R. C., and Seinfeld, J. H.: Gas particle partitioning and secondary

organic aerosol yields, Environ. Sci. Technol., 30, 2580–2585, doi:10.1021/es950943+, 1996.

Ono, R., Nakagawa, Y., Tokumitsu, Y., Matsumoto, H., and Oda, T.: Effect of humidity on the production of ozone and other radicals by low-pressure mercury lamps, J. Photoch. Photobio. A, 274, 13–19, doi:10.1016/j.jphotochem.2013.09.012, 2014.

Ortega, A. M., Day, D. A., Cubison, M. J., Brune, W. H., Bon, D., de Gouw, J. A., and Jimenez, J. L.: Secondary organic aerosol formation and primary organic aerosol oxidation from biomass-burning smoke in a flow reactor during FLAME-3, Atmos. Chem. Phys., 13, 11551–11571, doi:10.5194/acp-13-11551-2013, 2013.

Ortega, A. M., Hayes, P. L., Peng, Z., Palm, B. B., Hu, W., Day, D. A., Li, R., Cubison, M. J., Brune, W. H., Graus, M., Warneke, C., Gilman, J. B., Kuster, W. C., de Gouw, J. A., and Jimenez, J. L.: Real-time measurements of secondary organic aerosol formation and aging from ambient air in an oxidation flow reactor in the Los Angeles area, Atmos. Chem. Phys. Discuss., 15, 21907–21958, doi:10.5194/acpd-15-21907-2015, 2015.

Osburn, C. L., Retamal, L., and Vincent, W. F.: Photoreactivity of chromophoric dissolved organic matter transported by the Mackenzie River to the Beaufort Sea, Mar. Chem., 115, 10–20, doi:10.1016/j.marchem.2009.05.003, 2009.

O'Sullivan, D. W., Neale, P. J., Coffin, R. B., Boyd, T. J., and Osburn, C. L.: Photochemical production of hydrogen peroxide and methylhydroperoxide in coastal waters, Mar. Chem., 97, 14–33, doi:10.1016/j.marchem.2005.04.003, 2005.

Palm, B. B., Campuzano-Jost, P., Ortega, A. M., Day, D. A., Kaser, L., Jud, W., Karl, T., Hansel, A., Hunter, J. F., Cross, E. S., Kroll, J. H., Peng, Z., Brune, W. H., and Jimenez, J. L.: In situ secondary organic aerosol formation from ambient pine forest air using an oxidation flow reactor, Atmos. Chem. Phys., 16, 2943–2970, doi:10.5194/acp-16-2943-2016, 2016.

Peng, Z., Day, D. A., Stark, H., Li, R., Lee-Taylor, J., Palm, B. B., Brune, W. H., and Jimenez, J. L.: HO_x radical chemistry in oxidation flow reactors with low-pressure mercury lamps systematically examined by modeling, Atmos. Meas. Tech., 8, 4863–4890, doi:10.5194/amt-8-4863-2015, 2015.

Phillips, S. M. and Smith, G. D.: Light Absorption by Charge Transfer Complexes in Brown Carbon Aerosols, Environ. Sci. Technol. Lett., 1, 382–386, doi:10.1021/ez500263j, 2014.

Phillips, S. M. and Smith, G. D.: Further Evidence for Charge Transfer Complexes in Brown Carbon Aerosols from Excitation–Emission Matrix Fluorescence Spectroscopy, J. Phys. Chem. A, 119, 4545–4551, doi:10.1021/jp510709e, 2015.

Pitts, J. N. and Finlayson, B. J.: Mechanismen der photochemischen Luftverschmutzung, Angew. Chemie, 87, 18–33, doi:10.1002/ange.19750870103, 1975.

Platt, S. M., El Haddad, I., Zardini, A. A., Clairotte, M., Astorga, C., Wolf, R., Slowik, J. G., Temime-Roussel, B., Marchand, N., Ježek, I., Drinovec, L., Mocnik, G., Möhler, O., Richter, R., Barmet, P., Bianchi, F., Baltensperger, U., and Prévôt, A. S. H.: Secondary organic aerosol formation from gasoline vehicle emissions in a new mobile environmental reaction chamber, Atmos. Chem. Phys., 13, 9141–9158, doi:10.5194/acp-13-9141-2013, 2013.

Presto, A. A., Huff Hartz, K. E., and Donahue, N. M.: Secondary Organic Aerosol Production from Terpene Ozonolysis. 1. Effect of UV Radiation, Environ. Sci. Technol., 39, 7036–7045, doi:10.1021/es050174m, 2005.

Pretsch, E., Bühlmann, P., and Badertscher, M.: Structure Determination of Organic Compounds, Springer Berlin Heidelberg, Germany, 2009.

Renlund, A. M. and Trott, W. M.: ArF Laser-induced decomposition of simple energetic niolecules, Chem. Phys. Lett., 107, 555–560, doi:10.1016/S0009-2614(84)85155-6, 1984.

Roberts, J. M. and Fajer, R. W.: UV absorption cross sections of organic nitrates of potential atmospheric importance and estimation of atmospheric lifetimes, Environ. Sci. Technol., 23, 945–951, 1989.

Romonosky, D. E., Laskin, A., Laskin, J., and Nizkorodov, S. A.: High-Resolution Mass Spectrometry and Molecular Characterization of Aqueous Photochemistry Products of Common Types of Secondary Organic Aerosols, J. Phys. Chem. A, 119, 2594–2606, doi:10.1021/jp509476r, 2015.

Romonosky, D. E., Ali, N. N., Saiduddin, M. N., Wu, M., Lee, H. J., Aiona, P. K., and Nizkorodov, S. A.: Effective absorption cross sections and photolysis rates of anthropogenic and biogenic secondary organic aerosols, Atmos. Environ., 130, 172–179, doi:10.1016/j.atmosenv.2015.10.019, 2016.

Sander, S. P., Friedl, R. R., Barker, J. R., Golden, D. M., Kurylo, M. J., Wine, P. H., Abbatt, J. P. D., Burkholder, J. B., Kolb, C. E., Moortgat, G. K., Huie, R. E., and Orkin, V. L.: Chemical Kinetics and Photochemical Data for Use in Atmospheric Studies Evaluation Number 17, National Aeronautics and Space Administration and Jet Propulsion Laboratory, California Institute of Technology, Pasadena, CA, USA, 2011.

Saukko, E., Lambe, A. T., Massoli, P., Koop, T., Wright, J. P., Croasdale, D. R., Pedernera, D. A., Onasch, T. B., Laaksonen, A., Davidovits, P., Worsnop, D. R., and Virtanen, A.: Humidity-dependent phase state of SOA particles from biogenic and anthropogenic precursors, Atmos. Chem. Phys., 12, 7517–7529, doi:10.5194/acp-12-7517-2012, 2012.

Schmidt, G. A., Kelley, M., Nazarenko, L., Ruedy, R., Russell, G. L., Aleinov, I., Bauer, M., Bauer, S. E., Bhat, M. K., Bleck, R., Canuto, V., Chen, Y., Cheng, Y., Clune, T. L., Del Genio, A., de Fainchtein, R., Faluvegi, G., Hansen, J. E., Healy, R. J., Kiang, N. Y., Koch, D., Lacis, A. A., LeGrande, A. N., Lerner, J., Lo, K. K., Matthews, E. E., Menon, S., Miller, R. L., Oinas, V., Oloso, A. O., Perlwitz, J. P., Puma, M. J., Putman, W. M., Rind, D., Romanou, A., Sato, M., Shindell, D. T., Sun, S., Syed, R. A., Tausnev, N., Tsigaridis, K., Unger, N., Voulgarakis, A., Yao, M.-S., and Zhang, J.: Configuration and assessment of the GISS ModelE2 contributions to the CMIP5 archive, J. Adv. Model. Earth Syst., 6, 141–184, doi:10.1002/2013MS000265, 2014.

Seakins, P. W.: A brief review of the use of environmental chambers for gas phase studies of kinetics, chemical mechanisms and characterisation of field instruments, EPJ Web Conf., 9, 143–163, doi:10.1051/epjconf/201009012, 2010.

Sharpless, C. M. and Blough, N. V: The importance of charge-transfer interactions in determining chromophoric dissolved organic matter (CDOM) optical and photochemical properties, Environ. Sci. Process. Impacts, 16, 654–671, doi:10.1039/c3em00573a, 2014.

Smith, J. D., Kroll, J. H., Cappa, C. D., Che, D. L., Liu, C. L., Ahmed, M., Leone, S. R., Worsnop, D. R., and Wilson, K. R.: The heterogeneous reaction of hydroxyl radicals with sub-

micron squalane particles: a model system for understanding the oxidative aging of ambient aerosols, Atmos. Chem. Phys., 9, 3209–3222, doi:10.5194/acp-9-3209-2009, 2009.

Strollo, C. M. and Ziemann, P. J.: Products and mechanism of secondary organic aerosol formation from the reaction of 3-methylfuran with OH radicals in the presence of NO_x, Atmos. Environ., 77, 534–543, doi:10.1016/j.atmosenv.2013.05.033, 2013.

Tkacik, D. S., Lambe, A. T., Jathar, S., Li, X., Presto, A. A., Zhao, Y., Blake, D., Meinardi, S., Jayne, J. T., Croteau, P. L., and Robinson, A. L.: Secondary Organic Aerosol Formation from in-Use Motor Vehicle Emissions Using a Potential Aerosol Mass Reactor, Environ. Sci. Technol., 48, 11235–11242, doi:10.1021/es502239v, 2014.

Tsang, W.: Chemical kinetic data base for combustion chemistry part V. Propene, J. Phys. Chem. Ref. data, 20, 221–274, doi:10.1063/1.555880, 1991.

Turro, N. J., Ramamurthy, V., and Scaiano, J. C.: Principles of Molecular Photochemistry: An Introduction, University Science Books, Sausalito, CA, USA, available at: http://www.uscibooks.com/turro2.htm (last access: November 2015), 2009.

Updyke, K. M., Nguyen, T. B., and Nizkorodov, S. A.: Formation of brown carbon via reactions of ammonia with secondary organic aerosols from biogenic and anthropogenic precursors, Atmos. Environ., 63, 22–31, doi:10.1016/j.atmosenv.2012.09.012, 2012.

Wang, B., Lambe, A. T., Massoli, P., Onasch, T. B., Davidovits, P., Worsnop, D. R., and Knopf, D. A.: The deposition ice nucleation and immersion freezing potential of amorphous secondary organic aerosol: Pathways for ice and mixed-phase cloud formation, J. Geophys. Res., 117, D16209, doi:10.1029/2012JD018063, 2012.

Wang, J., Doussin, J. F., Perrier, S., Perraudin, E., Katrib, Y., Pangui, E., and Picquet-Varrault, B.: Design of a new multi-phase experimental simulation chamber for atmospheric photosmog, aerosol and cloud chemistry research, Atmos. Meas. Tech., 4, 2465–2494, doi:10.5194/amt-4-2465-2011, 2011.

Warneke, C., Roberts, J. M., Veres, P., Gilman, J., Kuster, W. C., Burling, I., Yokelson, R., and de Gouw, J. A.: VOC identification and inter-comparison from laboratory biomass burning using PTR-MS and PIT-MS, Int. J. Mass Spectrom., 303, 6–14, doi:10.1016/j.ijms.2010.12.002, 2011.

Wong, J. P. S., Zhou, S., and Abbatt, J. P. D.: Changes in Secondary Organic Aerosol Composition and Mass due to Photolysis: Relative Humidity Dependence, J. Phys. Chem. A, 119, 4309–4316, doi:10.1021/jp506898c, 2015.

Zhang, X., Cappa, C. D., Jathar, S. H., McVay, R. C., Ensberg, J. J., Kleeman, M. J., and Seinfeld, J. H.: Influence of vapor wall loss in laboratory chambers on yields of secondary organic aerosol, P. Natl. Acad. Sci. USA, 111, 5802–5807, doi:10.1073/pnas.1404727111, 2014.

Zhang, Y., Xie, H., and Chen, G.: Factors Affecting the Efficiency of Carbon Monoxide Photoproduction in the St. Lawrence Estuarine System (Canada), Environ. Sci. Technol., 40, 7771–7777, doi:10.1021/es0615268, 2006.

Ziemann, P. and Atkinson, R.: Kinetics, products, and mechanisms of secondary organic aerosol formation, Chem. Soc. Rev., 41, 6582, doi:10.1039/c2cs35122f, 2012.

Supplement of Atmos. Chem. Phys., 16, 4283–4305, 2016
http://www.atmos-chem-phys.net/16/4283/2016/
doi:10.5194/acp-16-4283-2016-supplement

Atmospheric Chemistry and Physics Open Access EGU

Supplement of

Non-OH chemistry in oxidation flow reactors for the study of atmospheric chemistry systematically examined by modeling

Zhe Peng et al.

Correspondence to: Jose L. Jimenez (jose.jimenez@colorado.edu)

- acp-16-4283-2016-supplement-title-page.pdf
- OFR_Exposure_Estimator.xlsx
- Supplement.pdf

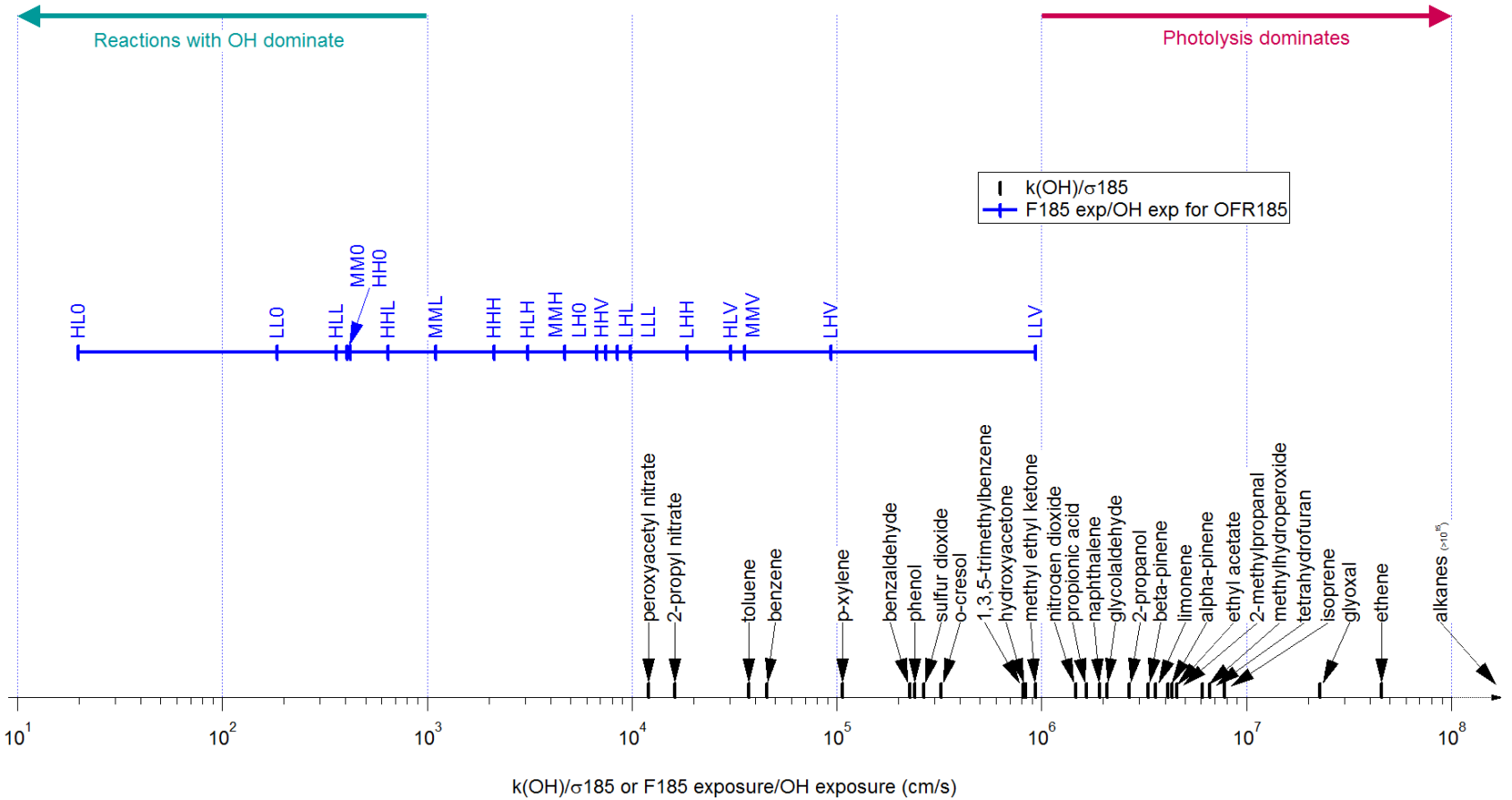

Figure S1. Ratios between rate constants of several species of atmospheric interest with OH and their photoabsorption cross-sections at 185 nm (black markers) and ratios between 185 nm-photon (F185) and OH exposures for OFR185 (blue). The former are also equal to F185 exposure/OH exposure at which photons at 185 nm and OH consume species equally. Ratios between 185 nm photon and OH exposures in typical OFR cases are shown by markers. The reaction of the considered species with OH is preponderant over photolysis at 185 nm at a certain value of F185 exposure/OH exposure, when this value is located on the left of the considered species' black marker, as the turquoise solid arrow on the top indicates. The reverse is true when this value is on the right, as the carmine solid arrow on the top indicates.

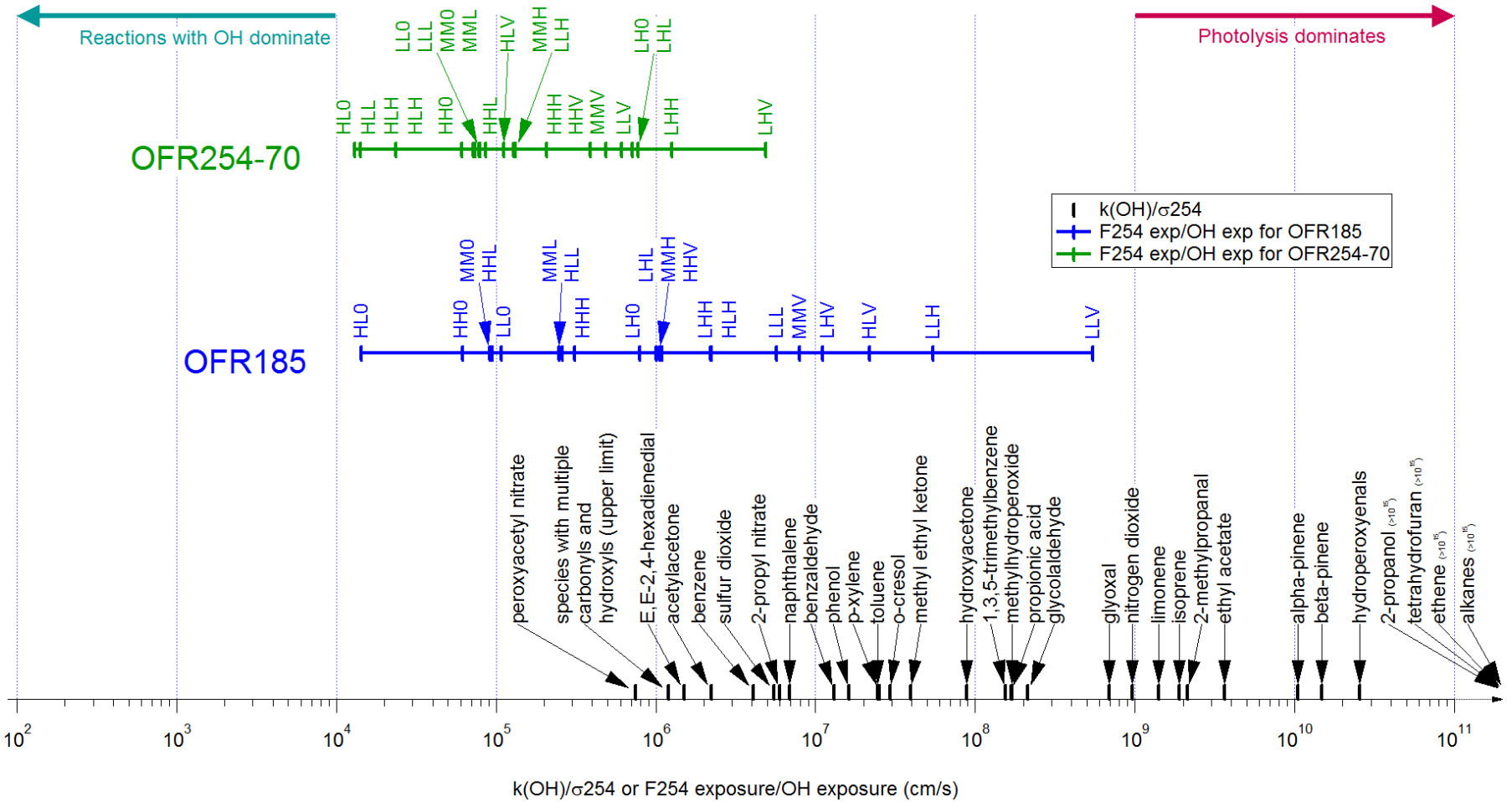

Figure S2. Same as Fig. S1, but for ratios of rate constants with OH and photoabsorption cross-sections at 254 nm and F254 exposure/OH exposure for OFR185 and OFR254-70.

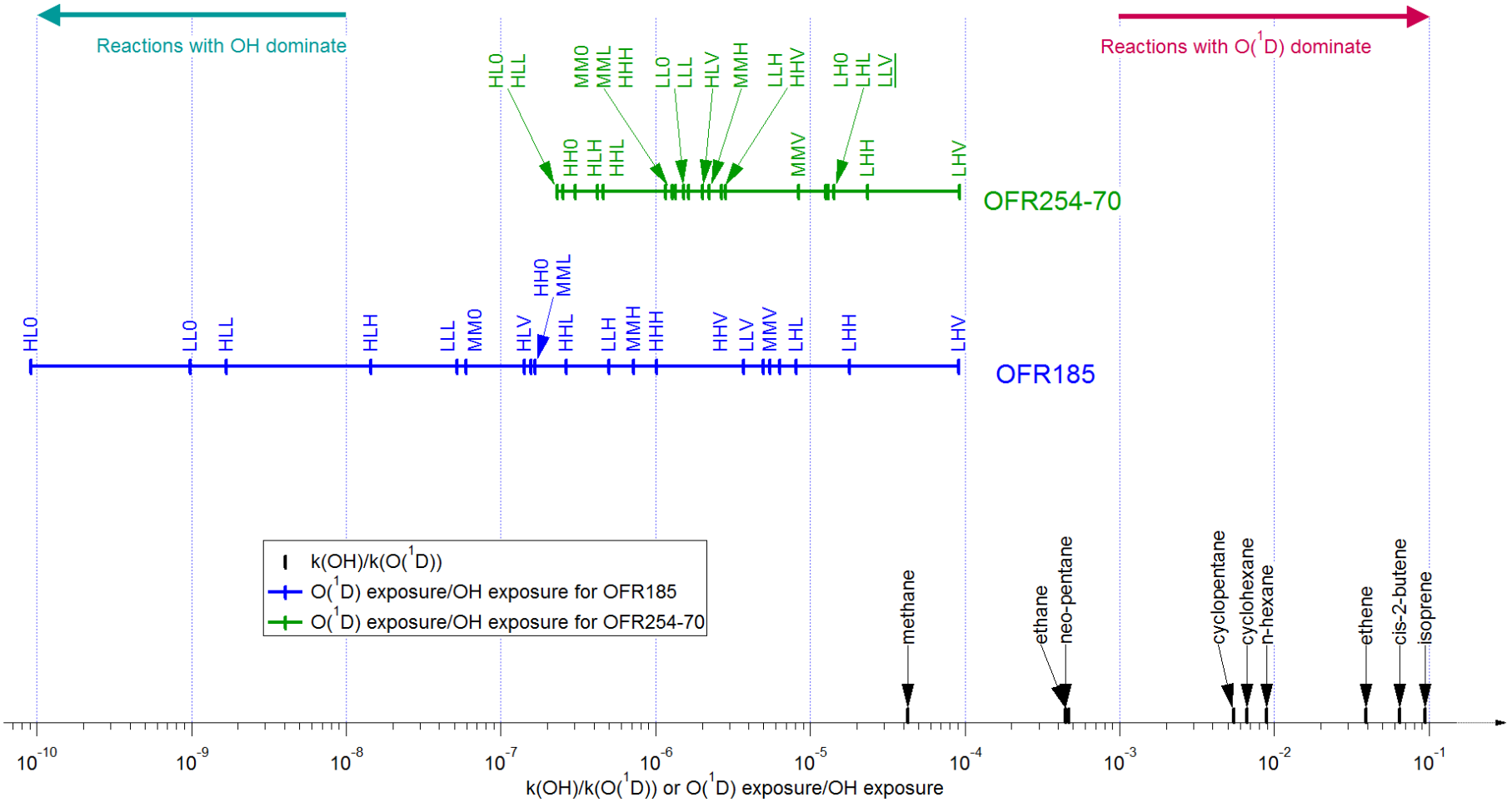

Figure S3. Same as Fig. S1, but for ratios of rate constants with OH and $O(^1D)$ and $O(^1D)$ exposure/OH exposure for OFR185 and OFR254-70.

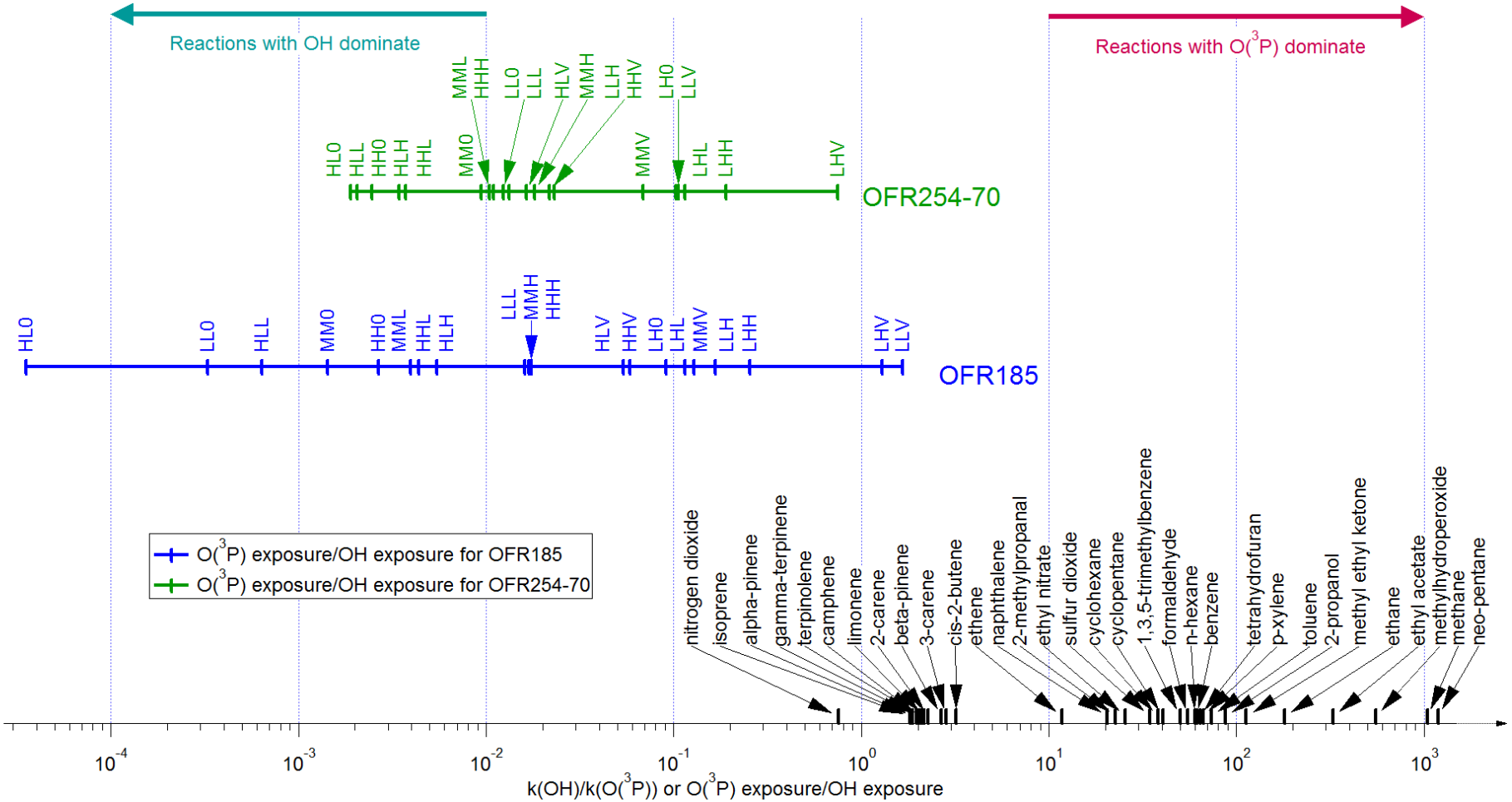

Figure S4. Same as Fig. S1, but for ratios of rate constants with OH and O(^{3}P) and O(^{3}P) exposure/OH exposure for OFR185 and OFR254-70.

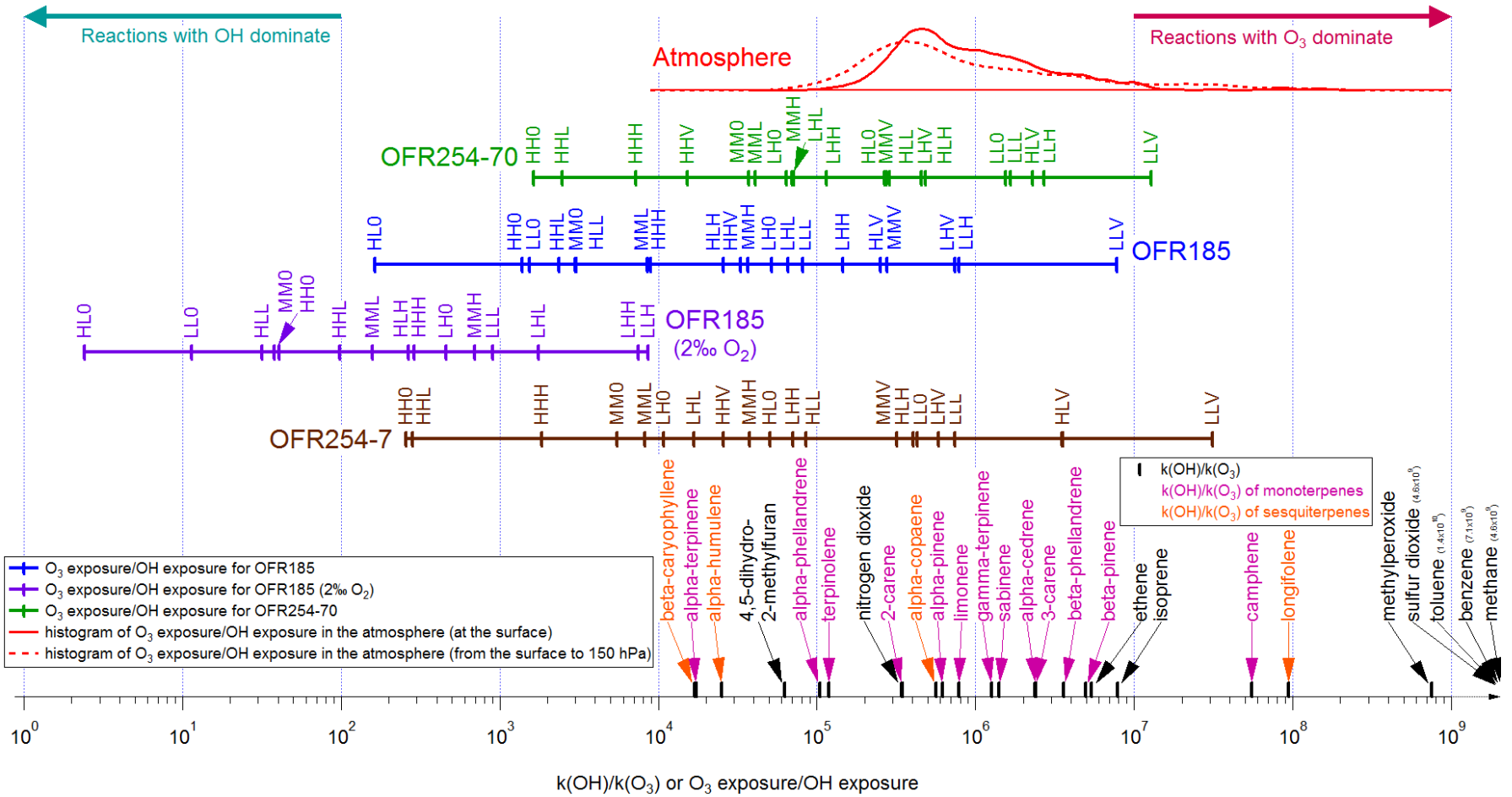

Figure S5. Same as Fig. S1, but for ratios of rate constants with OH and O_3 of species of atmospheric interest and O_3 exposure/OH exposure for OFR185 (blue), OFR185 with 0.2% O_2 (purple), OFR254-70 (dark green), and OFR254-7 (brown), and in the atmosphere (red).
Species names corresponding to ratios between rate constants of OH and of O_3 with monoterpenes, sesquiterpenes, and other species are in magenta, dark orange, and black, respectively. O_3 exposure/OH exposure at the Earth's surface (solid line) and throughout the column from the surface to a height with a pressure of 150 hPa (dashed line) in the atmosphere are shown by histograms, as simulated by the GISS ModelE2.

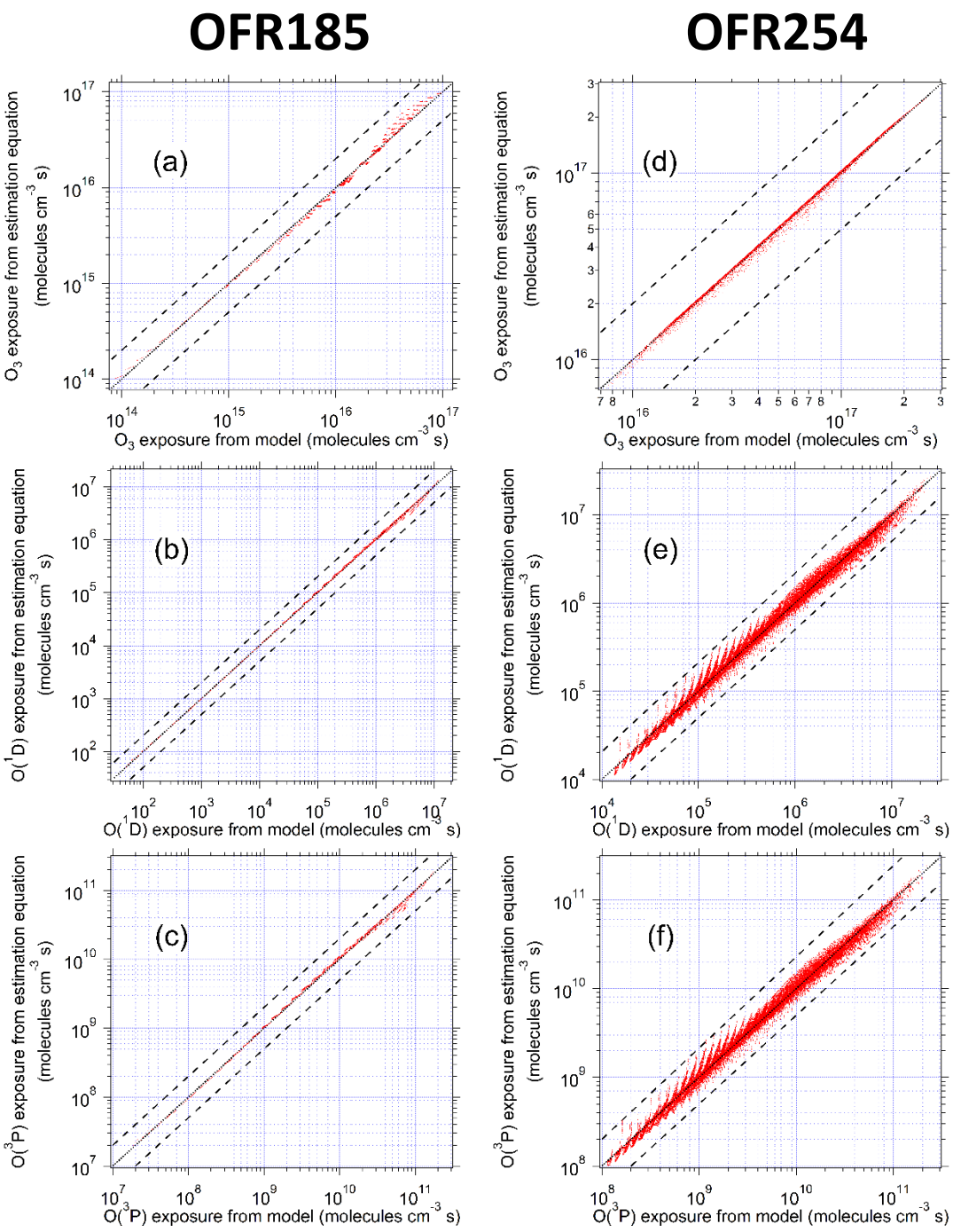
OFR185
OFR254
(a)
(b)
(c)
(d)
(e)
(f)
O3 exposure from estimation equation (molecules cm-3 s)
O3 exposure from model (molecules cm-3 s)
O(1D) exposure from estimation equation (molecules cm-3 s)
O(1D) exposure from model (molecules cm-3 s)
O(3P) exposure from estimation equation (molecules cm-3 s)
O(3P) exposure from model (molecules cm-3 s)

OFR185

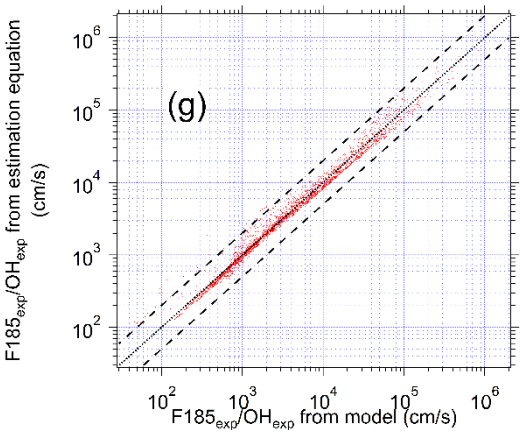

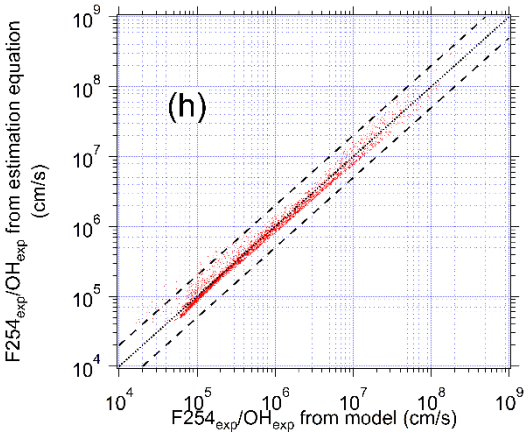

OFR254

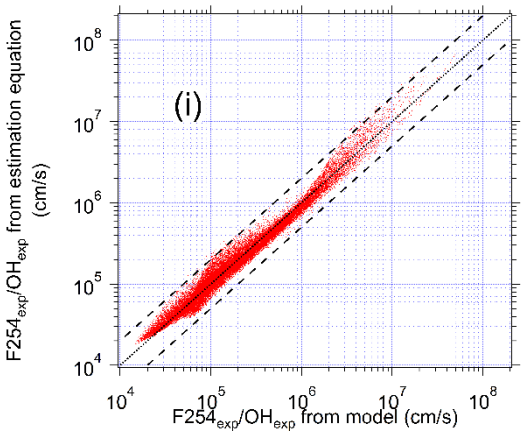

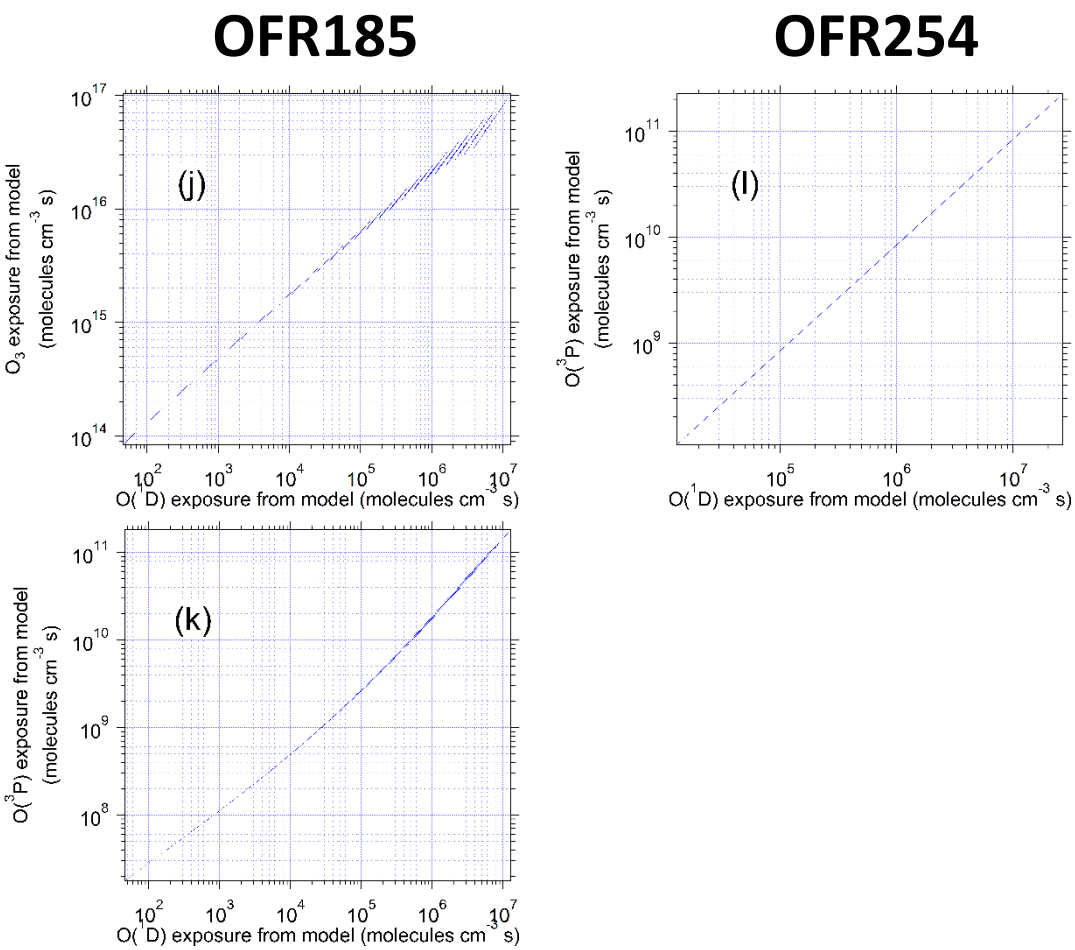

Figure S6. O_3, $O(^1D)$, and $O(^3P)$ exposures and ratios of F185 and F254 exposures to OH exposure from estimation equations vs. those from the model for (a–c, g, h) OFR185 and (d–f, i) OFR254. 1:1 (dotted), 1:2, and 2:1 (dashed) lines are shown in (a–i) to facilitate comparison. Scatter plots between modeled exposures for (j, k) OFR185 and (l) OFR254 are also shown.

Table S1. Photoabsorption cross-sections (in cm^2 $molecule^{-1}$) of several species of atmospheric interest at 185 and 254 nm and rate constants (in cm^3 $molecule^{-1}$ s^{-1}) of these species with OH at room temperature (298 K).

Species	σ(185)	Ref	σ(254)	Ref	k(OH)	Ref
isoprene	1.28E-17	(Keller-Rudek et al., 2015)	5.28E-20	(Keller-Rudek et al., 2015)	1.00E-10	(Atkinson and Arey, 2003)
α-pinene	1.27E-17	(Keller-Rudek et al., 2015)	~5E-21	(Keller-Rudek et al., 2015)[*1]	5.23E-11	(Atkinson and Arey, 2003)
β-pinene	2.25E-17	(Keller-Rudek et al., 2015)	~5E-21	(Keller-Rudek et al., 2015)[*2]	7.43E-11	(Atkinson and Arey, 2003)
limonene	4.58E-17	(Keller-Rudek et al., 2015)	1.16E-19	(Keller-Rudek et al., 2015)	1.64E-10	(Atkinson and Arey, 2003)
sulfur dioxide	3.47E-18	(Keller-Rudek et al., 2015)	1.67E-19	(Keller-Rudek et al., 2015)	9.20E-13	(Sander et al., 2011)
nitrogen dioxide	6.88E-18	(Keller-Rudek et al., 2015)	1.05E-20	(Keller-Rudek et al., 2015)	1.01E-11	(Sander et al., 2011)
benzene	2.68E-17	(Keller-Rudek et al., 2015)	3.00E-19	(Keller-Rudek et al., 2015)	1.22E-12	(Atkinson and Arey, 2003)
toluene	1.52E-16	(Keller-Rudek et al., 2015)	2.29E-19	(Keller-Rudek et al., 2015)	5.63E-12	(Atkinson and Arey, 2003)
benzaldehyde	~5.3E-17	this work[*3]	9.20E-19	(Keller-Rudek et al., 2015)	1.20E-11	(Trost et al., 1997)
o-cresol	~1.3E-16	this work[*3]	1.43E-18	(Keller-Rudek et al., 2015)	4.20E-11	(Trost et al., 1997)
phenol	~1.1E-16	this work[*3]	1.63E-18	(Keller-Rudek et al., 2015)	2.63E-11	(Atkinson and Arey, 2003)
p-xylene	1.34E-16	(Keller-Rudek et al., 2015)	5.70E-19	(Keller-Rudek et al., 2015)	1.43E-11	(Atkinson and Arey, 2003)
1,3,5-trimethylbenzene	6.96E-17	(Keller-Rudek et al., 2015)	3.68E-19	(Keller-Rudek et al., 2015)	5.67E-11	(Atkinson and Arey, 2003)
naphthalene	1.20E-17	(Halasinski et al., 2005)	3.33E-18	(Ferguson et al., 1957)	2.30E-11	(Atkinson and Arey, 2003)
methylhydroperoxide	~9E-19	(Keller-Rudek et al., 2015)[*4]	3.23E-20	(Keller-Rudek et al., 2015)	3.80E-12	(Sander et al., 2011)
hydroperoxyenals	N/A	N/A	3.23E-20	(Keller-Rudek et al., 2015)[*5]	~5.1E-11	(Wolfe et al., 2012)[*6]
E,E-2,4-hexadienedial	N/A	N/A	3.32E-17	(Keller-Rudek et al., 2015)[*7]	~5E-11	(Ziemann and Atkinson, 2012)[*8]
acetylacetone	N/A	N/A	4.00E-17	(Messaadia et al., 2015)	8.89E-11	(Messaadia et al., 2015)
species with multiple carbonyls and hydroxyls	N/A	N/A	~5E-17[*9]	(Foster, 1969)	~6E-12	(Atkinson and Arey, 2003)[*10]
2-propanol	2.16E-18	(Keller-Rudek et al., 2015)	0	N/A	5.80E-12	(Atkinson and Arey, 2003)
glyoxal	4.80E-19	(Keller-Rudek et al., 2015)[*11]	1.59E-20	(Keller-Rudek et al., 2015)	1.10E-11	(Atkinson and Arey, 2003)
2-methylpropanal	5.71E-18	(Keller-Rudek et al., 2015)	1.22E-20	(Keller-Rudek et al., 2015)	2.60E-11	(Atkinson and Arey, 2003)
glycolaldehyde	3.85E-18	(Keller-Rudek et al., 2015)	3.76E-20	(Keller-Rudek et al., 2015)	8.00E-12	(Ammann et al., 2015)
methyl ethyl ketone	1.31E-18	(Keller-Rudek et al., 2015)	3.09E-20	(Keller-Rudek et al., 2015)	1.22E-12	(Atkinson and Arey, 2003)
hydroxyacetone	5.40E-18	(Keller-Rudek et al., 2015)	5.07E-20	(Keller-Rudek et al., 2015)	4.50E-12	(Ammann et al., 2015)
ethyl acetate	4.21E-19	(Keller-Rudek et al., 2015)	5.00E-22	(Keller-Rudek et al., 2015)[*12]	1.82E-12	(El Boudali et al., 1996)

propionic acid	7.25E-19	(Keller-Rudek et al., 2015)	7.11E-21	(Keller-Rudek et al., 2015)	1.20E-12	(Ammann et al., 2015)
pyruvic acid	N/A	N/A	1.61E-20	(Keller-Rudek et al., 2015)	1.20E-13	(Mellouki and Mu, 2003)
tetrahydrofuran	2.27E-18	(Keller-Rudek et al., 2015)	0	N/A	1.50E-11	(Atkinson, 1986)
2-propyl nitrate	1.79E-17	(Keller-Rudek et al., 2015)	4.86E-20	(Keller-Rudek et al., 2015)	2.90E-13	(Atkinson and Arey, 2003)
peroxyacetyl nitrate	6.20E-18	(Sander et al., 2011)[*13]	1.00E-19	(Sander et al., 2011)	7.50E-14	(Tsalkani et al., 1988)
ethene	1.87E-19	(Keller-Rudek et al., 2015)	0	N/A	8.52E-12	(Atkinson and Arey, 2003)
alkanes	0	N/A	0	N/A	~1E-12	(Atkinson and Arey, 2003)

*1: approximate average value between 245 and 250 nm
*2: approximate average value between 245 and 250 nm
*3: estimate based on quantum chemical calculations. See details below.
*4: extrapolation from the data between 210 and 280 nm, whose logarithm manifests a good linear wavelength-dependence
*5: value of a proxy, methylhydroperoxide, as the proxy used in Wolfe et al. (2012), E-2-hexanal, does not contain a hydroperoxy group and hence has little absorption at 254 nm.
*6: value of a proxy, C_6-hydroperoxyenal
*7: value at 248 nm
*8: estimated according to quantitative structure-activity relationship in Ziemann and Atkinson (2012)
*9: upper limit estimated according to relevant data in Foster (1969)
*10: typical value of saturated ketones
*11: value at 193 nm
*12: value at 252 nm
*13: linear extrapolation from the data between 196–206 nm

Table S2. Rate constants (in cm^3 $molecule^{-1}$ s^{-1}) of several species of atmospheric interest with $O(^1D)$, $O(^3P)$, and OH at room temperature (298 K).

Species	k($O(^1D)$)	Ref	k($O(^3P)$)	Ref	k(OH)	Ref
sulfur dioxide	N/A	N/A	2.67E-14	(Atkinson et al., 1997)	9.19E-13	(Sander et al., 2011)
nitrogen dioxide	N/A	N/A	1.34E-11	(Sander et al., 2011)	1.01E-11	(Sander et al., 2011)
methane	1.50E-10	(Ammann et al., 2015)	6.12E-18	(Cohen and Westberg, 1991)	6.40E-15	(Atkinson and Arey, 2003)
ethane	5.30E-10	(Michaud et al., 1974)	1.38E-15	(Cohen and Westberg, 1991)	2.48E-13	(Atkinson and Arey, 2003)
neo-pentane	1.84E-09	(Pitts et al., 1974)	6.91E-16	(Cohen and Westberg, 1991)	8.25E-13	(Atkinson and Arey, 2003)
cyclopentane	9.05E-10	(Michaud et al., 1974)	1.23E-13	(Cohen and Westberg, 1991)	4.97E-12	(Atkinson and Arey, 2003)
n-hexane	5.80E-10	(Dillon et al., 2008)	8.69E-14	(Cohen and Westberg, 1991)	5.20E-12	(Atkinson and Arey, 2003)
cyclohexane	1.05E-09	(Michaud et al., 1974)	1.83E-13	(Cohen and Westberg, 1991)	6.97E-12	(Atkinson and Arey, 2003)
ethene	2.19E-10	(Kajimoto and Fueno, 1979)	7.25E-13	(Cvetanović, 1987)	8.52E-12	(Atkinson and Arey, 2003)
cis-2-butene	8.70E-10	(Kajimoto and Fueno, 1979)	1.76E-11	(Cvetanović, 1987)	5.64E-11	(Atkinson and Arey, 2003)
methylhydroperoxide	N/A	N/A	1.00E-14	(Baulch et al., 1994)	5.50E-12	(Atkinson and Arey, 2003)
benzene	N/A	N/A	1.99E-14	(Cvetanović, 1987)	1.22E-12	(Atkinson and Arey, 2003)
toluene	N/A	N/A	7.63E-14	(Baulch et al., 1994)	5.63E-12	(Atkinson and Arey, 2003)
p-xylene	N/A	N/A	2.15E-13	(Baulch et al., 1994)	1.43E-11	(Atkinson and Arey, 2003)
1,3,5-trimethylbenzene	N/A	N/A	1.13E-12	(Cvetanović, 1987)	5.67E-11	(Atkinson and Arey, 2003)
naphthalene	N/A	N/A	1.13E-12	(Frerichs et al., 1990)	2.30E-11	(Atkinson and Arey, 2003)
isoprene	1.06E-09	(Kajimoto and Fueno, 1979)	5.52E-11	(Cvetanović, 1987)	1.00E-10	(Atkinson and Arey, 2003)
α-pinene	N/A	N/A	2.79E-11	(Luo et al., 1996)	5.23E-11	(Atkinson and Arey, 2003)
β-pinene	N/A	N/A	2.80E-11	(Luo et al., 1996)	7.43E-11	(Atkinson and Arey, 2003)
3-carene	N/A	N/A	3.12E-11	(Luo et al., 1996)	8.80E-11	(Atkinson and Arey, 2003)
2-carene	N/A	N/A	3.54E-11	(Luo et al., 1996)	8.00E-11	(Atkinson and Arey, 2003)
camphene	N/A	N/A	2.60E-11	(Luo et al., 1996)	5.30E-11	(Atkinson and Arey, 2003)
limonene	N/A	N/A	7.60E-11	(Luo et al., 1996)	1.64E-10	(Atkinson and Arey, 2003)
γ-terpinene	N/A	N/A	9.00E-11	(Luo et al., 1996)	1.77E-10	(Atkinson and Arey, 2003)
terpinolene	N/A	N/A	1.07E-10	(Luo et al., 1996)	2.25E-10	(Atkinson and Arey, 2003)
2-propanol	N/A	N/A	6.64E-14	(Herron, 1988)	5.80E-12	(Atkinson and Arey, 2003)
2-methylpropanal	N/A	N/A	1.15E-12	(Herron, 1988)	2.60E-11	(Atkinson and Arey, 2003)

methyl ethyl ketone	N/A	N/A	1.09E-14	(Herron, 1988)	1.22E-12	(Atkinson and Arey, 2003)
ethyl acetate	N/A	N/A	5.59E-15	(Herron, 1988)	1.82E-12	(El Boudali et al., 1996)
tetrahydrofuran	N/A	N/A	2.36E-13	(Herron, 1988)	1.50E-11	(Atkinson, 1986)
ethyl nitrate	N/A	N/A	7.02E-15	(Salter and Thrush, 1977)	1.80E-13	(Atkinson and Arey, 2003)
formaldehyde	N/A	N/A	1.70E-13	(Herron, 1988)	9.37E-12	(Atkinson and Arey, 2003)

Table S3. Rate constants (in cm^3 $molecule^{-1}$ s^{-1}) of several species of atmospheric interest with O_3, and OH at room temperature (298 K).

Species	k(OH)	Ref	k(O_3)	Ref
isoprene	1.00E-10	(Atkinson and Arey, 2003)	1.27E-17	(Atkinson and Arey, 2003)
camphene	5.30E-11	(Atkinson and Arey, 2003)	9.60E-19	(Atkinson and Arey, 2003)
2-carene	8.00E-11	(Atkinson and Arey, 2003)	2.30E-16	(Atkinson and Arey, 2003)
3-carene	8.80E-11	(Atkinson and Arey, 2003)	3.70E-17	(Atkinson and Arey, 2003)
limonene	1.64E-10	(Atkinson and Arey, 2003)	2.10E-16	(Atkinson and Arey, 2003)
α-phellandrene	3.13E-10	(Atkinson and Arey, 2003)	3.00E-15	(Atkinson and Arey, 2003)
β-phellandrene	1.68E-10	(Atkinson and Arey, 2003)	4.70E-17	(Atkinson and Arey, 2003)
α-pinene	5.23E-11	(Atkinson and Arey, 2003)	8.40E-17	(Atkinson and Arey, 2003)
β-pinene	7.43E-11	(Atkinson and Arey, 2003)	1.50E-17	(Atkinson and Arey, 2003)
sabinene	1.17E-10	(Atkinson and Arey, 2003)	8.30E-17	(Atkinson and Arey, 2003)
α-terpinene	3.63E-10	(Atkinson and Arey, 2003)	2.10E-14	(Atkinson and Arey, 2003)
γ-terpinene	1.77E-10	(Atkinson and Arey, 2003)	1.40E-16	(Atkinson and Arey, 2003)
terpinolene	2.25E-10	(Atkinson and Arey, 2003)	1.90E-15	(Atkinson and Arey, 2003)
α-cedrene	6.70E-11	(Atkinson and Arey, 2003)	2.80E-17	(Atkinson and Arey, 2003)
α-copaene	9.00E-11	(Atkinson and Arey, 2003)	1.60E-16	(Atkinson and Arey, 2003)
β-caryophyllene	1.97E-10	(Atkinson and Arey, 2003)	1.16E-14	(Atkinson and Arey, 2003)
α-humulene	2.93E-10	(Atkinson and Arey, 2003)	1.17E-14	(Atkinson and Arey, 2003)
longifolene	4.70E-11	(Atkinson and Arey, 2003)	5.00E-19	(Atkinson and Arey, 2003)
methane	6.40E-15	(Atkinson and Arey, 2003)	1.40E-24	(Schubert et al., 1956)
ethene	8.52E-12	(Atkinson and Arey, 2003)	1.59E-18	(Atkinson and Arey, 2003)
benzene	1.22E-12	(Atkinson and Arey, 2003)	1.72E-22	(Toby et al., 1985)
toluene	5.63E-12	(Atkinson and Arey, 2003)	3.90E-22	(Toby et al., 1985)
methylperoxide	5.50E-12	(Atkinson and Arey, 2003)	7.30E-21	(Chen and Wang, 2006)
4,5-dihydro-2-methylfuran	2.18E-10	(Atkinson and Arey, 2003)	3.49E-15	(Atkinson and Arey, 2003)
sulfur dioxide	9.20E-13	(Sander et al., 2011)	2.00E-22	(Sander et al., 2011)
nitrogen dioxide	1.01E-11	(Sander et al., 2011)	2.97E-17	(Sander et al., 2011)

Table S4. Summary of the previous studies using OFRs. In case of multiple experiments with a certain source in a certain study, only the most (low water mixing ratio and high external OH reactivity) and the least (high water mixing ratio and low external OH reactivity) pathological cases are shown. Source, external OH reactivity (Ext. OHR), OH exposure (OH exp.), and relative humidity (RH) in each experiment are collected from the literature. Exposure ratios and percentages of the rate of a type of reactions [r(X), X=185 nm photons, 254 nm photons, $O(^1D)$, $O(^3P)$, and O_3] in the sum of the rates of these reactions and those with OH [r(X)+r(OH)] are estimated by our model. Photolysis at 185 and 254 nm is considered as non-tropospheric reactions (NTR). An example of the improvement of study using OFR is also shown for comparison.

Study	Source type	Source mixing ratio (ppb)	Ext. OHR (s^{-1})	OH exp. (molec cm^{-3} s)	RH (%)	Examined species	F185 exp./OH exp. (cm/s)	r(185) /(r(185) +r(OH)) (%)	F254 exp./OH exp. (cm/s)	r(254) /(r(254) +r(OH)) (%)	$O(^1D)$ exp. /OH exp.	$r(O(^1D))$ /($r(O(^1D))$ +r(OH)) (%)*8	$O(^3P)$ exp. /OH exp.	$r(O(^3P))$ /($r(O(^3P))$ +r(OH)) (%)	O_3 exp. /OH exp.	$r(O_3)$ /($r(O_3)$ +r(OH)) (%)*9	r(non-OH) /(r(total)) (%)	r(NTR) /(r(total)) (%)
Kang et al. 2011	α-pinene	39	49	2.8E+11	3	α-pinene			3.1E+06	0.03	7.7E-06	0.02	5.3E-02	2.88	1.8E+05	23.45	26.38	0.02
				2.3E+12	42				3.3E+05	0.00	6.0E-07	0.00	4.2E-03	0.23	1.7E+04	2.81	3.04	0.00
	m-xylene	170	94	2.4E+11	4	m-xylene			4.3E+06	8.47	1.0E-05	0.05	7.3E-02	0.13	2.1E+05	0.01	8.62	8.46
				2.4E+12	48				5.6E+05	1.21	8.4E-07	0.00	5.8E-03	0.01	1.4E+04	0.00	1.22	1.21
	p-xylene	180	62	2.1E+11	4	p-xylene			2.6E+06	9.58	6.7E-06	0.05	4.6E-02	0.06	2.5E+05	0.02	9.68	9.57
				1.6E+12	32				5.4E+05	2.11	1.0E-06	0.01	7.2E-03	0.01	2.6E+04	0.00	2.13	2.11
	mixture	*1	88	1.8E+11	3	α-pinene			5.8E+06	0.06	1.5E-05	0.03	1.0E-01	5.32	2.9E+05	32.40	37.81	0.04
						m-xylene				11.23		0.06		0.17		0.01	11.42	11.20
						p-xylene				18.88		0.10		0.14		0.02	19.05	18.84
				2.3E+12	44	α-pinene			5.6E+05	0.01	8.7E-07	0.00	6.0E-03	0.75	1.5E+04	2.41	3.13	0.01
						m-xylene				1.19		0.00		0.01		0.00	1.21	1.19
						p-xylene				2.17		0.01		0.01		0.00	2.19	2.17
Lambe et al. 2011	n-decane	330	87	1.6E+11	30	n-decane			1.7E+05	0.00	1.2E-06	0.12	8.6E-03	0.00	4.1E+05	0.00	0.12	0.00
		102	27	2.5E+12	40				1.5E+05	0.00	8.7E-07	0.09	6.0E-03	0.00	2.2E+04	0.00	0.09	0.00
	isoprene	330	792	1.6E+11	30	isoprene			2.2E+05	0.01	1.1E-06	0.00	7.9E-03	0.43	4.1E+05	4.95	5.36	0.01
				2.5E+12	40				1.3E+05	0.01	6.1E-07	0.00	4.2E-03	0.23	2.2E+04	0.28	0.52	0.01
	α-pinene	50	63	1.6E+11	30	α-pinene			1.3E+05	0.00	9.5E-07	0.00	6.6E-03	0.36	4.1E+05	40.73	41.10	0.00
				2.5E+12	40				2.0E+05	0.00	1.1E-06	0.00	7.9E-03	0.44	2.1E+04	3.43	3.87	0.00
	β-pinene	50	89	1.6E+11	30	β-pinene			1.8E+05	0.00	1.3E-06	0.00	8.7E-03	0.54	4.1E+05	7.61	8.07	0.00
				2.5E+12	40				2.4E+05	0.00	1.3E-06	0.00	9.3E-03	0.58	2.1E+04	0.41	0.99	0.00
	toluene	80	11	1.6E+11	30	toluene			5.4E+04	0.24	3.9E-07	0.01	2.7E-03	0.00	4.2E+05	0.00	0.25	0.24
				2.5E+12	40				1.2E+05	0.53	7.5E-07	0.01	5.2E-03	0.01	2.2E+04	0.00	0.55	0.53
	m-xylene	103	57	1.6E+11	30	m-xylene			1.2E+05	0.27	8.8E-07	0.00	6.1E-03	0.01	4.1E+05	0.02	0.30	0.27
		86	48	2.5E+12	40				1.7E+05	0.38	1.0E-06	0.00	7.1E-03	0.01	2.2E+04	0.00	0.40	0.38
	1,3,5-trimethyl-benzene	150	204	1.6E+11	30	1,3,5-trimethyl-benzene			3.9E+05	0.26	2.8E-06	0.00	1.9E-02	4.55	4.1E+05	0.01	4.80	0.25
		120	163	2.5E+12	40				3.7E+05	0.25	1.9E-06	0.00	1.3E-02	3.22	1.9E+04	0.00	3.45	0.24
Klems et al. 2015	dodecanoic acid	400	123*4	1.7E+09*5	3	dodecanoic acid			1.6E+07	0.36	5.2E-06	0.04	4.3E-02	0.06	1.5E+04	0.00	0.46	0.36
Tkacik et al. 2014	tunnel air	*2	~300	7.4E+10	42*6	toluene*7	9.8E+03	20.97	1.5E+06	5.86	2.5E-07	0.00	1.0E-02	0.01	1.8E+04	0.00	24.69	24.67
		*3	~100	2.4E+12	42*6		1.3E+03	3.48	1.5E+05	0.60	1.6E-07	0.00	2.7E-03	0.00	3.8E+03	0.00	4.04	4.04
FLAME-3	wood smoke		~250	2.5E+11*5	22*6	benzene*7	2.6E+04	36.31	4.4E+06	51.97	1.7E-06	0.14	4.1E-02	0.07	1.6E+05	0.00	62.32	62.25
						α-pinene*7		0.63		0.04		0.00		2.15		20.32	22.10	0.52
BEACHON	ambient air		~15	2.1E+12*5	63*6	α-pinene*7	8.8E+02	0.02	1.5E+05	0.00	1.3E-07	0.00	2.8E-03	0.15	6.3E+03	1.00	1.17	0.02
SOAS			~20	1.4E+12*5	83*6	isoprene*7	8.1E+02	0.01	1.5E+05	0.01	5.7E-08	0.00	1.4E-03	0.08	5.4E+03	0.07	0.16	0.02
CalNex			~25	8.8E+11*5	43*6	toluene*7	1.1E+03	2.85	2.0E+05	0.82	1.2E-07	0.00	3.1E-03	0.00	1.2E+04	0.00	3.63	3.62
Improvement for FLAME-3	wood smoke		~50	8.7E+11*5	22*6	benzene*7	3.8E+03	7.72	4.8E+05	10.53	6.2E-07	0.05	1.0E-02	0.02	2.2E+04	0.00	16.81	16.76
						α-pinene*7		0.09		0.00		0.00		0.53		3.38	3.96	0.09
Improvement for BEACHON	ambient air		~15	3.2E+12*5	92*10	α-pinene*7	7.5E+02	0.02	1.0E+05	0.00	6.3E-08	0.00	1.1E-03	0.06	3.2E+03	0.51	0.59	0.02

*1: 37 ppb α-pinene, 46 ppb m-xylene, and 47 ppb p-xylene
*2: 785 ppb NO_x, 1.9 ppm CO, and VOC of an OH reactivity of 49.7 s^{-1}, estimated from a linear CO-VOC relationship [VOC of 26.1 s^{-1} OH reactivity per ppm CO (Borbon et al., 2013)]
*3: 310 ppb NO_x, 0.2 ppm CO, and VOC of an OH reactivity of 5.2 s^{-1}, according to the same linear relationship
*4: estimated according to the rate constant of dodecane reported in Atkinson and Arey (2003)
*5: calculated by our model
*6: average value
*7: a typical species in source, not the only component
*8: rate constants of reactions of examined species with $O(^1D)$ that are not available are assumed to be 10^{-9} cm^3 molecule s^{-1}
*9: rate constants of reactions of n-decane and alkylbenzenes with O_3 are taken from their upper limits reported in Atkinson and Arey (2003)
*10: corresponding to a water vapor mixing ratio of 2.3%

Table S5. Absorption cross-sections at 185 and 254 nm for several atmospheric oxidation intermediates from Keller-Rudek et al. (2015), ambient photolysis rate constants from Hodzic et al. (2015), and photolysis percentages in OFR185 and OFR254-70 (under the condition of 70% relative humidity and 25 s^{-1} initial OHR_{ext}) and in the troposphere at an OH exposure equivalent to a photochemical age of 1 week (assuming an ambient OH concentration of $1.5x10^6$ molecules cm^{-3}). "N/A" in the table stands for "not available".

Species	Cross-sections (cm^2)		Ambient photolysis rate constant (s^{-1})	Photolysis percentage		
	185 nm	254 nm		OFR185	OFR254-70	Ambient
acrolein	2.82E-17	7.00E-22	1.39E-06	4.1	0.002	57
methacrolein	6.77E-18	1.78E-21	1.34E-05	1.0	0.005	100
acetone	2.91E-18	3.01E-20	3.82E-07	1.1	0.083	21
biacetyl	1.46E-18	3.71E-20	2.29E-04	1.0	0.103	100
pyruvic acid	N/A	1.61E-20	1.03E-04	N/A	0.045	100
methyl vinyl ketone	N/A	2.41E-21	4.72E-06	N/A	0.007	94
methylglyoxal	N/A	2.76E-20	7.79E-05	N/A	0.076	100
hydroxyacetone	5.40E-18	5.07E-20	1.51E-06	1.9	0.140	60
2,4-dimethyl-3-pentanone	N/A	1.66E-20	8.30E-06	N/A	0.046	99
2-methylpropanal	5.71E-18	1.22E-20	3.80E-05	1.1	0.034	100
4-methyl-2-pentanone	N/A	2.75E-20	5.48E-06	N/A	0.076	96
5-methyl-2-hexanone	N/A	2.39E-20	4.34E-06	N/A	0.066	93
2-propyl nitrate	1.79E-17	4.86E-20	1.93E-06	3.7	0.135	69
crotonaldehyde	1.05E-17	2.80E-21	9.87E-06	1.6	0.008	100
acetaldehyde	7.83E-20	1.57E-20	3.51E-06	0.4	0.044	88
3-pentanone	N/A	3.00E-20	3.07E-06	N/A	0.083	84
methyl ethyl ketone	1.31E-18	3.09E-20	2.98E-06	0.9	0.086	83
propanal	1.42E-17	1.75E-20	1.30E-05	2.5	0.048	100
n-butanal	7.99E-18	1.45E-20	1.14E-05	1.5	0.040	100
n-pentanal	N/A	1.43E-20	1.63E-06	N/A	0.040	63

n-hexanal	N/A	1.14E-20	1.18E-05	N/A	0.032	100
1-butyl nitrate	1.81E-17	4.60E-20	1.71E-06	3.6	0.127	64
1-propyl nitrate	1.81E-17	4.40E-20	1.84E-06	3.6	0.122	67
ethyl nitrate	1.71E-17	4.10E-20	1.16E-06	3.4	0.114	50
methyl nitrate	2.10E-17	3.34E-20	7.27E-07	3.8	0.093	36
methylhydroperoxide	9.00E-19	3.23E-20	4.25E-06	0.9	0.089	92
glyoxal	4.80E-19	1.59E-20	4.72E-04	0.4	0.044	100
peroxyacetyl nitrate	6.20E-18	1.00E-19	6.24E-07	3.1	0.277	31
glycolaldehyde	3.85E-18	3.76E-20	6.82E-06	1.4	0.104	98
hydroxymethyl hydroperoxide	N/A	2.88E-20	3.90E-06	N/A	0.080	91

Table S6. Percentage of non-OH fate of α-pinene and toluene in the "corner" cases (highest and lowest water mixing ratio, lamp setting, and external OH reactivity) in OFR185, OFR254-70, and OFR254-7. The cases with 0 external OH reactivity actually show non-OH VOC consumption at external OH reactivity very close but not equal to 0.

	OFR185		OFR254-70		OFR254-7	
Case	α-pinene	toluene	α-pinene	toluene	α-pinene	toluene
LL0	0.4	0.1	81.9	0.1	55.7	0.0
L"L"0	1.5	0.3	65.7	0.1	32.3	0.1
LH0	13.9	2.4	19.9	0.4	4.6	0.2
HL0	0.0	0.0	44.0	0.0	12.9	0.0
H"L"0	0.1	0.0	21.4	0.0	4.2	0.0
HH0	0.6	0.2	0.6	0.0	0.1	0.0
LLV	95.1	77.4	97.4	0.6	98.9	2.8
L"L"V	93.6	71.9	94.0	0.9	97.1	4.2
LHV	68.2	24.0	63.7	3.0	72.1	8.8
HLV	40.6	12.2	87.2	0.1	91.3	0.3
H"L"V	36.6	10.6	68.4	0.1	73.0	0.4
HHV	11.2	3.1	5.6	0.1	11.1	0.7

Table S7. Photoabsorption cross-sections (in cm^2 $molecule^{-1}$) of several surrogate SOA components at 185 and 254 nm and number of e-fold decays of photolysis of these species in the case of high H_2O, high UV, and high OHR_{ext} (Case HHH). Numbers of e-fold decays in OFR no less than 0.1 are in bold, and those no less than 1 are highlighted in gray cell. Ambient e-fold decay numbers corresponding to the same photochemical age as Case HHH are also shown for comparison.

Species	σ(185)	Ref	σ(254)	Ref	Number of e-fold decay of photolysis		
					185 nm	254 nm	Ambient
sulfuric acid	<1E-19	(Keller-Rudek et al., 2015)	<1E-21	(Keller-Rudek et al., 2015)	<1.8E-03	<1.5E-03	0
nitric acid	1.71E-17	(Keller-Rudek et al., 2015)	1.95E-20	(Keller-Rudek et al., 2015)	**0.31**	2.9E-02	7.1
benzaldehyde	5.30E-17	this work[*1]	9.20E-19	(Keller-Rudek et al., 2015)	**0.95**	**1.4**	7700
o-cresol	1.30E-16	this work[*1]	1.43E-18	(Keller-Rudek et al., 2015)	**2.3**	**2.1**	0
phenol	1.10E-16	this work[*1]	1.63E-18	(Keller-Rudek et al., 2015)	**2.0**	**2.4**	0
naphthalene	1.20E-17	(Halasinski et al., 2005)	3.33E-18	(Ferguson et al., 1957)	**0.22**	**5.0**	0
methylhydroperoxide	9.00E-19	(Keller-Rudek et al., 2015)[*2]	3.23E-20	(Keller-Rudek et al., 2015)	1.6E-02	4.8E-02	57
2-propanol	2.16E-18	(Keller-Rudek et al., 2015)	0	N/A	3.9E-02	0	0
glyoxal	4.80E-19	(Keller-Rudek et al., 2015)[*3]	1.59E-20	(Keller-Rudek et al., 2015)	8.6E-03	2.4E-02	640
2-methylpropanal	5.71E-18	(Keller-Rudek et al., 2015)	1.22E-20	(Keller-Rudek et al., 2015)	**0.10**	1.8E-02	510
glycolaldehyde	3.85E-18	(Keller-Rudek et al., 2015)	3.76E-20	(Keller-Rudek et al., 2015)	6.9E-02	5.6E-02	91
methyl ethyl ketone	1.31E-18	(Keller-Rudek et al., 2015)	3.09E-20	(Keller-Rudek et al., 2015)	2.4E-02	4.6E-02	40
hydroxyacetone	5.40E-18	(Keller-Rudek et al., 2015)	5.07E-20	(Keller-Rudek et al., 2015)	9.7E-02	7.6E-02	34
ethyl acetate	4.21E-19	(Keller-Rudek et al., 2015)	5.00E-22	(Keller-Rudek et al., 2015)[*4]	7.6E-03	7.5E-04	0
pentanoic acid	1.44E-18	(Keller-Rudek et al., 2015)	3.00E-21	(Keller-Rudek et al., 2015)	2.6E-02	4.5E-03	0
tetrahydrofuran	2.27E-18	(Keller-Rudek et al., 2015)	0	N/A	4.1E-02	0	0
alkanes	0	N/A	0	N/A	0	0	0
2-propyl nitrate	1.79E-17	(Keller-Rudek et al., 2015)	4.86E-20	(Keller-Rudek et al., 2015)	**0.32**	7.3E-02	26
peroxyacetyl nitrate	6.20E-18	(Sander et al., 2011)[*5]	1.00E-19	(Sander et al., 2011)	**0.11**	**0.15**	8.3
Ambient average	-	-	-	-	-		44[*6]

*1: estimate based on quantum chemical calculations. See details below.
*2: extrapolation from the data between 210 and 280 nm, whose logarithm manifests a good linear wavelength-dependence
*3: value at 193 nm
*4: value at 252 nm
*5: linear extrapolation from the data between 196–206 nm
*6: estimated based on i) ambient OH concentration of 1.5×10^{6} molecules cm^{-3} (Mao et al., 2009), ii) OH_{exp} of ~2×10^{13} molecules cm^{-3} s in Case HHH (1.8×10^{13} molecules cm^{-3} s for OFR185; 2.3×10^{13} molecules cm^{-3} s for OFR254-70), and iii) average ambient SOA photolysis lifetime of 3.5 d (Hodzic et al., 2015)

Table S8. Number of e-fold decays of photolysis and percentage of photolyzed OA of several SOA samples at an equivalent photochemical age of 1 week under atmospheric conditions in Romonosky et al. (2015a) and in OFR254-70 at 44% relative humidity (water vapor mixing ratio of 1.4%) and 25 s^{-1} initial OHR_{ext}. Absorption cross-sections at 254 nm and effective ambient photolysis lifetimes of SOA samples are taken from or calculated according to Romonosky et al. (2015a). Ambient photolysis data are obtained assuming quantum yields of SOA samples to be those of H_2O_2 or acetone.

SOA type	Cross-section at 254 nm (cm^2)	Effective ambient photolysis lifetime (min)		Number of e-fold decays due to photolysis			Percentage of photolyzed OA at equivalent photochemical age of 1 week		
		Using QY of H_2O_2	Using QY of acetone	OFR254-70	Ambient using QY of H_2O_2	Ambient using QY of acetone	OFR254-70	Ambient using QY of H_2O_2	Ambient using QY of acetone
2-methylpyrrole/O_3	1.66E-17	1	85	0.461	10080	119	36.9	100	100
guaiacol/OH	9.34E-18	1.7	190	0.259	5929	53	22.8	100	100
catechol/O_3	7.97E-18	3	260	0.221	3360	39	19.8	100	100
2-methylpyrrole/OH/NO_x	6.82E-18	1	130	0.189	10080	78	17.2	100	100
p-xylene/OH/NO_x	6.46E-18	2.5	280	0.179	4032	36	16.4	100	100
p-xylene/OH	5.99E-18	5.5	430	0.166	1833	23	15.3	100	100
toluene/OH/NO_x	5.93E-18	1.3	190	0.164	7754	53	15.2	100	100
2-methylpyrrole/OH	5.61E-18	2.6	260	0.155	3877	39	14.4	100	100
naphthalene/OH	4.98E-18	0.62	64	0.138	16258	158	12.9	100	100
toluene/OH	3.42E-18	6.2	590	0.095	1626	17	9.1	100	100
ocimene/OH	2.27E-18	25	1700	0.063	403	5.9	6.1	100	99.7
myrcene/O_3	1.88E-18	58	3800	0.052	174	2.7	5.1	100	93.0
ocimene/OH/NO_x	1.59E-18	25	1800	0.044	403	5.6	4.3	100	99.6
farnesene/OH	1.44E-18	53	3500	0.040	190	2.9	3.9	100	94.4
farnesene/OH/NO_x	1.07E-18	47	3400	0.030	214	3.0	2.9	100	94.8
d-limonene/O_3	5.95E-19	230	7200	0.016	44	1.4	1.6	100	75.3
imidazole/O_3	5.76E-19	95	4800	0.016	106	2.1	1.6	100	87.8
α-pinene/O_3	5.54E-19	85	4800	0.015	119	2.1	1.5	100	87.8

isoprene/OH	5.07E-19	410	7600	0.014	25	1.3	1.4	100	73.5
b-pinene/O_3	4.68E-19	90	4000	0.013	112	2.5	1.3	100	92.0
isoprene/O_3	4.42E-19	88	5400	0.012	115	1.9	1.2	100	84.5
linalool/OH/NO_x	3.65E-19	100	7700	0.010	101	1.3	1.0	100	73.0
linalool/OH	2.92E-19	160	11000	0.008	63	0.9	0.8	100	60.0

Table S9. Estimation equations of $O(^3P)$, $O(^1D)$, and O_3 exposures and ratios of $F254_{exp}$ to OH_{exp} for both OFR185 and OFR254, and ratio of $F185_{exp}$ to OH_{exp} for OFR185. UV in the equations for OFR185 and OFR254 are the photon fluxes at 185 and 254 nm, respectively. Numbers of fitted datapoints and average absolute value of the relative deviations (AAVRD) of the estimates by the equations from the fitted datapoints are also shown. rO_3 is the ratio between O_3 at the reactor exit and entrance. For OFR254, one of rO_3 and UV can be obtained by collectively considering and solving Eqs. 11 and 12 in Peng et al. (2015b) if the other is known. OH, O_3, $O(^1D)$, and $O(^3P)$ exposures are in molecules cm^{-3} s, $F185_{exp}$ and $F254_{exp}$ in photons cm^{-2}, OHR_{ext} in s^{-1}, UV in photons cm^{-2} s^{-1}, $O_{3,in}$ in ppb, and H_2O and rO_3 unitless.

OFR type	Eq. No.	Estimation equation	Number of fitted datapoints	AAVRD (%)
OFR185	S1	$\log O_{3exp} = 3.1825 + 0.98741 \log UV + 40.352 H_2O - 3.8184 H_2O \cdot \log UV$	28800	6
	S2	$\log O(^3P)_{exp} = 313.61 - 558.66 \log(\log O_{3exp}) - 171.59 H_2O + 254.33 (\log(\log O_{3exp}))^2 + 147.27 H_2O \cdot \log(\log O_{3exp})$		6
	S3	$\log O(^1D)_{exp} = 90.595 - 208.28 \log(\log O_{3exp}) - 155.9 H_2O + 114.15 (\log(\log O_{3exp}))^2 + 134.4 H_2O \cdot \log(\log O_{3exp})$		4
	S4	$\log(F185_{exp}/OH_{exp}) = -2.7477 - 0.79645 \log H_2O + 0.25018 \log O_{3exp} + 3.8051 \log OHR_{ext} - 0.22685 \log OHR_{ext} \cdot \log O_{3exp} + 0.0086381 (\log OHR_{ext})^2 \cdot \log O_{3exp}$		14
	S5	$\log(F254_{exp}/OH_{exp}) = 3.325 - 0.8268 \log H_2O + 3.7467 \log OHR_{ext} - 0.22294 \log OHR_{ext} \cdot \log O_{3exp} + 0.0086345 (\log OHR_{ext})^2 \cdot \log O_{3exp}$		14
OFR254	S6	$\log O_{3exp} = 15.559 + \log O_{3,in} + 0.42073 \log rO_3$	316800	1
	S7	$\log O(^3P)_{exp} = 7.6621 + 0.16135 \log(-\log rO_3) - 1.1342 \log H_2O + 0.59182 \log O_{3,in} - 0.17007 \log H_2O \cdot \log(-\log rO_3) - 0.3797 (\log(-\log rO_3))^2 + 0.099902 \log OHR_{ext}$		12
	S8	$\log O(^1D)_{exp} = 3.7371 + 0.1608 \log(-\log rO_3) - 1.1344 \log H_2O + 0.59179 \log O_{3,in} - 0.17019 \log H_2O \cdot \log(-\log rO_3) - 0.37983 (\log(-\log rO_3))^2 + 0.099941 \log OHR_{ext}$		12
	S9	$\log(F254_{exp}/OH_{exp}) = 2.8045 - 0.888519 \log H_2O - 0.015648 \log(-\log rO_3) - 0.2607 \log OHR_{ext} - 0.1641 (\log(-\log rO_3))^2 + (OHR_{ext}/O_{3,in})^{0.25142}$		14

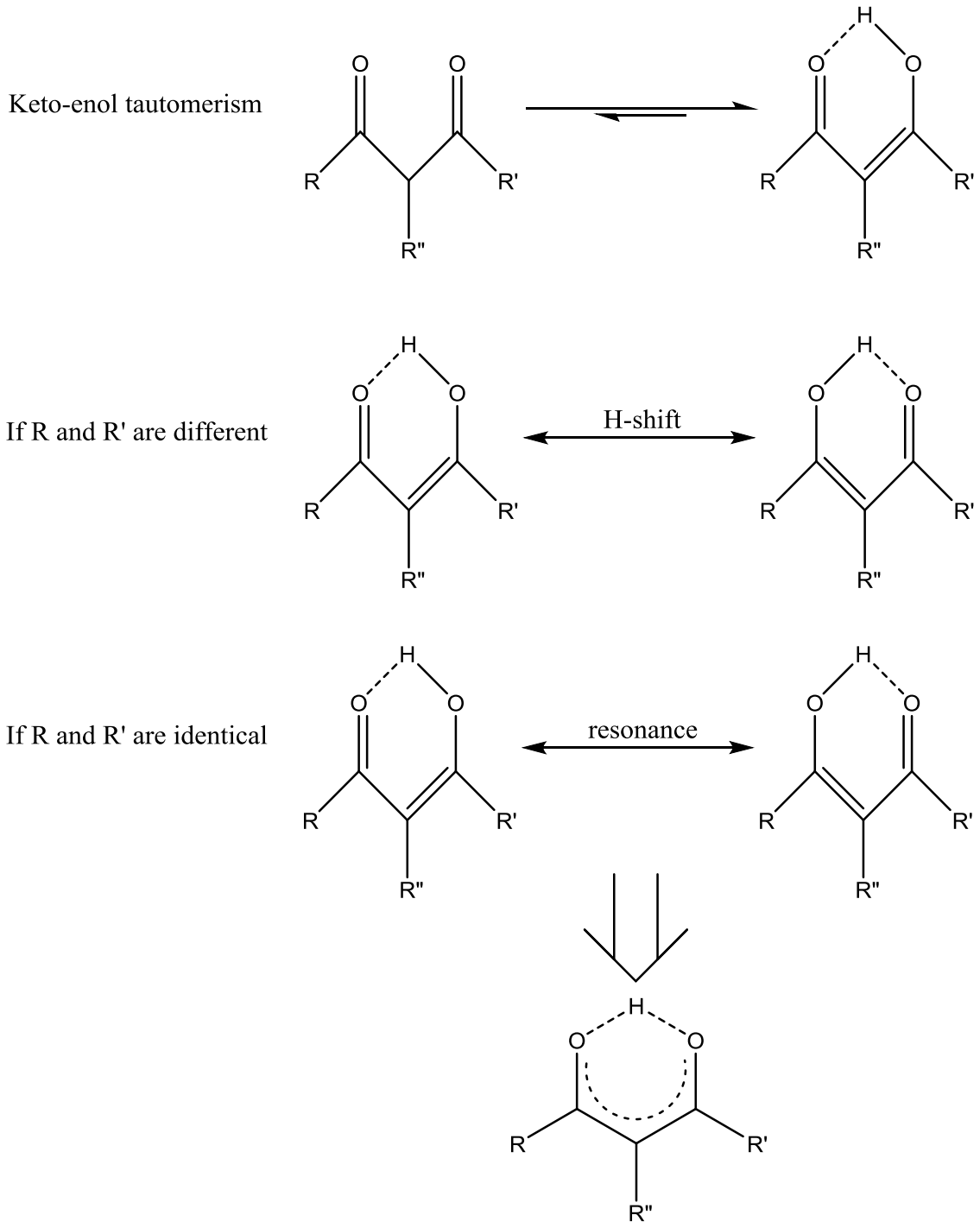

Scheme S1. Keto-enol tautomerism of β-diketone, and H-shift between O atoms or resonance of the enol form. Note that the tautomerism is generally favorable toward the enol form (Burdett and Rogers, 1964) and that the enol form, particularly its resonance, results in an extensive conjugated ring structure, which may have high absorptivity.

S1. Selection of kinetic data

This study involves photoabsorption cross-sections at 185 and 254 nm, rate constants of reactions with OH, $O(^1D)$, $O(^3P)$, and O_3 of a large variety of species of interest. Obviously, we are not able to include all possible reactants. Instead, we include one or two representative species for a category of species with certain functional group(s). The selection of presented species is subject to data availability. In principle, we choose species with available kinetic data to cover categories with different functional groups. However, for example, rate constants of reactions with $O(^1D)$ have seldom been measured. Some categories (e.g., aromatics) are thus not covered. In case of multiple available dataset for a single cross-section/rate constant, we apply the following rules:

i) Photoabsorption cross-section data from different sources are used in the priority order of MPI-Mainz UV/VIS Spectral Atlas of Gaseous Molecules of Atmospheric Interest (Keller-Rudek et al., 2015) > JPL Chemical Kinetic Data Evaluation (Sander et al., 2011) > other sources;

ii) The latest dataset is selected in case of multiple available references in MPI-Mainz UV/VIS Spectral Atlas of Gaseous Molecules of Atmospheric Interest;

iii) Data of rate constants of thermal reactions from different sources are used in the priority order of Atkinson and Arey (2003) > JPL Chemical Kinetic Data Evaluation (Sander et al., 2011) > IUPAC Task Group on Atmospheric Chemical Kinetic Data Evaluation (Ammann et al., 2015) > other sources.

In some cases, kinetic data are also collected under certain reliable approximations, despite no available direct measurements. For example, to obtain cross-section of methylhydroperoxide at 185 nm, we make an extrapolation from the data between 210 and 280 nm, whose logarithm manifests a good linear wavelength-dependence; we use cross-section of ethyl acetate at 252 nm as that at 254 nm.

According to data in Trost et al. (1997) and Atkinson and Arey (2003), photolysis of benzaldehydes and phenols at 254 nm is significant compared to their reactions with OH. It is important to assess their photolysis at 185 nm. However, no measured cross-section data are available. Moreover, no appropriate assumptions based on available data to obtain cross-sections at 185 nm can be made. We thus make an estimation of these cross-sections based on quantum chemical calculations.

S2. Estimation of 185 nm absorption cross-sections of several aromatics

We perform time-dependent density functional theory calculations (Runge and Gross, 1984) using GAMESS program (Schmidt et al., 1993) for the molecule of interest: ground state geometry is optimized at Perdew-Burke-Ernzerhof0/6-311g(d,p) level (Perdew et al., 1996). Oscillator strengths of transitions between 160 and 300 nm are obtained by time-dependent calculations at the same level with the first 10 excited states considered. Then cross-section at 185 nm is estimated under the assumption that the ratio between cross-sections at 185 nm and absorption maximum wavelength in the longer-wavelength range, where experimental data are available in Keller-Rudek et al. (2015), is equal to that between oscillator strengths of transitions closest to 185 nm and absorption maximum wavelength, respectively. This is a very rough approximation completely neglecting vibronic structure of absorption bands. However, in this study, we only seek cross-section values on the right order of magnitude, but not quantum chemical predictions quantitatively comparable to measurements, which require vibrational/vibronic wavefunctions of dissociative excited states and are far beyond this work's scope.

The main features that we find from theoretical estimates, i.e., estimated 185 nm cross-sections are around 10^{16} cm^2/molecule and 2 orders of magnitude larger than those at 254 nm, agree well with the available data for other aromatics, i.e., toluene and p-xylene (Table S1).

S3. Estimation equations of non-OH reactant exposures

In order that one may practically estimate exposure ratios between non-OH reactants and OH under any condition for OFR operation, we provide the estimation equations of $O(^3P)$, $O(^1D)$, and O_3 exposures obtained by fitting the modeling results (Table S9). The equations for OFR254 are

fitted from the results of the same runs as in Peng et al. (2015b), while those for OFR185 from the modeling data under conditions spanning the same H_2O, UV, and OHR_{ext} ranges as for OFR254, but without the initial O_3 ($O_{3,in}$) dimension. Exposures estimated from these equations compare very well with the modeled exposures (Fig. S6). Scatter plots between a few exposures are also shown in Fig. S6.

For OFR254, UV at 254 nm can be estimated by collectively considering and solving Eqs. 11 and 12 in Peng et al. (2015b), if rO_3 (i.e., ratio between O_3 at the reactor entrance and exit) is known, and vice versa. For OFR185, one of UV at 185 nm and O_{3exp} (or average O_3) can be obtained if the other is known according to Eq. S1 below. UV at 254 nm in OFR185 can be calculated by Eq. S1 in Li et al. (2015), and then photon flux exposures can be easily estimated.

The ratios of F185 and F254 exposures to OH exposure are the most important parameter in this work that determine the relative contribution of non-tropospheric VOC photolysis. Therefore, we also provide equations for directly estimating these parameters from measurable surrogates of UV (i.e., O_{3exp} in OFR185 and rO_3 in OFR254) (Table S9 and Fig. S6).

References

Ammann, M., Cox, R. A., Crowley, J. N., Jenkin, M. E., Mellouki, A., Rossi, M. J., Troe, J., Wallington, T. J., Cox, B., Atkinson, R., Baulch, D. L. and Kerr, J. A.: IUPAC Task Group on Atmospheric Chemical Kinetic Data Evaluation, [online] Available from: http://iupac.pole-ether.fr/#, 2015.

Atkinson, R.: Kinetics and mechanisms of the gas-phase reactions of the hydroxyl radical with organic compounds under atmospheric conditions, Chem. Rev., 86(1), 69–201, doi:10.1021/cr00071a004, 1986.

Atkinson, R. and Arey, J.: Atmospheric degradation of volatile organic compounds., Chem. Rev., 103(12), 4605–38, doi:10.1021/cr0206420, 2003.

Atkinson, R., Baulch, D. L., Cox, R. A., Hampson, R. F., Kerr, J. A., Rossi, M. J. and Troe, J.: Evaluated Kinetic and Photochemical Data for Atmospheric Chemistry: Supplement VI. IUPAC Subcommittee on Gas Kinetic Data Evaluation for Atmospheric Chemistry, J. Phys. Chem. Ref. Data, 26(6), 1329, doi:10.1063/1.556010, 1997.

Baulch, D. L., Cobos, C. J., Cox, R. A., Frank, P., Hayman, G., Just, T., Kerr, J. A., Murrells, T., Pilling, M. J., Troe, J., Walker, R. W. and Warnatz, J.: Evaluated Kinetic Data for Combustion Modeling. Supplement I, J. Phys. Chem. Ref. Data, 23(6), 847, doi:10.1063/1.555953, 1994.

Borbon, A., Gilman, J. B., Kuster, W. C., Grand, N., Chevaillier, S., Colomb, A., Dolgorouky, C., Gros, V., Lopez, M., Sarda-Esteve, R., Holloway, J., Stutz, J., Petetin, H., McKeen, S., Beekmann, M., Warneke, C., Parrish, D. D. and De Gouw, J. A.: Emission ratios of anthropogenic volatile organic compounds in northern mid-latitude megacities: Observations versus emission inventories in Los Angeles and Paris, J. Geophys. Res. Atmos., 118(4), 2041–2057, doi:10.1002/jgrd.50059, 2013.

El Boudali, A., Le Calvé, S., Le Bras, G. and Mellouki, A.: Kinetic Studies of OH Reactions with a Series of Acetates, J. Phys. Chem., 10(30), 12364–12368, doi:10.1021/jp9606218, 1996.

Burdett, J. L. and Rogers, M. T.: Keto-Enol Tautomerism in β-Dicarbonyls Studied by Nuclear Magnetic Resonance Spectroscopy. 1 I. Proton Chemical Shifts and Equilibrium Constants of Pure Compounds, J. Am. Chem. Soc., 86(11), 2105–2109, doi:10.1021/ja01065a003, 1964.

Chen, Z. and Wang, C.: Rate constants of the gas-phase reactions of CH3OOH with O3 and NOx at 293K, Chem. Phys. Lett., 424(4-6), 233–238, doi:10.1016/j.cplett.2006.04.026, 2006.

Cohen, N. and Westberg, K. R.: Chemical Kinetic Data Sheets for High-Temperature Reactions. Part II, J. Phys. Chem. Ref. Data, 20(6), 1211, doi:10.1063/1.555901, 1991.

Cvetanović, R. J.: Evaluated Chemical Kinetic Data for the Reactions of Atomic Oxygen O(3P) with Unsaturated Hydrocarbons, J. Phys. Chem. Ref. Data, 16(2), 261, doi:10.1063/1.555783, 1987.

Dillon, T. J., Horowitz, A. and Crowley, J. N.: The atmospheric chemistry of sulphuryl fluoride, SO2F2, Atmos. Chem. Phys., 8(6), 1547–1557, doi:10.5194/acp-8-1547-2008, 2008.

Ferguson, J., Reeves, L. W. and Schneider, W. G.: VAPOR ABSORPTION SPECTRA AND OSCILLATOR STRENGTHS OF NAPHTHALENE, ANTHRACENE, AND PYRENE, Can. J. Chem., 35(10), 1117–1136, doi:10.1139/v57-152, 1957.

Foster, R.: Organic Charge-Transfer Complexes, Academic Press, New York., 1969.

Frerichs, H., Tappe, M. and Wagner, H. G.: Comparison of the Reactions of Mono- and Polycyclic Aromatic Hydrocarbons with Oxygen Atoms, Berichte der Bunsengesellschaft für Phys. Chemie, 94(11), 1404–1407, doi:10.1002/bbpc.199000043, 1990.

Halasinski, T. M., Salama, F. and Allamandola, L. J.: Investigation of the Ultraviolet, Visible, and Near-Infrared Absorption Spectra of Hydrogenated Polycyclic Aromatic Hydrocarbons and Their Cations, Astrophys. J., 628(1), 555–566, doi:10.1086/430631, 2005.

Herron, J. T.: Evaluated Chemical Kinetic Data for the Reaction of Atomic Oxygen, O(3P), with Saturated Organic Compounds in the Gas Phase, J. Phys. Chem. Ref. Data., 17(3), 967–994, doi:10.1063/1.555810, 1988.

Hodzic, A., Madronich, S., Kasibhatla, P. S., Tyndall, G., Aumont, B., Jimenez, J. L., Lee-Taylor, J. and Orlando, J.: Organic photolysis reactions in tropospheric aerosols: effect on secondary organic aerosol formation and lifetime, Atmos. Chem. Phys., 15(16), 9253–9269, doi:10.5194/acp-15-9253-2015, 2015.

Kajimoto, O. and Fueno, T.: Relative rate constants of O(1D2)—olefin reactions, Chem. Phys. Lett., 64(3), 445–447, doi:10.1016/0009-2614(79)80218-3, 1979.

Keller-Rudek, H., Moortgat, G. K., Sander, R. and Sörensen, R.: The MPI-Mainz UV/VIS Spectral Atlas of Gaseous Molecules of Atmospheric Interest, [online] Available from: www.uv-vis-spectral-atlas-mainz.org, 2015.

Li, R., Palm, B. B., Ortega, A. M., Hu, W., Peng, Z., Day, D. A., Knote, C., Brune, W. H., de Gouw, J. and Jimenez, J. L.: Modeling the radical chemistry in an Oxidation Flow Reactor (OFR): radical formation and recycling, sensitivities, and OH exposure estimation equation, J. Phys. Chem. A, 119(19), 4418–4432, doi:10.1021/jp509534k, 2015.

Luo, D., Pierce, J. A., Malkina, I. L. and Carter, W. P. L.: Rate constants for the reactions of O(3P) with selected monoterpenes, Int. J. Chem. Kinet., 28(1), 1–8, doi:10.1002/(SICI)1097-4601(1996)28:1<1::AID-KIN1>3.0.CO;2-Z, 1996.

Mao, J., Ren, X., Brune, W. H., Olson, J. R., Crawford, J. H., Fried, a., Huey, L. G., Cohen, R. C., Heikes, B., Singh, H. B., Blake, D. R., Sachse, G. W., Diskin, G. S., Hall, S. R. and Shetter, R. E.: Airborne measurement of OH reactivity during INTEX-B, Atmos. Chem. Phys., 9(1), 163–173, doi:10.5194/acp-9-163-2009, 2009.

Mellouki, A. and Mu, Y.: On the atmospheric degradation of pyruvic acid in the gas phase, J. Photochem. Photobiol. A Chem., 157(2-3), 295–300, doi:10.1016/S1010-6030(03)00070-4, 2003.

Messaadia, L., El Dib, G., Ferhati, A. and Chakir, A.: UV–visible spectra and gas-phase rate coefficients for the reaction of 2,3-pentanedione and 2,4-pentanedione with OH radicals, Chem. Phys. Lett., 626, 73–79, doi:10.1016/j.cplett.2015.02.032, 2015.

Michaud, P., Paraskevopoulos, G. and Cvetanovic, R. J.: Relative rates of the reactions of O(1D2) atoms with alkanes and cycloalkanes, J. Phys. Chem., 78(15), 1457–1461, doi:10.1021/j100608a003, 1974.

Peng, Z., Day, D. A., Stark, H., Li, R., Lee-Taylor, J., Palm, B. B., Brune, W. H. and Jimenez, J. L.: HOx radical chemistry in oxidation flow reactors with low-pressure mercury lamps systematically examined by modeling, Atmos. Meas. Tech., 8(11), 4863–4890, doi:10.5194/amt-8-4863-2015, 2015.

Perdew, J. P., Burke, K. and Ernzerhof, M.: Generalized Gradient Approximation Made Simple, Phys. Rev. Lett., 77(18), 3865–3868, doi:10.1103/PhysRevLett.77.3865, 1996.

Pitts, J. N., Sandoval, H. L. and Atkinson, R.: Relative rate constants for the reaction of O(1D) atoms with fluorocarbons and N2O, Chem. Phys. Lett., 29(1), 31–34, doi:10.1016/0009-2614(74)80129-6, 1974.

Romonosky, D. E., Ali, N. N., Saiduddin, M. N., Wu, M., Lee, H. J. (Julie), Aiona, P. K. and Nizkorodov, S. A.: Effective absorption cross sections and photolysis rates of anthropogenic and biogenic secondary organic aerosols, Atmos. Environ., 130, 172–179, doi:10.1016/j.atmosenv.2015.10.019, 2016.

Runge, E. and Gross, E. K. U.: Density-functional theory for time-dependent systems, Phys. Rev. Lett., 52(12), 997–1000, doi:10.1103/PhysRevLett.52.997, 1984.

Salter, L. F. and Thrush, B. A.: Reaction of oxygen atoms with methyl and ethyl nitrates, J. Chem. Soc. Faraday Trans. 1, 73, 1098, doi:10.1039/f19777301098, 1977.

Sander, S. P., Friedl, R. R., Barker, J. R., Golden, D. M., Kurylo, M. J., Wine, P. H., Abbatt, J. P. D., Burkholder, J. B., Kolb, C. E., Moortgat, G. K., Huie, R. E. and Orkin, V. L.: Chemical Kinetics and Photochemical Data for Use in Atmospheric Studies Evaluation Number 17, Pasadena, CA, USA. [online] Available from: http://jpldataeval.jpl.nasa.gov/pdf/JPL%10-6%Final%15June2011.pdf, 2011.

Schmidt, M. W., Baldridge, K. K., Boatz, J. A., Elbert, S. T., Gordon, M. S., Jensen, J. H., Koseki, S., Matsunaga, N., Nguyen, K. A., Su, S., Windus, T. L., Dupuis, M. and Montgomery, J. A.: General atomic and molecular electronic structure system, J. Comput. Chem., 14(11), 1347–1363, doi:10.1002/jcc.540141112, 1993.

Schubert, C. C., Schubert, S. and Pease, R. N.: The Oxidation of Lower Paraffin Hydrocarbons. I. Room Temperature Reaction of Methane, Propane, n-Butane and Isobutane with Ozonized Oxygen 1, J. Am. Chem. Soc., 78(10), 2044–2048, doi:10.1021/ja01591a006, 1956.

Toby, S., Van de Burgt, L. J. and Toby, F. S.: Kinetics and chemiluminescence of ozone-aromatic reactions in the gas phase, J. Phys. Chem., 89(10), 1982–1986, doi:10.1021/j100256a034, 1985.

Trost, B., Stutz, J. and Platt, U.: UV-absorption cross sections of a series of monocyclic aromatic compounds, Atmos. Environ., 31(23), 3999–4008, doi:10.1016/S1352-2310(97)00214-8, 1997.

Tsalkani, N., Mellouki, a., Poulet, G., Toupance, G. and Bras, G.: Rate constant measurement for the reactions of OH and Cl with peroxyacetyl nitrate at 298 K, J. Atmos. Chem., 7(4), 409–419, doi:10.1007/BF00058713, 1988.

Wolfe, G. M., Crounse, J. D., Parrish, J. D., St. Clair, J. M., Beaver, M. R., Paulot, F., Yoon, T. P., Wennberg, P. O. and Keutsch, F. N.: Photolysis, OH reactivity and ozone reactivity of a proxy for isoprene-derived hydroperoxyenals (HPALDs), Phys. Chem. Chem. Phys., 14(20), 7276, doi:10.1039/c2cp40388a, 2012.

Ziemann, P. and Atkinson, R.: Kinetics, products, and mechanisms of secondary organic aerosol formation, Chem. Soc. Rev., 41(19), 6582, doi:10.1039/c2cs35122f, 2012.